ASSESSING THE FEASIBILITY OF DEEP GEOTHERMAL WELLS USING ADVANCED TECHNOLOGIES AND RESERVOIR SIMULATION: A CASE STUDY IN THE DJ BASIN, COLORADO

by

Ali Nassereddine

© Copyright by Ali Nassereddine, 2024

All Rights Reserved

A thesis submitted to the Faculty and the Board of Trustees of the Colorado School of Mines in partial fulfillment of the requirements for the degree of Master of Science (Petroleum Engineering).

Golden, Colorado
Date _____

Signed: _____
Ali Nassereddine

Signed: _____
Dr. Luis Zerpa
Thesis Advisor

Golden, Colorado
Date _____

Signed: _____
Dr. Jennifer Miskimins
Professor and Head
Department of Petroleum Engineering

ABSTRACT

This study explores the potential of extracting geothermal energy from the Wattenberg field's basement in the Denver-Julesburg (DJ) Basin. Recognizing the need for advanced drilling technologies and innovative reservoir management techniques due to the challenging conditions of deep geothermal wells, this research only focuses on assessing the flow performance of various well configurations and their heat extraction efficiencies. To be specific, the research centered on U-Shaped, V-Shaped, Inclined V-Shaped, and Pipe-in-Pipe on drilling and well completion compared to the known Enhanced Geothermal Systems (EGS) configurations.

Employing numerical modeling, the study investigates the thermal behavior under different operational scenarios, such as variations in well configurations and the impact of fracture states. Findings indicate that closed-loop systems provide moderate temperature increases, highlighting the critical influence of well architecture on thermal performance. Remarkably, EGS configurations demonstrate a significant potential for high-temperature geothermal energy extraction.

This research underscores the critical need for a comprehensive evaluation of well configurations in geothermal energy projects, especially in geologically complex regions like the DJ Basin. By focusing on the comparative performance of various well designs, this study contributes valuable insights into the strategic planning and development of geothermal energy resources. The advancements and knowledge gained from this investigation highlight the evolving landscape of geothermal technology, paving the way for future explorations and optimizations in geothermal energy extraction.

TABLE OF CONTENTS

ABSTRACT iii

LIST OF FIGURES viii

LIST OF TABLES xii

NOMENCLATURE xiii

LIST OF ABBREVIATION xv

ACKNOWLEDGEMENTS xvi

CHAPTER 1 INTRODUCTION 1

1.1 Research Background 1

1.2 Research Objectives and Questions 7

1.3 Significance of the Research 9

1.4 Thesis Organization 9

CHAPTER 2 GEOTHERMAL ENERGY 12

2.1 Overview 12

2.2 Geothermal Power Plants 15

2.2.1 Efficiency and Environmental Compatibility 17

2.2.2 Expanding the Utilization of Geothermal Energy 17

2.2.3 Operating Principles and Environmental Benefits 17

2.2.4 Case Studies: Quantifying the Impact of Binary Cycle Technology in Geothermal Power Generation 18

2.3 Geothermal Energy Extraction: Closed Loop vs. Open Loop Systems 20

2.3.1 Closed Loops: Geothermal Closed Loop Systems with ORC Technologies .. 20

2.3.2 Open Loops: Enhanced Geothermal Systems (EGS) with Supercritical ORC (sORC) 21

2.3.3 Optimal ORC Configurations for Geothermal Systems 21

2.3.4 Calculation of Electricity Generation in Geothermal Power Plants 22

2.4 Advancements in Geothermal Reservoir Simulation 24

2.4.1 Theoretical Framework in CMG-STARS 25

2.4.2 CMG-Stars FlexWell 26

2.5 Geothermal Well Configurations 27

CHAPTER 3 METHODOLOGY 35

3.1 Reservoir Simulation Approach 35

3.1.1 Defining Parameters and Simulation Setup 36

3.1.2 Reservoir Simulation Model 37

3.1.3 Simulation Setup and Parameter Definition 38

3.1.4 Performance Analysis and Model Validation 39

3.2 Description of Geothermal Well Configurations 39

3.2.1 Reservoir Grid and Properties 40

3.2.2 Definition of Reservoir Parameters 40

3.2.3 Thermal Properties 41

3.2.4 Components Configuration 42

3.2.5 Rock-Fluid Interactions 42

3.2.6 Initial Conditions 43

3.2.7 Wells Configuration and Fluid Dynamics 44

3.2.8 Integration of Empirical Data and Theoretical Models 59

CHAPTER 4 RESULTS 63

4.1 Long-Term Performance Analysis of U-Shaped Geothermal Well Models 63

4.1.1 Base Model 63

4.1.2 Fractured Models 67

4.1.3 U-Shaped Wells Models Comparison 69

4.2 Long-Term Performance Analysis of Pipe-in-Pipe Geothermal Well Models 70

4.3 Long-Term Performance Analysis of V-Shaped Geothermal Well Models 74

4.4 Long-Term Performance Analysis of Inclined V-Shaped Geothermal Well Models 78

4.5 Long-Term Performance Analysis of EGS Well Models 82

4.6 Long-Term Performance Analysis of Inclined EGS Well Models 86

4.7 Comparison of Closed-Loop Systems 90

4.8 Comparison of EGS Systems 91

4.9 Overall Performance Comparison 92

CHAPTER 5 CONCLUSION 95

CHAPTER 6 FUTURE IMPLICATIONS 98

REFERENCES CITED 99

APPENDIX A U-SHAPE CASE .DAT CODE..... 105

APPENDIX B V-SHAPE CASE .DAT CODE..... 131

APPENDIX C EGS CASE .DAT CODE..... 137

APPENDIX D LIST OF SUPPLEMENTAL FILES FOR COPYRIGHT PERMISSIONS 142

LIST OF FIGURES

Figure 1.1: Temperature vs Depth (EnvGeo EGS, Inc. 2020), reprinted by permission of EnvGeo EGS, Inc. Team. 3

Figure 1.2: Interpretive Geothermal Gradient Map of Colorado, USA (Colorado Geological Survey, Department of Natural Resources 2010), reprinted by permission of US Department of Natural Resources. 5

Figure 1.3: Map of Greater Wattenberg Area, located within the Denver-Julesburg Basin of Colorado. West–east cross section A–A' showing structural setting of the Denver Basin, Colorado, adapted from Robson and Banta (1987), reprinted by permission of USGS. 6

Figure 2.1: Temperature Gradient. Adapted from Panchuk (2019), reprinted by permission of Karla Panchuk and licensed under CC BY-NC-SA 4.0 12

Figure 2.2: Binary Cycle Geothermal Power Plant (Mines 2016), reprinted by permission of Elsevier Books. 15

Figure 2.3: Reservoir stimulation strategy, (a) two-wing fracturing of the center well and (b) double well symmetric fracturing (Lei et al. 2020), reprinted by permission of Elsevier Books. 29

Figure 2.4: Schematic of heat extraction for multilateral-well EGS (Song et al. 2018), reprinted by permission of Elsevier Books. 30

Figure 2.5: Schematic diagram of the fluid flow and thermal process for CLG (Song et al. 2018), reprinted by permission of Elsevier Books. 31

Figure 2.6: Structure diagram of Single Well Geothermal Heating (Bu, Jiang, and Li 2019), reprinted by permission of Elsevier Books. 32

Figure 2.7: Schematic showing heat extraction in horizontal-well open-loop geothermal system (Wang et al. 2020), reprinted by permission of Elsevier Books. 33

Figure 3.1: Geothermal Reservoir Model Grid System. 40

Figure 3.2: U-Shaped Closed Loop Well Model Description 45

Figure 3.3: V-Shaped Closed Loop Well Model Description 48

Figure 3.4: Inclined V-Shaped Closed Loop Well Model Description Geometric Configuration 49

Figure 3.5: Pipe-in-Pipe Closed Loop Well Model Description 51

Figure 3.6: EGS Well Model Description 55

Figure 3.7: Inclined EGS Well Model Description 58

Figure 3.8: Fervo vs CMG Model (Surface Temperature Comparison)..... 60

Figure 3.9: Fervo vs CMG Model (Injection and production Wells Comparison)..... 61

Figure 3.10: Amini's Model vs CMG Model (Surface Temperature Comparison) 62

Figure 4.1: U-Shaped Closed Loop Wells Reservoir Model (After 80 years)..... 64

Figure 4.2: U-Shaped (Base Model) – Temperature (°F) vs Time (years) 64

Figure 4.3: U-Shaped (Base Model) – Temperature Profile (°F) vs Depth (ft)..... 65

Figure 4.4: U-Shaped (Base Model) – P-h Diagram for Water up to 250 MPa 66

Figure 4.5: Thermal and Pressure Dynamics in U-Shaped Well Systems: Profiles and Projections..... 67

Figure 4.6: U-Shaped (Fracked - Closed) – Temperature (°F) vs Time (years) 68

Figure 4.7: U-Shaped (Fracked - Opened) – Temperature (°F) vs Time (years)..... 69

Figure 4.8: Temperature (°F) vs Time (years) – U-Shaped (All Models) Comparison..... 70

Figure 4.9: Pipe-in-Pipe Well Closed Loop Well Reservoir Model (After 80 years)..... 71

Figure 4.10: Pipe-in-Pipe Well – Temperature (°F) vs Time (years)..... 71

Figure 4.11: Pipe-in-Pipe Well – Temperature Profile (°F) vs Depth (ft) 72

Figure 4.12: Pipe-In-Pipe Model – P-h Diagram for Water up to 250 MPa..... 73

Figure 4.13: Thermal and Pressure Dynamics in Pipe-in-Pipe Well Systems: Profiles and Projections 74

Figure 4.14: V-Shaped Closed Loop Wells Reservoir Model (After 80 years) 75

Figure 4.15: V-Shaped Wells – Temperature (°F) vs Time (years) 75

Figure 4.16: V-Shaped Wells – Temperature Profile (°F) vs Depth (ft) 76

Figure 4.17: V-Shaped Model – P-h Diagram for Water up to 250 MPa 77

Figure 4.18: Thermal and Pressure Dynamics in V-Shaped Wells Systems: Profiles and Projections 78

Figure 4.19: Inclined V-Shaped Closed Loop Wells Reservoir Model (After 80 years) 79

Figure 4.20: Inclined V-Shaped Wells – Temperature (°F) vs Time (years) 79

Figure 4.21: Inclined V-Shaped Wells – Temperature Profile (°F) vs Depth (ft) 80

Figure 4.22: Inclined V-Shaped Model – P-h Diagram for Water up to 250 MPa 81

Figure 4.23: Thermal and Pressure Dynamics in V-Shaped Wells Systems: Profiles and Projections 82

Figure 4.24: EGS Well Reservoir Model (After 80 years) 83

Figure 4.25: EGS Wells – Temperature (°F) vs Time (years) 84

Figure 4.26: EGS Wells – Temperature Profile (°F) vs Depth (ft) 84

Figure 4.27: EGS Model – P-h Diagram for Water up to 250 MPa 85

Figure 4.28: Thermal and Pressure Dynamics in EGS Wells Systems: Profiles and Projections 86

Figure 4.29: Inclined EGS Well Reservoir Model (After 80 years) 87

Figure 4.30: EGS Wells – Temperature (°F) vs Time (years) 87

Figure 4.31: Inclined EGS Wells – Temperature Profile (°F) vs Depth (ft) 88

Figure 4.32: Inclined EGS Model – P-h Diagram for Water up to 250 MPa 89

Figure 4.33: Thermal and Pressure Dynamics in Inclined EGS Wells Systems: Profiles and Projections..... 90

Figure 4.34: Temperature Comparison of Closed-Loop Well Configurations after 20 Years ... 91

Figure 4.35: Temperature Outcomes of EGS and Inclined EGS Wells after 20 Years..... 91

Figure 4.36: Overall Temperature Comparison of All Geothermal Well Configurations after 20 Years..... 92

LIST OF TABLES

Table 3.1: Input Parameters for the Reservoir and Grid Section 41

Table 3.2: Component Properties for Simulation 42

Table 3.3: Relative Permeability Table 43

Table 3.4: Parameters for Initial Conditions 43

Table 3.5: Operational Parameters for 'Injector' Well 46

Table 3.6: Operational Parameters for 'Producer' Well 46

Table 3.7: Well Radius and Fluid Injection Parameters 46

Table 3.8: Diameter Specifications for FlexWells 47

Table 3.9: Operational Parameters for 'Casing' and 'Tubing' Wells 52

Table 3.10: Fluid Injection Parameters 52

Table 3.11: Perforation-Related Well Radius Specifications 53

Table 3.12: Casing and Insulation Parameters for Pipe Components 54

Table 3.13: Well Wall Diameter Specifications 54

Table 4.1: Well Models Temperature Performance Comparison 94

NOMENCLATURE

Ad_i ……..……..…. adsorbed component i

B …….…...……...…… exergy

C_f ……..……..…. fluid heat capacity [J/(kg °C)]

D_{wi} ……..…….……..…….. component dispersibilities

h ……..……..…….. enthalpy

H_w ……...……..……. water enthalpy

$\dot{m}$ ……...…….….. mass rate (kg/s)

m_{prod} …….……..……..…... mass flow rate of the produced fluid

P_{gross} ……...……..……. gross electric power

p_{inj} ……...…….….……... injection wellhead pressure

P_{net} ……...……..…….. net electric power generated

P_{pump} …….……..… electrical power for injection pumps

q_{inj} ……..……..……... injection flow rate

q_w ……...……...…….. water source/sink flow rate

q_{wk} ……...……...…….. water well phase rate

s ……..…….. entropy

S_w ……...……..……... water saturation

T_0 ……...……..…….…… ambient temperature

T_1 …….……..…...….. temperature inlet (°C)

T_2 ……...……..……... temperature inlet (°C)

U_i ……..……...……. internal energy for i phase

U_r ……..…..……... energy per rock volume

V ……...…….. total volume of the grid block

wi ……..……...…….…..….. concentration of component i

η_{pump} ……..……...……..……...……. pump efficiency

Greek Letters

ϕ_f ……..…….. fluid porosity

ϕ_v ……...….... void porosity

ρ_w ……..…….. water density

Δw_i …….…….. change in concentration of component i in aqueous phase

ϕ ……..…….….. absolute porosity

ΔT ……..…….….. temperature gradient

K ……..……..…….….. thermal conductivity

η ……..…..…….….. Carnot's efficiency (fraction)

LIST OF ABBREVIATION

BHP ……..…….....…….. Bottom Hole Pressure

CLG ……..…...…..…….. Closed-Loop Geothermal

CMG ……....…..…….. Computer Modelling Group

DFN …….....…….. Discrete Fracture Network

DJ ……..……..……...…….. Denver-Julesburg

EGS ……..…...…..…….. Enhanced Geothermal Systems

EH ……..…….…...…….. Extended Horizontally

GLADE ……...…...…….. Geothermal Limitless Approach to Drilling Efficiencies

HDR ……...……...……...…….. Hot Dry Rock

HTM ……..……...…….. hydro-thermo-mechanical

ID ……..……..…...…….. Inner Diameter

OD ……..……...…….. Outer Diameter

ORC ……..….....…….. Organic Rankine Cycle

PIP …….....…….. Pipe-in-Pipe

sORC ……....…….. Supercritical ORC

STW ……...…...…...…….. Surface Water Rate

UBA ……...……....…….. User Block Address

ACKNOWLEDGEMENTS

My journey through research, study, and daily life has been shaped by the generous support of many individuals. It is with deep gratitude that I acknowledge their invaluable contributions to my work.

During my time at the Colorado School of Mines, I have experienced tremendous growth and learning. The sense of family within the department has profoundly enhanced my experience. I am especially grateful to Dr. Kazemi, whose belief in my potential from the outset has been transformative. His wisdom and generosity have opened numerous doors for me to engage in meaningful projects. I would like to thank Dr. Zerpa for his unwavering support and constant availability, for his trust in my work, for always being there to answer my questions, for his wisdom, and for giving me the opportunity to complete my studies at Mines.

I must also acknowledge Kaveh, whose humility and expertise are truly exceptional. Working alongside him, particularly on his geothermal model, has significantly contributed to the success of my research. I am deeply honored to have learned from the distinguished faculty at CSM, including Dr. Kazemi, Dr. Ozkan, Dr. Sonnenberg, Dr. Prasad, and Dr. Battalora. Their teachings and insights have been invaluable.

The camaraderie with my peers, Mehryar, Hossein, Melak, Tsimur, Kaveh, Mohammad, Abdullah, Zenitha, Ozan, and Luiz, has made my time at CSM both enjoyable and enlightening, broadening my perspective on life.

Lastly, I owe a heartfelt thank you to my parents and sisters, whose unwavering support has been the cornerstone of my achievements. Every step of this journey has been inspired by and dedicated to them.

CHAPTER 1
INTRODUCTION

1.1 Research Background

Geothermal energy, a sustainable energy resource derived from the Earth's internal heat, has garnered significant attention due to its low carbon footprint and capacity for providing continuous baseload power (Glassley 2010). Despite its abundance, this renewable resource poses special difficulties for discovery, extraction, and use, especially in areas with deep geothermal reservoirs that are hot and have intricate geological features.

A notable geological feature spanning Colorado, Wyoming, and Nebraska, the Denver-Julesburg (DJ) Basin has gained attention as a possible hotspot for the production of geothermal energy. Known historically for its hydrocarbon wealth, the geothermal potential of the DJ Basin is still largely unexplored; the Wattenberg field's basement present particularly intriguing opportunities because of their high heat flow and thermal gradient (Vivas et al. 2023; Moska et al. 2023).

Such difficult terrain makes it necessary to use cutting-edge drilling technologies and creative reservoir management techniques to extract geothermal resources. It is projected that deep geothermal wells in the DJ Basin will descend to extremely high depths and experience temperatures of approximately 300°C (572°F), which presents considerable environmental and technological difficulties. To achieve effective and sustainable resource extraction under these conditions, a thorough understanding of the subsurface geology, reservoir dynamics, and fluid characteristics is necessary.

A complex web of interconnected geological, physical, and chemical characteristics controls the nuances of the dynamics within these reservoirs. The two most important of these are the

reservoir rock's porosity and permeability, which determine how much fluid the rock can hold and how easily these fluids can pass through its pore spaces. These factors together determine the reservoir's potential productivity and rate of heat extraction (Fournier 1999).

In addition, the geothermal gradient and reservoir temperature have a direct impact on the amount of heat energy that can be extracted, with greater temperatures and steeper gradients often indicating more effective energy extraction (Ye et al. 2022). As shown in Figure 1.1, the thermal gradient has a direct impact on the technology used to extract geothermal energy. This varies with depth, as we can find conventional hydrothermal systems at shallow depths with high reservoir temperatures, indicating a high thermal gradient (per unit depth). In contrast, a shallow depth with low temperature, indicating a lower temperature gradient, will result in a direct use of produced geothermal resources because of the limitation of extracting electricity from these temperatures. Finally, having high geothermal temperature in deep formations will require the use of enhanced geothermal systems (EGS), because of the limitation to find good porosity/permeability at very high depths. Using EGS, it will allow us to extract heat by fracking the reservoir and creating channels with high surface areas for the fluid to flow and extract the heat. The methods of heat storage and transfer from the rock matrix to the circulating fluid are greatly influenced by the mineralogical composition and thermal characteristics of the reservoir rock, such as its heat capacity and thermal conductivity (Clauser 2006).

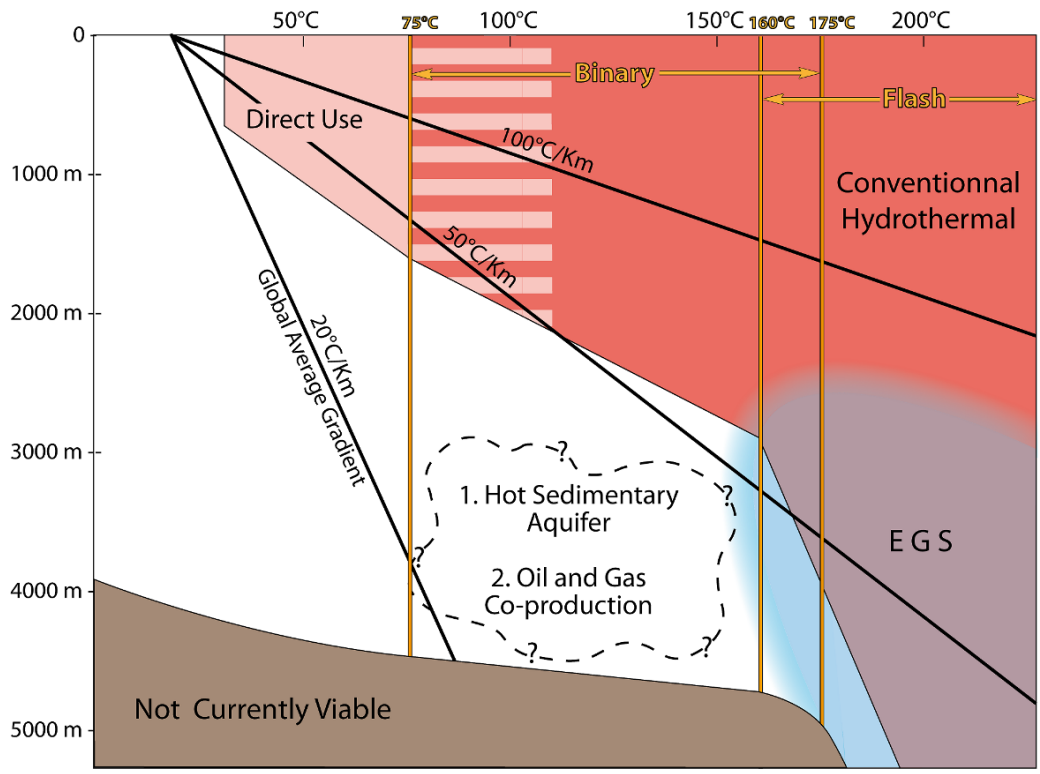

Figure 1.1: Temperature vs Depth (EnvGeo EGS, Inc. 2020), reprinted by permission of EnvGeo EGS, Inc. Team.

A critical component in this complex environment is the chemical makeup of geothermal fluids. In particular, the existence of dissolved gases and minerals can cause problems, affecting the effectiveness of heat transfer and perhaps causing mineral precipitation that obstructs reservoir pores (Axelsson 2010). Moreover, preserving the ideal fluid flow rates requires careful balancing and is necessary to prevent thermal breakthrough, which is the premature cooling of the reservoir and to maintain the reservoir's pressure (Cheng et al. 2021).

One more crucial factor affecting the reservoir's sustainable utilization is the placement and arrangement of the production and injection wells. In order to avoid interference and sustainably regulate reservoir pressure, this entails the strategic positioning of wells (Pratama and Saptadji 2021; Simmons et al. 2021).

Advanced reservoir engineering approaches, including reservoir simulation and monitoring, have been put to use in response to these complex difficulties. These advanced techniques, based on thorough data analysis and predictive modeling, are essential for maximizing heat extraction and guaranteeing the long-term viability of the reservoir (Xu et al. 2021; Chen et al. 2023). The field of geothermal technology is developing, which emphasizes the need for continued study and creative approaches to overcome the difficulties presented by these intricate natural systems.

Massachusetts Institute of Technology (2006) has identified Enhanced Geothermal Systems (EGS) as a feasible method for utilizing the geothermal potential of low-permeability, hot, dry rock formations such as the DJ Basin. EGS involves the artificial generation of permeability through hydraulic stimulation. Although promising, EGS technologies need to take induced seismicity, environmental effects, and economic viability into serious account (Majer et al. 2007).

The DJ Basin presents a promising opportunity for geothermal exploration due to its geothermal gradient and geophysical features. Higher than average geothermal gradients are caused by the radioactive decay of minerals and residual heat from the Earth's creation, which affect the basin's thermal regime (Abdelrahman et al. 2023; Zhang et al. 2022).

Figures 1.2 illustrates the geothermal gradient of the DJ Basin and highlights the regions with the greatest potential for geothermal energy use. An important use of this type of cartographic depiction is to show the spatial differences in subsurface temperature regimes, which helps identify potential locations for geothermal drilling projects (Colorado Geological Survey, Department of Natural Resources 2010).

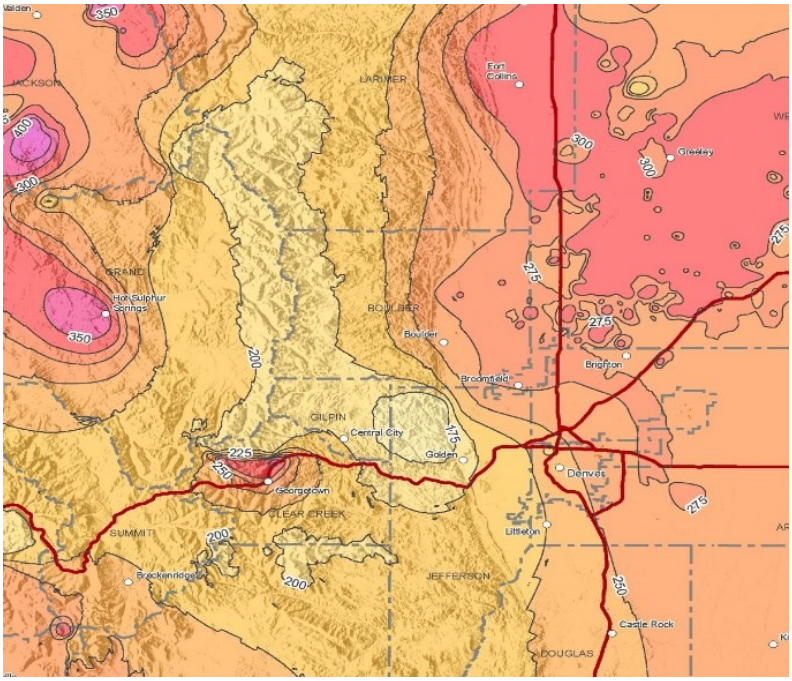

Figure 1.2: Interpretive Geothermal Gradient Map of Colorado, USA (Colorado Geological Survey, Department of Natural Resources 2010), reprinted by permission of US Department of Natural Resources.

Due to the influence of its geological past, the geothermal profile of the DJ Basin shows a complex network of structural elements that are favorable to Hot Dry Rock (HDR) geothermal systems.

These characteristics include a complex network of fault networks and cracked substrates that may facilitate improved circulation of geothermal fluids in addition to exhibiting strong temperature variations.

A cross-sectional representation of the basin's subsurface is provided in Figure 1.3, which also explains the different geological strata, fault zones, and potential HDR reservoirs.

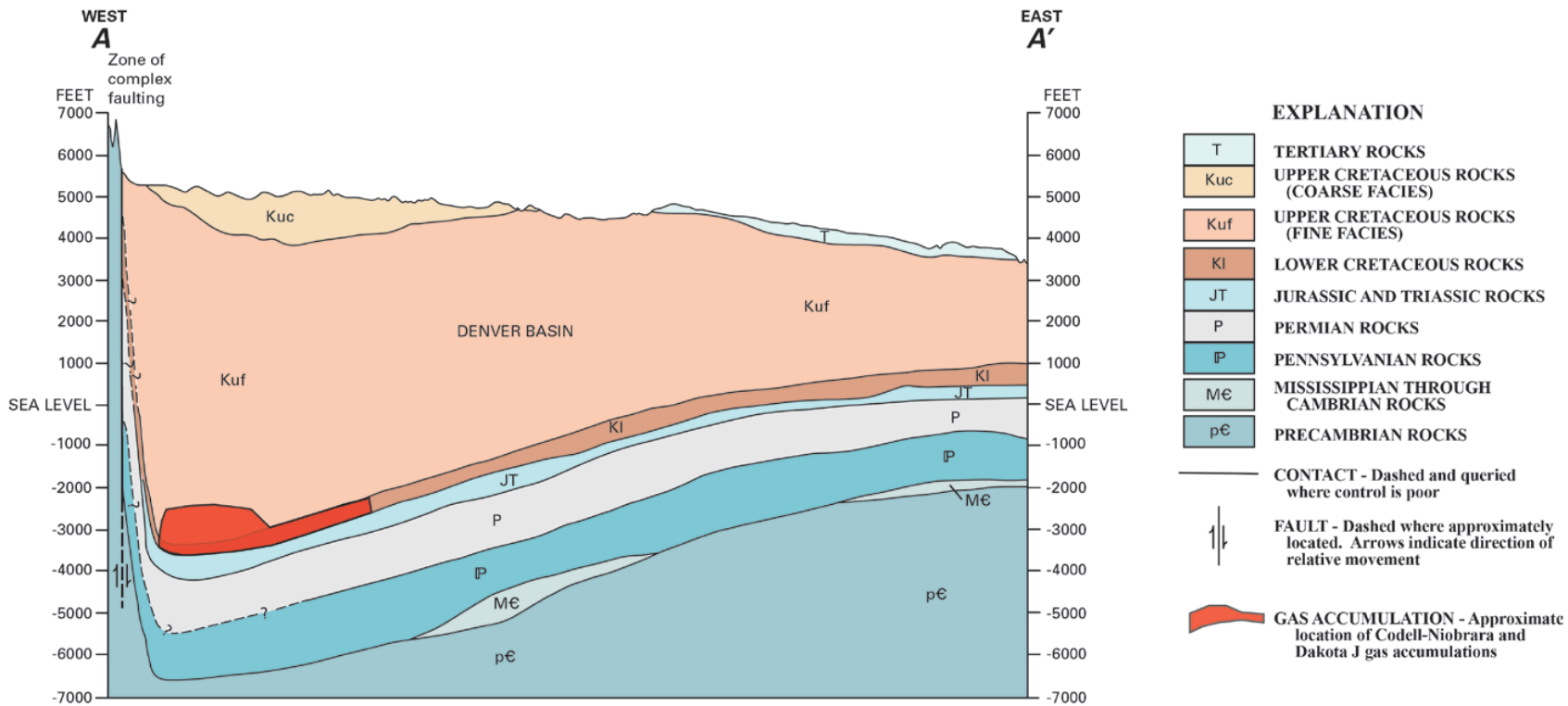

Figure 1.3: Map of Greater Wattenberg Area, located within the Denver-Julesburg Basin of Colorado. West–east cross section A–A' showing structural setting of the Denver Basin, Colorado, adapted from Robson and Banta (1987), reprinted by permission of USGS.

1.2 Research Objectives and Questions

The primary objective of this research project is to carry out a thorough reservoir simulation to investigate the geothermal energy production potential of deep wells drilled down to the granitic basement of the Wattenberg field in the DJ Basin, Colorado. At the writing of this thesis, the Geothermal Limitless Approach to Drilling Efficiencies (GLADE) project is planning to drill two deep, high-temperature geothermal wells in this particular area, with conditions that can reach temperatures of roughly 572°F and depths of up to 20,000 feet.

While the broader project context involves the use of advanced drilling technologies for these challenging conditions, this research will thoroughly examine and assess several well configuration and injection/production strategies using numerical simulation. This evaluation encompasses a thorough examination of both open-hole and closed-hole systems relevant to these geothermal wells operating at high temperatures in the granitic formation.

The goal is to forecast the behavior of the reservoir under various operating situations and comprehend its dynamics through in-depth simulations. This will help us guide the best drilling trajectories and production practices. In the following sections of this study, the simulation methods, parameters, and major conclusions will be thoroughly examined.

The study's objectives are to:

1. Conduct a thorough reservoir simulation in the Wattenberg field's granitic formations to understand reservoir dynamics and predict behavior under various operating circumstances.

2. Compare and analyze open-hole and closed-hole geothermal system configurations to discern their respective advantages and challenges.

3. Investigate a novel strategy that combines the advantages of closed-loop and enhanced geothermal systems with the goal of increasing geothermal energy output.

4. Maximize the longevity, effectiveness, and performance of the geothermal systems under consideration.

5. Establish the best configuration for the DJ Basin's geothermal system to reach maximum energy output and maintain system longevity.

To achieve these objectives, the research will address the following questions:

1. How can geothermal system design in the Denver-Julesburg Basin be optimized through the use of reservoir simulation?

2. What fundamental reservoir properties impact the efficiency of geothermal systems in the DJ Basin, and how can they be measured or estimated?

3. What are the benefits and drawbacks of integrating improved and closed-loop technology into a hybrid geothermal system?

The following tasks have been created in order to address these questions and fulfill the goals of the research:

- Task 1: Perform a comprehensive reservoir simulation in order to understand the granitic formation dynamics in the Wattenberg field. This will entail adjusting conditions and parameters to evaluate the reservoir's response in various scenarios.
- Task 2: Analyze the performance of the granitic formation's open- and closed-hole geothermal systems. This will entail comparing the systems in order to ascertain which one provides the best energy extraction.

- Task 3: An innovative hybrid geothermal system that combines the advantages of improved and closed-loop technologies should be proposed and evaluated. This will entail modeling the hybrid system's performance under the circumstances of the DJ Basin.
- Task 4: Provide a thorough analysis of the simulations' main conclusions, parameters, and techniques. This will entail a careful examination and interpretation of the simulation data, offering perceptions into the best practices for producing geothermal energy in the DJ Basin.

1.3 Significance of the Research

The exploration of geothermal energy in the Denver-Julesburg (DJ) Basin holds transformative potential for the energy landscape. The significance of this study encompasses multiple elements:

1. Meeting Energy Needs: Leveraging the geothermal resources of the DJ Basin can assist in addressing the increasing demand for energy while lowering dependency on fossil fuels.
2. Environmental Benefits: Geothermal energy presents an environmentally friendly substitute, resulting in a decrease in greenhouse gas emissions.
3. Economic Growth: Successful geothermal extraction in the DJ Basin can result in lower costs, the creation of jobs, and the growth of the local economy.
4. Technological Advancement: Insights from this research may spur new developments in geothermal extraction methods, which would help other geothermal-rich areas.

1.4 Thesis Organization

This thesis is structured into six chapters, with each chapter dedicated to a specific aspect of geothermal energy extraction and its optimization in the Denver-Julesburg (DJ) Basin,

particularly within the Wattenberg field's granitic basement. The organization of the thesis is outlined as follows:

- Chapter 1: Provides a foundation for the study by presenting the research background, delineating the research objectives and questions, and underscoring the significance of the research. This chapter also includes an overview of the thesis organization.
- Chapter 2: Delves into the fundamentals of geothermal energy, including an overview of geothermal power plants and their efficiency, environmental compatibility, and the potential for expanding their utilization. This chapter explores the distinctions between closed-loop and open-loop systems for geothermal energy extraction, advancements in geothermal reservoir simulation, and different geothermal well configurations.
- Chapter 3: Outlines the comprehensive approach employed in this study, including reservoir simulation techniques, definition of parameters, model validation, and a detailed examination of various geothermal well configurations and their impact on energy extraction efficiency.
- Chapter 4: Presents the findings from the long-term performance analysis of several geothermal well models, including U-Shaped, Pipe-in-Pipe, V-Shaped, Inclined V-Shaped, and Enhanced Geothermal Systems (EGS), both standard and inclined. It also offers a comparative analysis of closed-loop systems versus EGS configurations and summarizes the overall performance comparison.
- Chapter 5: Encapsulates the key findings, achievements, and contributions of the study, providing a conclusive summary of the research and its implications for the field of geothermal energy.

- Chapter 6: Suggests directions for future research, building upon the findings of this study to propose areas for continued exploration and development in geothermal energy extraction technologies.

CHAPTER 2

GEOTHERMAL ENERGY

2.1 Overview

Geothermal energy, a form of renewable energy, is derived from the Earth's internal heat. In certain countries, people have been using this energy source for heating and cooking for thousands of years. It is the internal heat of the Earth that can also be captured and transformed into electrical power. Using the Earth's enormous internal heat reservoir, steam is produced, which drives turbines to produce energy (Montesdeoca-Martínez and Velázquez-Medina 2023).

Iron makes up the majority of the Earth's core, which is thought to reach temperatures of over 9,000°F (5,000°C) and is encircled by a layer of molten rock (Figure 2.1). The mantle, the layer of rock beneath the Earth's crust, is heated by the constant outflow of heat from the core. Geothermal energy production is common is areas where the heat from the mantle rises closer to the Earth's surface (Panchuk 2019).

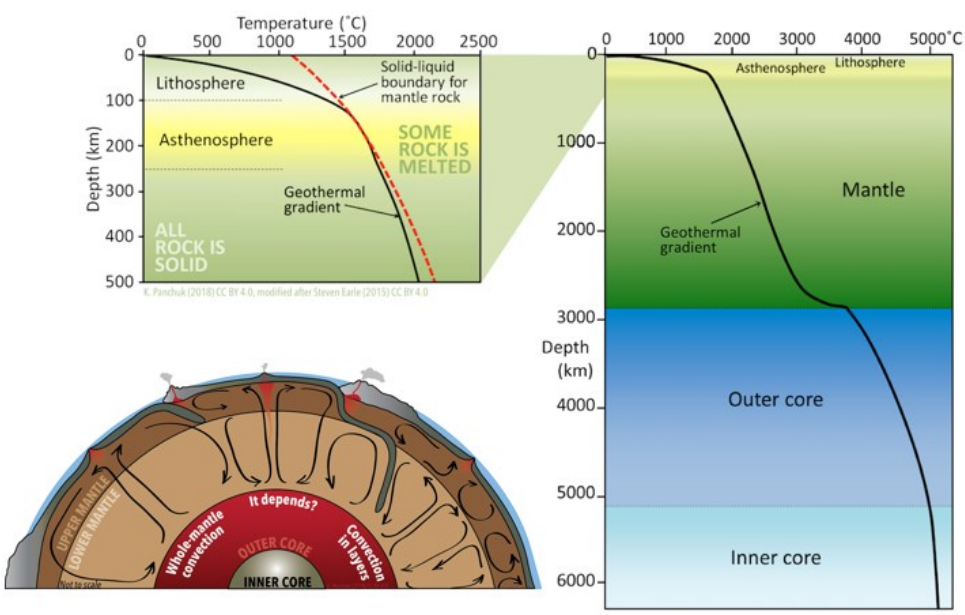

Figure 2.1: Temperature Gradient. Adapted from Panchuk (2019), reprinted by permission of Karla Panchuk and licensed under CC BY-NC-SA 4.0

In general, there are three main uses for geothermal energy systems: geothermal heat pumps for heating and cooling buildings using the steady Earth surface temperatures, direct use applications such as heating buildings, greenhouses, drying crops, and industrial processes like pasteurizing milk using geothermal hot water directly, and electric power production (Beckers et al. 2014; De Souza et al. 2021; Morrone and Algieri 2020).

High surface temperatures are required to produce steam from water, which is an essential step in the electricity production process. However, this requirement varies depending on the type of power plant. For example, the binary cycle—in which water from the geothermal well is used to heat another fluid with a lower boiling point—is frequently the most effective method in Hot Dry Rock (HDR) systems.

For effective energy conversion in these systems, the surface temperature requirements are crucial. While some systems are built for heat source temperatures of 170°C, 150°C, and 130°C (Zhai, An, and Shi 2014), it has been proved that a binary-cycle electrical generator may employ geothermal fluid at 132°C to boil Freon R-114 for power generation (Cremer 1981). These instances show how surface temperature needs might vary based on the particulars of the geothermal reservoir and the power plant's architecture (Hu et al. 2022). This emphasizes how each geothermal project needs to be approached uniquely in order to match surface temperatures with subsurface conditions and technology design for optimal performance.

The Denver-Julesburg (DJ) Basin has a substantial potential for the production of geothermal energy due to its distinct geological features. The basin is a great option for geothermal energy research and production due to its strong thermal gradient and advantageous geological characteristics. The depth of the basin and the characteristics of its rock formations make it an excellent place to explore for deep geothermal energy.

One particularly notable feature of the DJ Basin is the Wattenberg field. Its granitic deposits and other geological features make it an excellent choice for the extraction of geothermal energy. The possibility that high-temperature geothermal reservoirs could be found in the granitic rocks in particular makes them extremely interesting (Figure 1.2). These granitic rocks are expected to be appropriate for deep geothermal energy extraction because they can reach as deep as 20,000 feet and have temperatures as high as around 572°F.

The exploration of Hot Dry Rock (HDR) geothermal reservoirs marks a significant advancement in the field of renewable energy. In contrast to traditional hydrothermal systems, HDR reservoirs are not naturally hydrated, and their utilization depends on heat from dry rocks at significant depths. Geothermal energy extraction from these types of reservoirs presents a number of exciting potential as well as significant hurdles.

Understanding the hydro-thermo-mechanical (HTM) dynamics that emerge when fluid is added to the system is a major barrier to the use of HDR reservoirs. The injected fluid, the natural geothermal heat, and the mechanical characteristics of the rock interact in a complicated way in this process. For instance, the introduction of fluid into a single crack in a two-dimensional rock matrix in a standard HDR setup can drastically modify the stress distribution because of variations in pore pressure and temperature.

These changes may have an impact on the stress state of the matrix and, in turn, the permeability of the fracture. Furthermore, a key factor in determining the long-term sustainability of the energy extraction process is the heat transfer that occurs both through direct conduction and fluid-driven advection within the fracture and the surrounding rock.

The possibility of induced seismicity related to HDR reservoir stimulation, which is commonly accomplished via hydraulic fracturing, presents another difficulty (Andrés et al.

2022). This mechanism has the potential to create seismic events, some of which may be large enough to be concerning. It is imperative to tackle the hazards linked to this level of seismicity in order to responsibly exploit HDR geothermal resources.

2.2 Geothermal Power Plants

Geothermal energy, derived from the Earth's internal heat, is a sustainable and clean power source that has been increasingly harnessed through various technologies. Among these, Binary Cycle Power Plants stand out for their efficiency and environmental compatibility (DiPippo 2016). Traditional geothermal systems typically require high-temperature resources to operate effectively. However, Binary Cycle Power Plants are uniquely designed to exploit lower temperature geothermal fluids, making them instrumental in expanding the utilization of geothermal energy across diverse geological settings (Figure 2.2).

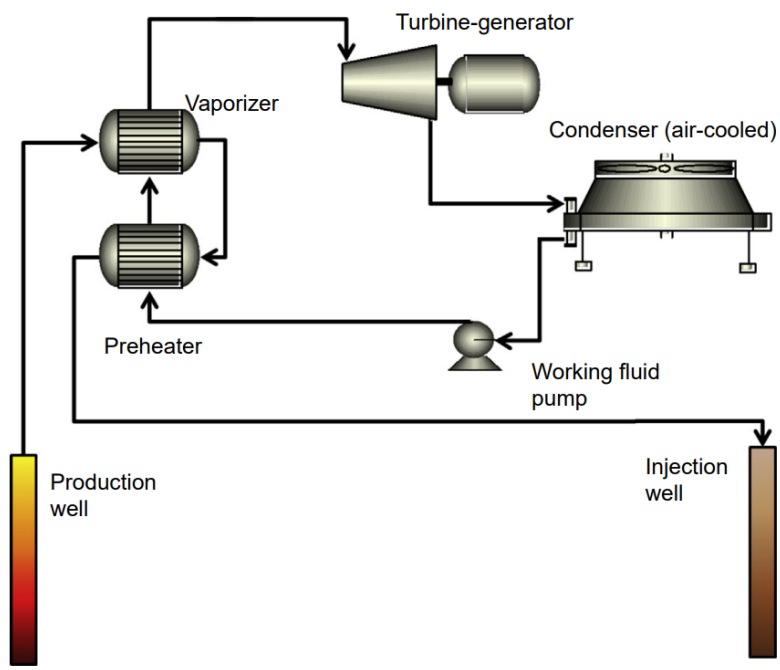

Figure 2.2: Binary Cycle Geothermal Power Plant (Mines 2016), reprinted by permission of Elsevier Books.

Binary Cycle Power Plants represent a significant advancement in the field of geothermal power generation. These plants employ a sophisticated heat exchange mechanism, enabling them to efficiently use geothermal fluids with temperatures ranging between 85-170°C.

Unlike conventional geothermal systems that depend on high-temperature steam, binary plants use a secondary fluid with a lower boiling point, such as isobutane or R245fa. This secondary fluid vaporizes at lower temperatures, driving a turbine to generate electricity. The process operates within a closed-loop system, minimizing environmental impact by preventing emissions and conserving geothermal fluids (DiPippo 2016).

Many components are essential to evaluate and optimize the performance of a geothermal power plant. Two main factors contribute the most in this evaluation, which are the 'thermal efficiency' and 'exergy'. Thermal efficiency would simply indicate the effectiveness of converting heat into work or energy. Yet, to better understand and evaluate the potential of these power plants, the exergy concept was introduced. Exergy evaluates the thermodynamic efficiency of a system by accounting for energy quality and system losses at each step. It identifies where the loss of energy is happening and quantifies it to implement better improvements in the power generation efficiency. For instance, Ibrahim et al. (2017) demonstrated in their study that optimizing the air-fuel ratio in the combustion chambers and enhancing the design of the turbine can significantly reduce the exergy destruction while enhancing the overall performance. Therefore, exergy analysis identifies the major losses that usually occur in a power plant, specifically in the combustion chambers, boilers, and turbines due to the irreversible processes, while leaving the space for a better improvement.

2.2.1 Efficiency and Environmental Compatibility

The efficiency of Binary Cycle Power Plants in converting thermal energy from low-enthalpy geothermal sources into electrical energy is notable. Their closed-loop system not only maximizes thermal energy extraction but also preserves geothermal reservoirs by re-injecting cooled water back into the Earth. This approach underscores the environmental compatibility of binary cycle plants, aligning with global renewable energy goals (Manente, Da Lio, and Lazzaretto 2016).

2.2.2 Expanding the Utilization of Geothermal Energy

Binary Cycle Power Plants' adaptability to various temperatures enhances their applicability across different geothermal settings. By facilitating the exploitation of previously uneconomical geothermal resources, binary cycle technology significantly broadens the potential for geothermal energy generation. This is particularly crucial for regions lacking access to high-temperature geothermal resources, offering a viable, clean energy solution that contributes to the diversification of the renewable energy mix (Nasruddin et al. 2018).

2.2.3 Operating Principles and Environmental Benefits

The operation of binary cycle power plants is grounded in the heat exchange between geothermal fluid and a secondary working fluid, guided by fundamental thermodynamic principles. The process includes heat extraction, vaporization of the secondary fluid, electricity generation by driving a turbine, and condensation and recirculation of the working fluid. These steps are crucial for the plant's efficiency and are enhanced through engineering optimizations.

Binary cycle power plants provide substantial environmental benefits, including zero emissions during operation, sustainable use of resources, low visual and land footprint, and

adaptability to lower temperature resources. These advantages make binary cycle plants an essential component of the global transition to renewable energy sources.

2.2.4 Case Studies: Quantifying the Impact of Binary Cycle Technology in Geothermal Power Generation

The adoption of binary cycle technology across the globe showcases its significant efficiency in utilizing lower temperature geothermal resources for electricity generation. This technology has seen a notable increase in total installed capacity by more than 50% in the last five years, highlighting its transformative impact on the renewable energy landscape. Binary cycle plants have proven to be effective in recovering heat from geothermal fluid in the range of 100–200°C, demonstrating their potential to significantly expand the scope of geothermal energy development worldwide (Tomarov and Shipkov 2017).

A. Chena Hot Springs Geothermal Power Plant, Alaska

The Chena Hot Springs Geothermal Power Plant is a testament to the potential of binary cycle technology in climates not typically associated with geothermal energy production. Operating efficiently with geothermal fluids at temperatures as low as 74°C (165°F), this plant has achieved operational efficiencies of 8% to 18%, a remarkable feat for geothermal power generation in colder regions. The Chena Hot Springs plant illustrates the feasibility of extending geothermal energy development to areas with lower geothermal resource temperatures, contributing significantly to diversifying the renewable energy portfolio in colder climates (Erkan et al. 2008).

B. Hatchobaru Geothermal Power Plant, Japan

Situated within Japan's volcanic terrain, the Hatchobaru Geothermal Power Plant exemplifies binary cycle technology's adaptability to challenging geological conditions. This facility's strategic use of binary cycle technology allows it to efficiently exploit geothermal fluids

at the optimal temperatures required for this innovative power generation method. Japan's reliance on Hatchobaru and similar plants reinforces the country's commitment to increasing renewable energy production, highlighting binary cycle technology's role in enhancing geothermal energy's contribution to the national energy mix, while reducing dependence on imported fossil fuels (Gunatilake 2023).

C. Tuzla Geothermal Power Plant, Turkey

Tuzla Geothermal Power Plant in Turkey utilizes binary cycle technology to convert geothermal energy into electricity with an emphasis on efficiency and sustainability. A thermodynamic analysis of this operational plant reveals energetic and exergetic performances, with energy and exergy efficiencies indicative of binary technology's effectiveness in geothermal power generation (Coskun, Oktay, and Dincer 2011).

D. Ampallas Geothermal Power Plant, West Sulawesi, Indonesia

The Ampallas Geothermal Power Plant in West Sulawesi, Indonesia, has been the subject of exergy, exergoeconomic, and exergoenvironmental optimization studies. These studies have shown that the organic Rankine cycle (ORC) system, using isopentane as the working fluid, achieves high exergy efficiency (82.12%), with a unit cost of produced energy at 8.19 US cent/kWh, demonstrating the effectiveness of binary cycle technology in maximizing both the economic and environmental benefits of geothermal energy production (Nasruddin et al. 2020).

The case studies of Chena Hot Springs, Hatchobaru, Tuzla, and Ampallas Geothermal Power Plants illustrate the global impact of binary cycle technology in the geothermal power generation sector. By achieving good efficiencies in lower temperature geothermal resources, these plants have collectively demonstrated the technology's potential to significantly expand the scope of geothermal energy development worldwide. This quantifiable success underscores

binary cycle technology's adaptability, efficiency, and critical contribution to advancing sustainable and renewable energy utilization across diverse geographical and geological settings.

2.3 Geothermal Energy Extraction: Closed Loop vs. Open Loop Systems

This section examines the technical details of both closed-loop and open-loop geothermal systems, as well as their various approaches and levels of efficiency in utilizing the heat that exists beneath the surface of the Earth. Open Loop systems make use of the natural fluids in the geothermal reservoir, whereas Closed Loop systems recycle heat without coming into direct contact with it. The discourse that follows compares these systems, highlighting the operational dynamics and technological advancements that define the current state and future trajectory of geothermal energy exploitation.

2.3.1 Closed Loops: Geothermal Closed Loop Systems with ORC Technologies

In the realm of geothermal energy extraction, U-Shaped Closed Loop systems employing Organic Rankine Cycle (ORC) technologies have emerged as a promising solution for harnessing heat from deep geothermal resources at relatively lower temperatures. These innovative systems minimize reliance on natural reservoirs, opting instead to circulate a working fluid through U-shaped boreholes to extract heat from the surrounding rocks (Nondy and Gogoi 2021).

Efficiency in these systems is paramount, with recuperative and regenerative ORC configurations demonstrating notable efficiencies around 13.2%, surpassing the approximately 12% efficiency of basic and reheated ORCs. This efficiency gain underscores the advantage of employing specific ORC configurations and working fluids, such as R245fa at an evaporation temperature of 130°C, which are optimized for the lower temperature ranges typically encountered in closed loop systems (Nondy and Gogoi 2021). Additionally, the choice of working fluids becomes crucial as temperatures vary; for example, R245fa is deemed most efficient for

temperatures below 140°C, whereas ethanol, benzene, and toluene show higher efficiencies at around 170°C, with efficiencies of 24.2%, 23.2%, and 22.9% respectively (Algieri and Šebo 2017).

2.3.2 Open Loops: Enhanced Geothermal Systems (EGS) with Supercritical ORC (sORC)

Enhanced Geothermal Systems (EGS) represent a pivotal advancement, employing the concept of artificially enhancing the permeability of deep geothermal reservoirs to access higher temperatures. The integration of Supercritical Organic Rankine Cycle (sORC) technologies is critical within EGS, attributed to their efficiency in higher temperature conditions (Liu et al. 2016).

Supercritical ORCs, utilizing high critical temperature fluids such as R152a, exhibit efficiencies up to 11.18%. The incorporation of zeotropic mixtures can further elevate thermal efficiencies by approximately 3.8%, highlighting the enhanced performance potential of sORC in EGS applications (Liu et al. 2016). Supercritical ORCs also outperform their subcritical counterparts, producing up to 20% more power with exergy efficiency values around 46% when using fluids like R1234yf, R134a, and R1234ze(E) (Liu et al. 2016). Moreover, at temperatures exceeding 150°C, supercritical cycles benefit significantly, with working fluids such as R1233zd(E), butane, isopentane, pentane, and neopentane achieving the highest efficiencies, underscoring the criticality of selecting appropriate working fluids for maximizing efficiency in open loop systems (Liu et al. 2016).

2.3.3 Optimal ORC Configurations for Geothermal Systems

The selection of an appropriate Organic Rankine Cycle (ORC) configuration is contingent upon the specific characteristics of the geothermal resource. For Closed Loop systems, particularly U-Shaped Closed Loops, recuperative and regenerative ORCs are most suited due to the relatively lower temperatures encountered. These configurations enhance

system efficiency by optimizing thermal energy utilization within the system, making them ideal for maximizing energy extraction from the geothermal source (Nondy and Gogoi 2021).

Conversely, Supercritical ORCs (sORC) are particularly apt for Open Loop systems, such as Enhanced Geothermal Systems (EGS). Their ability to operate efficiently at higher temperatures and pressures enables the extraction of maximum energy from the geothermal fluid, thus being a preferred choice for exploiting the high-temperature resources available through EGS (Liu et al. 2016).

In conclusion, the intricate balance between system configuration, working fluid selection, and operational temperatures plays a pivotal role in the efficiency and effectiveness of both Closed Loop and Open Loop geothermal energy extraction systems. The advancements in ORC technology, particularly in the development and application of recuperative, regenerative, and supercritical cycles, have significantly enhanced the potential for sustainable and efficient geothermal energy utilization.

2.3.4 Calculation of Electricity Generation in Geothermal Power Plants

Electricity generation from geothermal sources entails harnessing the thermal energy stored beneath the Earth's surface. This section outlines a refined approach to estimating the electrical power output from geothermal power plants, primarily focusing on the use of air-cooled Organic Rankine Cycle (ORC) technology, recognized for its suitability in converting low- to medium-grade heat to electricity.

The conversion efficiency of geothermal energy to electrical power significantly depends on the thermodynamic processes involved in the power plant. Recent advancements in ORC technology have opened new avenues for the efficient utilization of geothermal resources. A critical aspect of this process is the calculation of gross electrical power production, which can

be expressed as a function of the system's utilization efficiency and the exergy of the produced geothermal fluid (Altun and Kilic 2020; Briola, Gabbrielli, and Bischi 2019).

A. Gross Electric Power Production

The gross electric power (P_{gross}) generated by the system is determined by the formula:

$$P_{\text{gross}} = \eta_u \cdot B \tag{2.1}$$

where η_u represents the utilization efficiency of the power plant, and B denotes the exergy of the produced geothermal fluid. The exergy (B) is computed based on the specific enthalpy (h) and specific entropy (s) of the geothermal fluid at production ($prod$) and ambient (0) conditions:

$$B = m_{\text{prod}} \cdot \left[h_{\text{prod}} - h_0 - T_0 \cdot \left(s_{\text{prod}} - s_0\right)\right] \tag{2.2}$$

Here, m_{prod} is the mass flow rate of the produced fluid, and T_0 is the ambient temperature.

B. Pumping Power and Net Electric Power

The electrical power required for the injection pumps (P_{pump}) is calculated considering the volumetric injection rate (q_{inj}), the injection wellhead pressure (p_{inj}), and the pump efficiency (η_{pump}):

$$P_{\text{pump}} = \left(q_{inj} \cdot p_{inj}\right)/\eta_{pump} \tag{2.3}$$

The net electric power (P_{net}) generated by the system is the difference between the gross electric power and the power consumed by the pumps:

$$P_{\text{net}} = P_{\text{gross}} - P_{\text{pump}} \tag{2.4}$$

C. Practical Applications and Performance Insights

Empirical data from field tests provide a foundation for evaluating the electric power output across various operational conditions. Notably, the efficiency of air-cooled ORC technology, as applied in Fervo's geothermal power plants, has been scrutinized under differing ambient temperatures to reveal fluctuations in net power output, demonstrating a significant drop in efficiency from winter to summer months (Altun and Kilic 2020).

Furthermore, the integration of an internal heat recovery system has been proposed to enhance the plant's energy and exergy efficiencies, potentially improving performance by up to 15% (Altun and Kilic 2020). This innovation underscores the evolving landscape of geothermal power generation, where optimizing operational parameters and integrating advanced technologies are paramount for maximizing efficiency and sustainability.

2.4 Advancements in Geothermal Reservoir Simulation

Geothermal energy extraction has seen significant advancements through the adoption of sophisticated numerical modeling. These simulations, applied globally, draw upon and extend methodologies developed for oil and gas reservoirs to the thermal complexities of geothermal systems. Such cross-disciplinary applications have proven essential for understanding and harnessing geothermal energy, as exhibited by the utility of CMG-STARS software. This tool has validated its prowess across a spectrum of geothermal applications, embracing both traditional open-loop systems like Enhanced Geothermal Systems (EGS) and innovative Closed Loop Geothermal (CLG) setups.

Simulators like CMG-STARS integrate two fundamental models: one representing the subsurface reservoir and another depicting the operational well. The reservoir model simulates the multiphase fluid flow and heat transfer within the geothermal formation, while the well

model captures the dynamics of fluid extraction or injection processes (Computer Modelling Group Ltd. 2024). These models are crucial for both open-loop systems, which interact directly with the geothermal reservoir, and closed-loop systems, which circulate a working fluid in a subsurface heat exchanger.

Through CMG-STARS, conservation equations for mass and energy are deftly applied to geothermal contexts, allowing for detailed predictions of the reservoir's thermal and fluid behavior. The software's flexibility in handling different fluid properties and rock interactions makes it suitable for the challenges posed by EGS, where hydraulic stimulation is used to enhance reservoir permeability. The integration of these conservation principles within CMG-STARS demonstrates its capacity to model the intricate thermal phenomena inherent to both EGS and CLG systems.

2.4.1 Theoretical Framework in CMG-STARS

CMG-STARS employs a set of fundamental conservation equations to describe the variations within a specified zone. As noted by Computer Modelling Group Ltd. (2024), STARS applies mass and energy conservation laws tailored for water to predict reservoir behavior under varying thermal and fluid conditions. The mass conservation equation, which focuses on the water phase, is structured as follows:

$$V\frac{\partial}{\partial t}\left(\phi_f(\rho_w S_w w_i) + \phi_v A_{di}\right) = \rho_w S_w w_i + \phi\rho_w D_{wi}\Delta w_i + \rho_w q_{wk} w_i \tag{2.5}$$

In the case of a system with multiple phases, the general mass conservation equation encapsulates these complexities:

$$\begin{aligned} &V\frac{\partial}{\partial t}\left(\phi_f\left(\rho_w S_w w_i + \rho_o S_o x_i + \rho_g S_g y_i\right) + \phi_v A_{di}\right) - \rho_w S_w w_i + \rho_o S_o x_i + \rho_g S_g y_i + \\ &\phi\rho_w D_{wi}\Delta w_i + \phi\rho_o D_{oi}\Delta x_i + \phi\rho_g D_{gi}\Delta y_i + \rho_w q_{wk} w_i + \rho_o q_{ok} x_i + \rho_g q_{gk} y_i \end{aligned} \tag{2.6}$$

Here, V represents the volume of the grid block, ϕ_f is the fluid porosity, and ϕ is the absolute porosity, among other parameters.

Energy conservation is equally vital, with equations taking into account the water phase and the geological framework of the reservoir:

$$V\frac{\partial}{\partial t}\left(\phi_f(\rho_w S_w U_w + \phi_v c_s U_s + (1-\phi_v)U_r\right) - \rho_w V_w H_w + K\Delta T + \rho_w q_{wk} H_w \tag{2.7}$$

And for a system entailing multiple fluid phases as well as solid rock, the comprehensive energy conservation equation would be:

$$V\frac{\partial}{\partial t}\left(\phi_f\left(\rho_w S_w U_w + \rho_o S_o U_o + \rho_g S_g U_g\right) + \phi_v c_s U_s + (1-\phi_v)U_r\right) - \rho_w V_w H_w + \rho_o V_o H_o + \rho_g V_g H_g + K\Delta T + \rho_w q_{wk} H_w + \rho_o q_{ak} H_o + \rho_g q_{gk} H_g \tag{2.8}$$

This framework within CMG-STARS allows for the transformation of data from a Black Oil fluid model to a compositional model of STARS, addressing temperature dependencies through conversion of properties like density and viscosity.

With advancements in CMG software, there is now a sophisticated flexible wellbore modeling component that precisely simulates special well configurations. These models can capture complex interactions between the well and the reservoir, essential for understanding heat transfer and fluid dynamics.

2.4.2 CMG-Stars FlexWell

At the heart of this software is FlexWell technology, a sophisticated discretized mechanistic wellbore model developed by CMG. FlexWell is adept at modeling both fluid and heat flow within the wellbore and between the wellbore and the surrounding reservoir, making it an indispensable tool for our simulations. It shines in handling complex flow regimes, especially in long horizontal wells, by accurately managing multiple tubing streams, cross-flow, phase segregation, and transient behavior. Moreover, FlexWell's ability to model the wellbore on a

separate grid allows it to accurately represent a well's undulating trajectory through various geological layers, enhancing the realism and precision of our simulations.

FlexWell technology also excels in detailing the interaction between multiple tubings within a casing, including scenarios where the casing is shut-in or tubing is disconnected. It models fluid discharges uniquely at the tubing's toe and facilitates communication between the reservoir and casing through a defined flow term. The technology thoroughly evaluates flow regimes based on gas and fluid velocities and calculates friction pressure drops and slip between gas and liquid phases. Furthermore, it conducts a detailed analysis of radial conductive heat transfer along the full length of the tubing, factoring in the complex interplay of fluid composition, velocity, tubing and annular wall properties, and the thermal characteristics of the reservoir rock.

This deep integration of FlexWell technology across all our proposed geothermal well configurations ensures a nuanced, precise simulation of thermal and fluid dynamics, enabling us to optimize the design and operational parameters of each configuration to maximize energy extraction efficiency from Hot Dry Rock reservoirs.

2.5 Geothermal Well Configurations

The exploration and optimization of geothermal well configurations in deep Hot Dry Rock (HDR) reservoirs are pivotal in advancing geothermal energy extraction technologies. This quest has inspired a plethora of innovative approaches designed to enhance heat extraction efficiency and leverage the vast untapped energy potential within deep geothermal systems. The landscape of geothermal energy extraction is rich with diverse well configurations, each uniquely designed to optimize resource utilization in various geothermal reservoirs. There are numerous well configurations available, each of which is appropriate for the particulars of the geothermal

reservoir and the objectives of the geothermal project. Wells that are oriented vertically, horizontally, or slanted or deviated are common configurations. The configuration of the well determines the flow dynamics, the contact area with the geothermal reservoir, and ultimately the heat extraction efficiency (Zhu et al. 2023; Hoteit et al. 2023).

Among the forefront of these innovations is the development of single-well geothermal systems. A significant contribution by Huang et al. (2018) introduced a novel mining system that combines a heat pipe with an artificial reservoir saturated with CO_2. This design capitalizes on the thermosyphon effect of CO_2 fluid, stimulating stronger natural convection within the reservoir and thus, enhancing thermal power production. This method not only demonstrated superior heat extraction performance compared to conventional downhole heat exchanger (DHE) systems but also presented a promising solution to common issues such as corrosion, scaling, and water loss in HDR projects (Huang, Cao, and Jiang 2018).

Parallel to the evolution of single-well systems, the application of Enhanced Geothermal Systems (EGS) with horizontal wells has garnered significant attention. Lei et al. (2020) explored the potential of electricity generation from a three-horizontal-well EGS configuration in the Qiabuqia geothermal field, China (Figure 2.3). Their work underscored the impact of slickwater fracturing treatments on reservoir stimulation, revealing that optimized EGS scenarios could significantly enhance installed capacity and total power generation, alongside offering substantial environmental benefits by reducing greenhouse gas emissions (Lei et al. 2020).

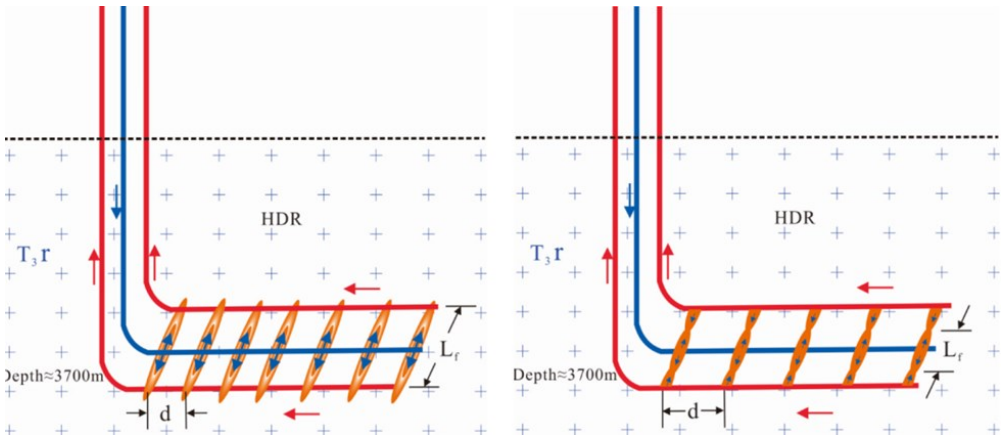

Figure 2.3: Reservoir stimulation strategy, (a) two-wing fracturing of the center well and (b) double well symmetric fracturing (Lei et al. 2020), reprinted by permission of Elsevier Books.

The advent of closed-loop systems in horizontal wells further underscores the continuous search for more efficient geothermal energy extraction methods. Cui et al. (2017) presented a groundbreaking approach that circumvents the need for complex hydro-fracturing. By recycling heat transmission fluid in a horizontal well, their method demonstrated the potential for achieving high heat mining rates, making it a viable option for low-temperature geothermal reservoirs and indicating a shift towards more sustainable and cost-effective solutions (Cui et al. 2017).

Moreover, the exploration of multilateral well configurations in EGS by Song et al. (2018) represents another leap forward. Their proposed system, which features multiple injection and production wells branching from a main wellbore, aims to optimize the interaction between the working fluid and the hot dry rock, thereby maximizing heat extraction (Figure 2.4). This innovative configuration offers a promising alternative to conventional EGS, promising greater heat extraction performance and operational flexibility (Song et al. 2018).

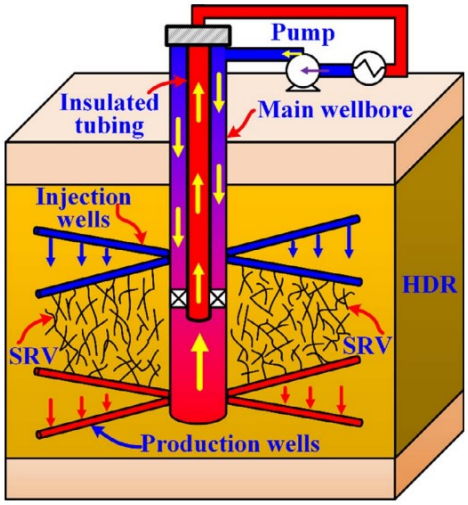

Figure 2.4: Schematic of heat extraction for multilateral-well EGS (Song et al. 2018), reprinted by permission of Elsevier Books.

Geothermal energy extraction efficiency can be greatly increased by well layouts that are optimized and customized to the unique characteristics of the geothermal reservoir (Jiang et al. 2023). For example, compared to vertical wells, horizontal wells can provide superior sweep efficiency and hence improved energy extraction because of their extended contact with the reservoir.

In the realm of Enhanced Geothermal Systems (EGS), the integration of advanced drilling and fracturing techniques has marked a significant advancement. Evaluating this field, Kazemi et al. (2019) demonstrated the effectiveness of hydraulic fractures in in the Western Canada Sedimentary Basin, balancing increased heat output against the risk of thermal breakthroughs. Furthering this exploration, Sun et al. (2017) approached the reservoir as a fractured porous medium, delving into the synergistic effects of fluid dynamics, heat transfer, and mechanical responses.

Additionally, U-Shaped Closed Loop Systems have gained attention through the work of researchers like Song et al. (2018), who explored the heat production performance of these systems (Figure 2.5).

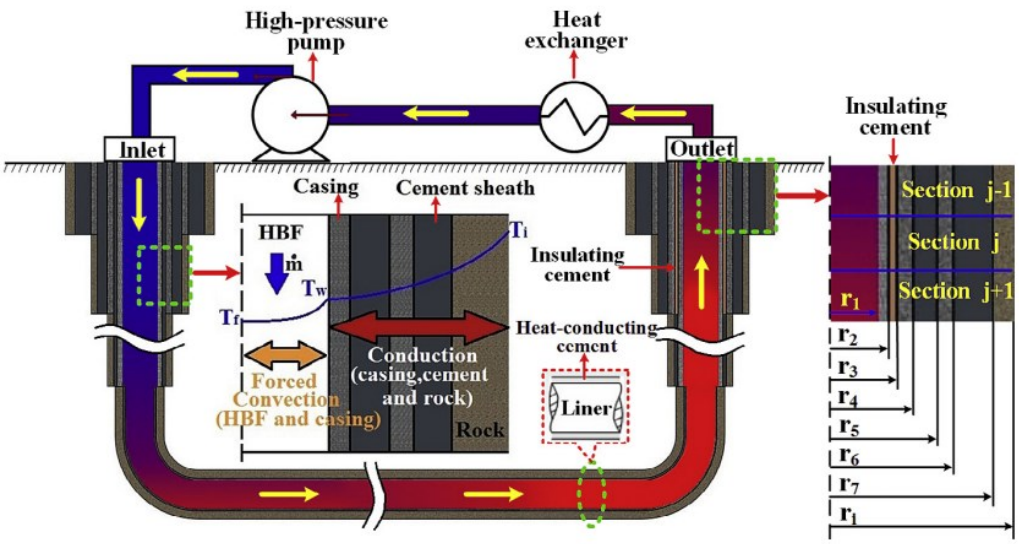

Figure 2.5: Schematic diagram of the fluid flow and thermal process for CLG (Song et al. 2018), reprinted by permission of Elsevier Books.

This innovative approach, further examined by Xiao et al. (2022) and Sun et al. (2018), utilizes U-shaped boreholes with closed-loop systems and different working fluids, presenting a viable solution to common challenges in EGS, such as water loss and thermal short-circuiting.

Moreover, Pipe-in-Pipe Closed Loop Systems have been brought into the spotlight by Bu, Jiang, and Li (Bu, Jiang, and Li 2019), who focused on their efficiency in heat exchange. This configuration, a form of single well closed loop, has been further explored for its adaptability and effectiveness in various geothermal settings, particularly when integrated with hydraulic fracturing techniques (Figure 2.6).

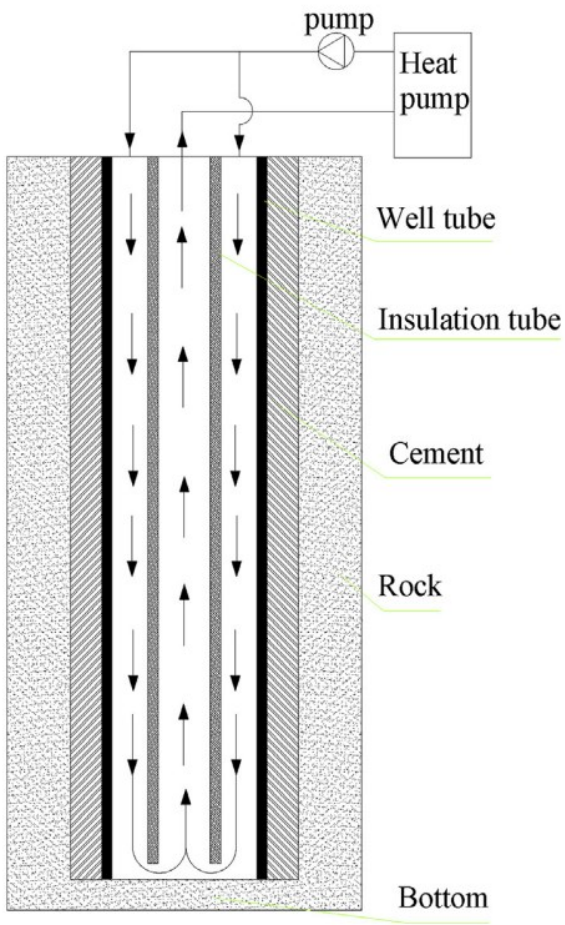

Figure 2.6: Structure diagram of Single Well Geothermal Heating (Bu, Jiang, and Li 2019), reprinted by permission of Elsevier Books.

Transitioning to Coaxial Closed-Loop Geothermal Systems, Zhang et al. (2019) have conducted comprehensive studies to analyze the performance and feasibility of different working fluids for coaxial designs. Their work contributes significantly to understanding the practicality of these systems in geothermal energy extraction. In addition, Wang et al. (2020) provides a comparative analysis of various coaxial closed-loop geothermal systems, offering insights into their heat extraction performance and potential applications.

Lastly, the potential of Horizontal Pipe-in-Pipe Open Loop Systems has been highlighted in other studies by Wang et al. (2020). These systems, particularly effective in lower temperature

reservoirs, represent a significant advancement in geothermal technology, offering new avenues for energy extraction.

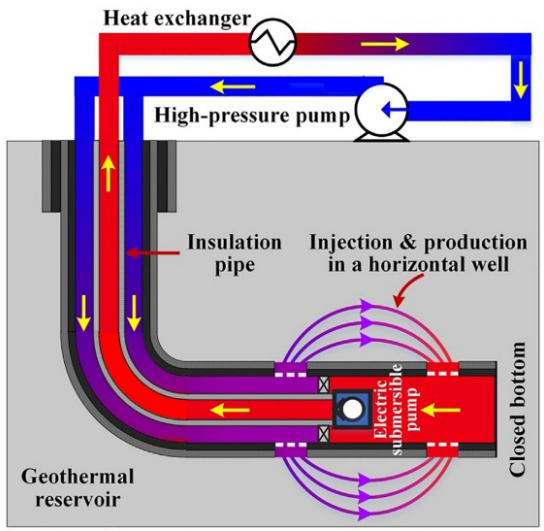

Figure 2.7: Schematic showing heat extraction in horizontal-well open-loop geothermal system (Wang et al. 2020), reprinted by permission of Elsevier Books.

Each of these configurations, with their distinct advantages and challenges, underscores the importance of tailoring geothermal energy extraction methods to specific reservoir characteristics, environmental considerations, and technological capabilities. The ongoing research in these areas continues to deepen the understanding of optimal methods for geothermal energy extraction, paving the way for more efficient and sustainable energy solutions.

These studies collectively contribute to the evolving landscape of geothermal energy extraction, each offering novel insights and methodologies tailored to overcome the unique challenges presented by deep HDR reservoirs. However, despite these advancements, a significant gap remains in the exploration of geothermal well configurations at extreme depths, particularly those reaching up to 20,000 ft.

Our research endeavors to bridge this gap by modeling various well configurations, including U-Shaped, V-Shaped, EGS, and Pipe-in-Pipe systems, in the context of deep geothermal HDR

reservoirs. By venturing into depths previously unexplored, our study not only extends the current boundaries of geothermal research but also presents a critical examination of the feasibility, efficiency, and potential of these configurations in harnessing the Earth's deep thermal energy. This pioneering effort is poised to contribute significantly to the field, offering valuable insights and opening new avenues for sustainable energy extraction from one of the planet's most abundant yet underutilized resources.

CHAPTER 3
METHODOLOGY

3.1 Reservoir Simulation Approach

The modeling and prediction of geothermal reservoir behavior under various situations is made possible by reservoir simulation, which is a crucial tool in the geothermal energy industry. Understanding the dynamics of the granitic formations in the Wattenberg field in the DJ Basin, Colorado, is the main goal of this research, especially in relation to the processes involved in the extraction of geothermal energy.

The methodology's basis is derived from numerical modeling. The governing equations for mass, momentum, and energy conservation can be solved at each grid block by discretizing the reservoir into a grid system. A thorough depiction of the physical and thermal characteristics of the reservoir, as well as the interactions between the geothermal fluid, fractures, and the rock matrix, are made possible by this granular method.

Several scenarios that depict various operational settings are simulated in order to have a thorough knowledge. This includes adjustments to well layouts, temperature changes in the injected fluid, and variations in injection and output rates. Every scenario is intended to answer a particular research topic on maximizing the extraction of geothermal energy.

This research employs a comprehensive reservoir simulation approach to assess the potential of geothermal energy extraction in the specified study area. The development of our simulation models is guided by the objective to enhance the accuracy and reliability of geothermal reservoir predictions under various operational scenarios. Central to our methodology is the incorporation of empirical data and theoretical insights gleaned from a

carefully curated set of literature, ensuring that our simulations are grounded in both proven models and cutting-edge research.

3.1.1 Defining Parameters and Simulation Setup

The foundation of the reservoir simulation strategy for the Wattenberg field in the DJ Basin is rooted in a thorough comprehension of the region's distinct geological and geothermal features. The precise definition of parameters and setup are critical to the simulation's accuracy and dependability.

The basis of this simulation is the characteristics of rocks and fluids, specifically, the deepest targeted formation at 6100 m depth. The Wattenberg field's granitic rocks have unique physical characteristics, including permeability, porosity, and thermal conductivity. It's also critical to determine the specific heat and viscosity of the geothermal fluid—typically brine in these conditions—given the high temperatures predicted. These characteristics are crucial in defining how the fluid moves through the reservoir and how well it can transfer heat.

Our geothermal models will focus on the impact of the deepest targeted Wattenberg formation on the geothermal output. The shallower formations, comprising sedimentary rocks have the same characteristics as the deeper ones, with low porosity and permeability. For this purpose, all production wells have been insulated to evaluate the direct impact of these deep formations while minimizing the influence of the shallower ones.

We divide the reservoir into a grid system in order to capture its complex dynamics. Every grid block denotes a distinct reservoir volume. This grid's granularity finds a compromise between resolution and computing efficiency. Highly relevant areas, particularly those close to the well regions, will be depicted using a more refined grid.

Finally, different operational situations are used to see how they affect the extraction of geothermal energy. This includes tweaking well layouts, changing the temperature of the injected fluid, and modulating fluid injection and production rates. Every scenario provides information about how the reservoir might react to various geothermal operations. This meticulous methodology guarantees the simulation outcomes are precise and significant, providing significant perspectives on the extraction of geothermal energy in the DJ Basin.

3.1.2 Reservoir Simulation Model

The assessment and enhancement of energy output from the proposed well configurations in Geothermal (Hot Dry Rock) are anchored on a systematic and comprehensive approach.

Initially, a thorough geological and geophysical characterization of the reservoir is carried out to comprehend its inherent properties like temperature, pressure, permeability, porosity, and thermal properties. This foundational step is critical for the subsequent model development.

Following this, reservoir simulation models are meticulously crafted using the CMG STARS software, which is capable of handling the complex thermal, hydraulic, and mechanical behaviors of geothermal systems. The model incorporates the essential reservoir properties, rock-fluid interactions, and well configurations to evaluate the efficiency and sustainability of the geothermal energy extraction process. This stage is crucial for accurately representing the geothermal reservoir and the proposed well configurations, laying the groundwork for precise simulation exercises.

The identification of key parameters and assumptions forms the next step. This includes delineating initial and boundary conditions as well as material properties, which are indispensable for this simulation.

The execution phase encompasses the running of reservoir simulations to assess the performance of the proposed well configurations in extracting geothermal energy under an array of reservoir conditions. The findings from this phase are pivotal for performance analysis.

Performance analysis entails a thorough examination of simulation results to gauge the energy output, efficiency, and operational feasibility of each well configuration. This stage is instrumental in understanding the merits and demerits of each configuration.

3.1.3 Simulation Setup and Parameter Definition

Our simulation model is meticulously configured to reflect the complex interplay of geological, thermal, and operational parameters critical to the evaluation of extraction of geothermal energy. The definition and calibration of these parameters are informed by the comprehensive review of literature outlined above, ensuring that our model reflects the current state of knowledge in the field.

- Rock and Fluid Characteristics: Parameters related to the thermal properties of rock formations and geothermal fluids are derived from Frash et al. (2024), encompassing thermal conductivity, specific heat capacity, and injection temperatures. These parameters are crucial for modeling the heat transfer mechanisms within the reservoir.
- Well Integrity and Material Properties: Drawing on Won et al. (2016), our model incorporates detailed specifications of casing materials, including their thermal and mechanical properties. This is essential for assessing the stability of geothermal wells and their performance over time.
- System Performance and Validation: Leveraging the validated EGS model from Norbeck and Latimer (2023), our simulation aims to replicate and extend their findings, applying their insights to our specific geothermal context. Additionally, the modeling approach use

in this work was compared against an independently built model (Amini, personal communication) and validated for the U-shaped geothermal well configuration, aiming to explore alternative configurations and their potential to enhance geothermal energy extraction.

3.1.4 Performance Analysis and Model Validation

The execution of our reservoir simulations is designed to assess the performance of proposed well configurations and operational strategies. Through the application of the aforementioned parameters and models, our research endeavors to provide a comprehensive analysis of energy output, efficiency, and operational feasibility. This iterative process of simulation and analysis is pivotal in refining our understanding of geothermal reservoir dynamics and the optimization of extraction processes.

3.2 Description of Geothermal Well Configurations

The description of Geothermal Well Configurations represents the most critical section of this study, delineating each well configuration adopted, including both closed and open loop systems. These configurations range from Closed-Loop Geothermal (CLG) setups, such as Pipe-in-Pipe, U-Shaped, V-Shaped, and Inclined V-Shaped designs. In contrast, the EGS category comprises the standard EGS and an Inclined EGS configuration. This section aims to provide a comprehensive overview of the various geothermal configurations employed in our study, highlighting their distinctive features and roles in enhancing geothermal energy extraction efficiency.

3.2.1 Reservoir Grid and Properties

Initially, the simulation employs a Cartesian grid structured along the I, J, and K directions, comprising 141, 59, and 86 blocks, respectively. Each block is uniquely identified by a User Block Address (UBA). To enhance model convergence and accurately represent thermal dynamics, the grid size is selectively refined around the wellbore locations, enabling a precise depiction of temperature variations within the surrounding rock matrix (Figure 3.1).

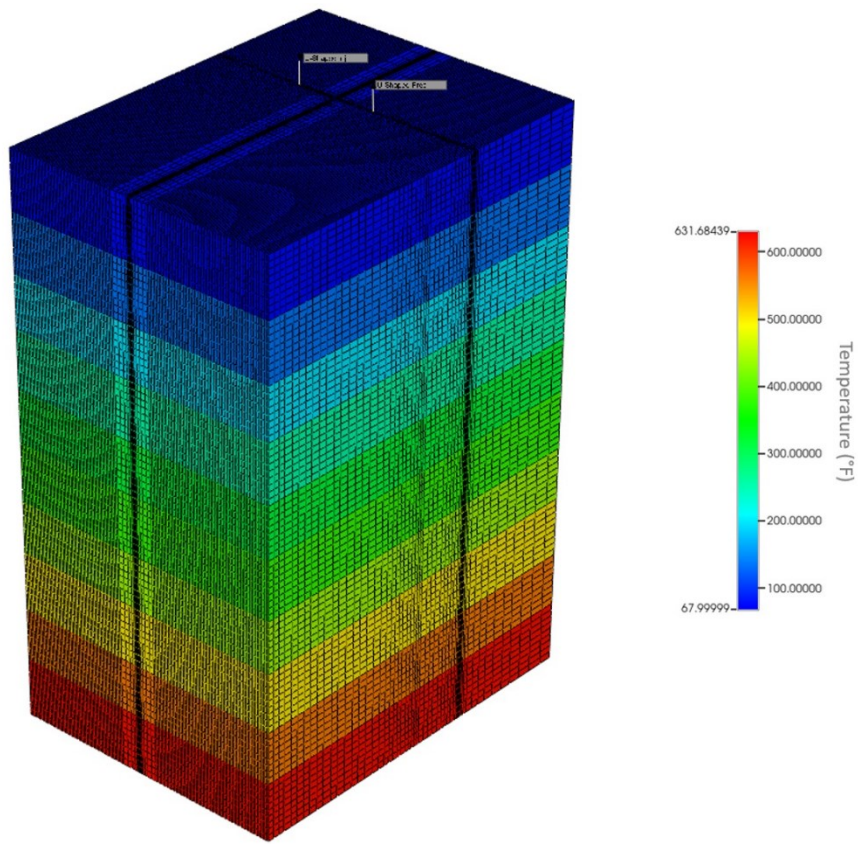

Figure 3.1: Geothermal Reservoir Model Grid System

3.2.2 Definition of Reservoir Parameters

For the closed-loop configurations under study, interactions between the injected fluid and the rock matrix are not modeled, leading to the specification of reservoir properties as

constants. Porosity and permeability are set at 1% and 1e-6 millidarcies (md), respectively, with complete water saturation (100%) assumed throughout the reservoir. Although the model configurations lack open perforations, defining the reservoir pressure is essential for the simulation. A standard hydrostatic gradient of 10 kPa/m is employed to establish the pressure distribution, complemented by an assumed rock compressibility of 4.35e-7 1/kPa. These properties, critical for initializing the numerical simulation, are summarized in Table 3.1.

Table 3.1: Input Parameters for the Reservoir and Grid Section

Parameter	**Value**
Porosity	1%
Permeability	1e-6 md
Water Saturation	100%
Hydrostatic Gradient	10 kPa/m
Rock Compressibility	4.35e-7 kPa^{-1}
Formation Thermal Conductivity	252,720 J/(m·day·°C)
Formation Volume Heat Capacity	2,667,500 J/(m^3·°C)
Working Fluid Volume Capacity	53,500 J/(m·day·°C)
Temperature Gradient	50 °C/km

3.2.3 Thermal Properties

The accurate definition of thermal properties is crucial, as they significantly impact the simulation's outcomes. Based on Frash et al. (2024), the best-case scenario utilizes a formation volumetric heat capacity of 2,667,500 J/(m^3·°C), a formation thermal conductivity of 252,720 J/(m·day·°C), and a working fluid volumetric heat capacity of 53,500 J/(m·day·°C). Given the bottom hole temperature of 300 °C, a temperature gradient of 50 °C/km is applied to model the thermal distribution within the reservoir accurately. This approach allows for an informed

analysis of the system's thermal behavior, albeit with an acknowledgment of the atypical temperature gradient.

3.2.4 Components Configuration

The simulation employs freshwater as the working fluid, integrated into the CMG simulation software by selecting H_2O with its default settings. The liquid phase's properties, including densities and viscosities, are crucial for accurate modeling. Specifically, viscosity values of AVISC at 0.0047352 cp and BVISC at 1515.7°C align with recommendations from the STARS manual for the specified temperature conditions (Computer Modelling Group Ltd, 2009). The simulation framework also requires the definition of reference and surface conditions — atmospheric pressure (101 kPa) at the surface with a temperature of 20°C, and a reference pressure calculated based on the geothermal gradient at the bottom hole depth of 6100m, amounting to 61,000 kPa, with a corresponding temperature of 300°C (Table 3.2).

Table 3.2: Component Properties for Simulation

Parameter	Value
AVISC	0.0047352 cp
BVISC	1515.7 °C
Reference Pressure	61,000 kPa
Reference Temperature	300 °C
Surface Pressure	101 kPa
Surface Temperature	20 °C

3.2.5 Rock-Fluid Interactions

Given the scope of this study, which includes Enhanced Geothermal Systems (EGS) and accounts for Hot Dry Rock (HDR) formations, it is acknowledged that direct interaction between

the injected fluid and the rock is limited. This simplification is based on the primary focus being on thermal extraction efficiency rather than comprehensive rock-fluid interaction dynamics. However, the initialization of the simulation necessitates the definition of relative permeability tables, thereby providing a basic framework for the software to accurately simulate fluid movement within the reservoir. A straightforward approach is adopted, with relative permeability values inputted as shown in Table 3.3.

Table 3.3: Relative Permeability Table

Sw	krw	krow
0	0	1
1	1	0

3.2.6 Initial Conditions

The establishment of initial conditions is critical for simulating phase equilibrium within the porous media of the reservoir, despite the minimized emphasis on fluid-rock interactions. The model presumes complete water saturation, with the reservoir characterized by a reference pressure of 61,000 kPa and a depth of 6100m to reflect realistic subterranean conditions consistent with the targeted geothermal systems (Table 3.4).

Table 3.4: Parameters for Initial Conditions

Parameter	Value
Reference Pressure	61,000 kPa
Reference Depth	6100 m

Numerical Approach: In alignment with the CMG-STARS user guide (Computer Modelling Group Ltd. 2024), the numerical configuration of our models maintains default settings to ensure consistency across simulations.

Adjustments to numerical values will be considered only to address and rectify convergence issues, should they arise during the simulation process, thus safeguarding the stability and reliability of our modeling outcomes.

Geomechanical Interactions: Given the focus on thermal energy extraction and fluid dynamics within the wells, geomechanical interactions within the reservoir rock are not explicitly modeled in this study. This decision is based on the closed-loop and EGS configurations' operational premise, where direct fluid-rock interactions are minimal or non-existent.

3.2.7 Wells Configuration and Fluid Dynamics

This section delves into the detailed configuration of wells within each model, highlighting the necessity of distinct well types and their respective operational parameters. The model's complexity is underscored by various well configurations, emphasizing the critical role of fluid dynamics in the energy extraction process.

A. Well Creation for the U-Shaped Model

The U-Shaped Closed Loop System is a novel approach designed for the efficient extraction of geothermal energy from Hot Dry Rock (HDR) reservoirs. By employing a single pipe configured in a U-shape, this model promotes a continuous flow of heat transfer fluid through the reservoir, aiming to simplify construction and reduce costs while enhancing heat extraction (Figure 3.2).

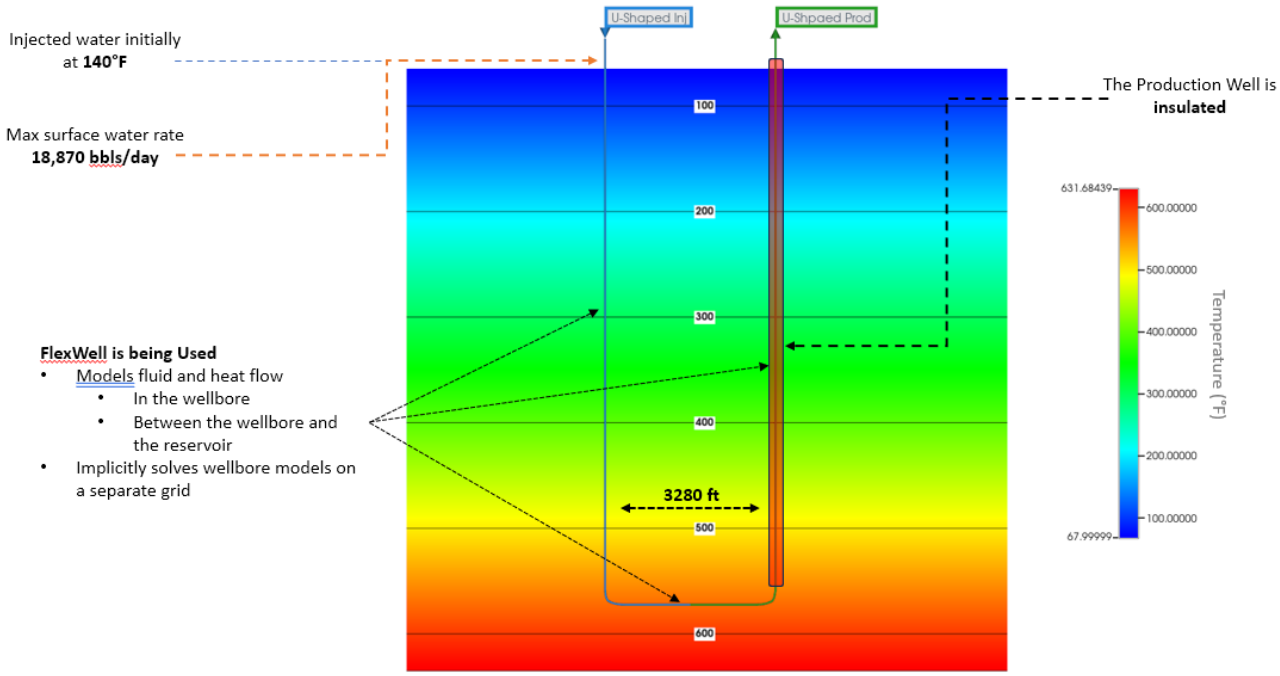

Figure 3.2: U-Shaped Closed Loop Well Model Description

The U-Shaped Well configuration, while seemingly a single entity, is conceptually bifurcated into two distinct sections - the injection and production wells, interconnected at a depth of 6,100 meters with an additional 1,000 meters horizontal section to facilitate fluid movement.

Injection Well Configuration:

The "Injector" serves as the entry point for the working fluid into the geothermal system. It is meticulously designed to align with refined grid blocks, ensuring precision in modeling fluid dynamics. The trajectory extends from UBA (48, 17, 1) at the surface to UBA (48, 17, 77) and proceeds to UBA (67, 17, 77) marking the halfway of the horizontal section. The "Injector" is categorized under the "ID & Type" tab as an injection well, with a specified maximum surface

water rate (STW) of 3000 m³/day (Table 3.5). The radius of the well is standardized at 0.14 m to maintain consistency across the model (Table 3.8).

Table 3.5: Operational Parameters for 'Injector' Well

Constraint	Parameter	Value
OPERATE	STW surface water rate	MAX 3000 m³/day

Production Well Configuration:

Following the setup of the "Injector" well, the "Producer" is established using a similar methodology. Its trajectory is aligned from UBA (87, 17, 1) to UBA (87, 17, 76) and finally to UBA (67, 17, 77). It operates under a maximum surface water rate of 3000 m³/day (Table 3.6), mirroring the "Injector" to ensure balanced fluid flow within the system. The "Producer" well also features a radius of 0.14 m, aligning with the injector for uniformity (Table 3.8).

Table 3.6: Operational Parameters for 'Producer' Well

Constraint	Parameter	Value
OPERATE	STW surface water rate	MAX 3000 m³/day

Fluid Dynamics:

The working fluid, freshwater, is characterized by a temperature of 60°C, steam quality of 0, and pressure of 6875 kPa, tailored to match the operational conditions (Table 3.7).

Table 3.7: Well Radius and Fluid Injection Parameters

Parameter	Injection Well Radius	Production Well Radius	Temperature	Steam Quality	Pressure
Value	0.14 m	0.14 m	60 °C	0	6875 kPa

FlexWell Configuration for the U-Shaped Model

This pivotal section outlines the FlexWell configuration process, integral for simulating the U-shaped model's thermal and fluid mechanics. Upon defining well trajectories and operational parameters, FlexWell integration commences with the selection of the "Injector" well, adopting a straightforward approach for casing properties and diameter definitions. A similar procedure is employed for the "Producer" well, ensuring both sections are accurately modeled within the FlexWell framework.

Table 3.8: Diameter Specifications for FlexWells

Well	Wall Inner Diameter (ID)	Wall Outer Diameter (OD)
Injector	0.14 m	0.152 m
Producer	0.14 m	0.152 m

The completion of parameter input across the FlexWell model marks the readiness of the simulation to accurately depict the operational dynamics and thermal behavior of the U-Shaped geothermal well configuration, setting the stage for an in-depth performance analysis.

B. V-Shaped Closed-Loop System Model Description

The V-Shaped Closed-Loop System, also referred to as the U-Shaped Extended Horizontally (EH) model, represents an evolution in geothermal well design that aims to fully capitalize on the high-temperature zones of Hot Dry Rock (HDR) reservoirs by extending horizontally at significant depths (Figure 3.3).

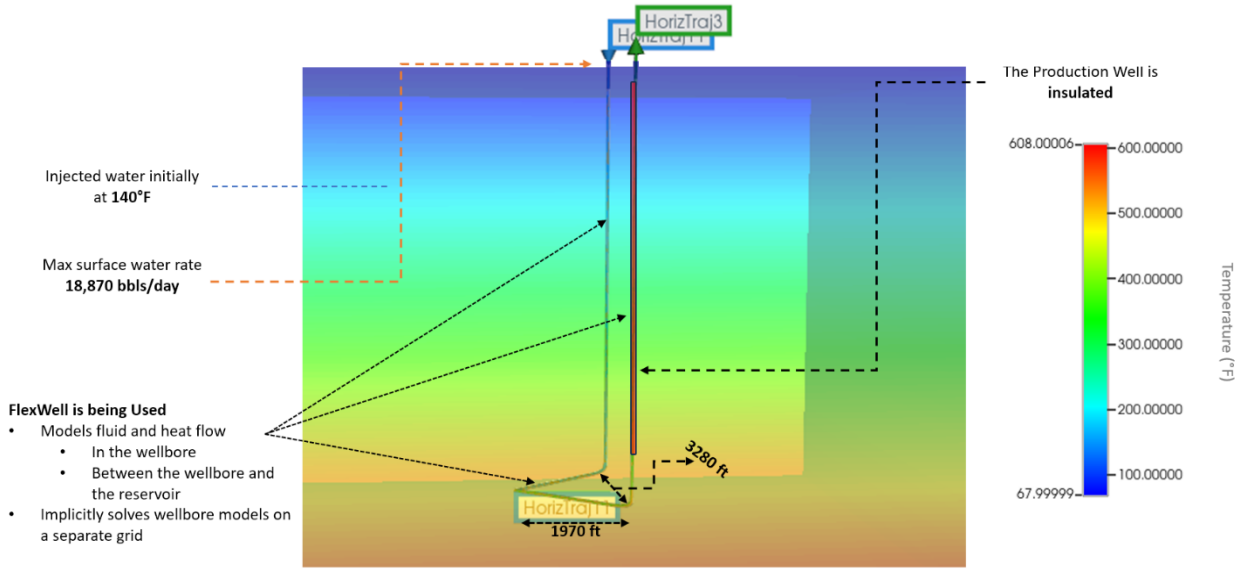

Figure 3.3: V-Shaped Closed Loop Well Model Description

Geometric Configuration

In the V-Shaped model, the wells descend vertically to a depth of 6100 meters, where temperatures are substantially higher, thus providing an advantageous thermal environment for energy extraction. Upon reaching this depth, the wells extend 600 meters laterally within the reservoir. This horizontal extension is parallel to the bottom of the reservoir, creating a broadened area of contact between the heat transfer fluid and the geothermally heated rock, allowing for an increased rate of heat absorption.

Well Configurations and Operational Parameters

The horizontal wells in this configuration are designed to exploit the consistent and elevated temperatures available at these depths. Similar to the U-Shaped version, the injection parameters involve a maximum surface water rate of 3000 m^3/day, with water being injected at a temperature of 60°C.

The production well in this model is also insulated to preserve the thermal energy obtained from the deep geothermal reservoir, minimizing any heat losses during the ascent of the fluid to the surface. This design choice underscores the importance of insulation in maintaining the efficiency of the heat exchange process, particularly in horizontally extended systems where the fluid travels a greater distance in the reservoir's high-temperature regions.

C. Inclined V-Shaped Closed-Loop System Model Description

The Inclined V-Shaped model is a sophisticated iteration of geothermal well configurations, devised to enhance the efficacy of heat extraction from Hot Dry Rock (HDR) reservoirs through strategic well placement and advanced simulation techniques (Figure 3.4).

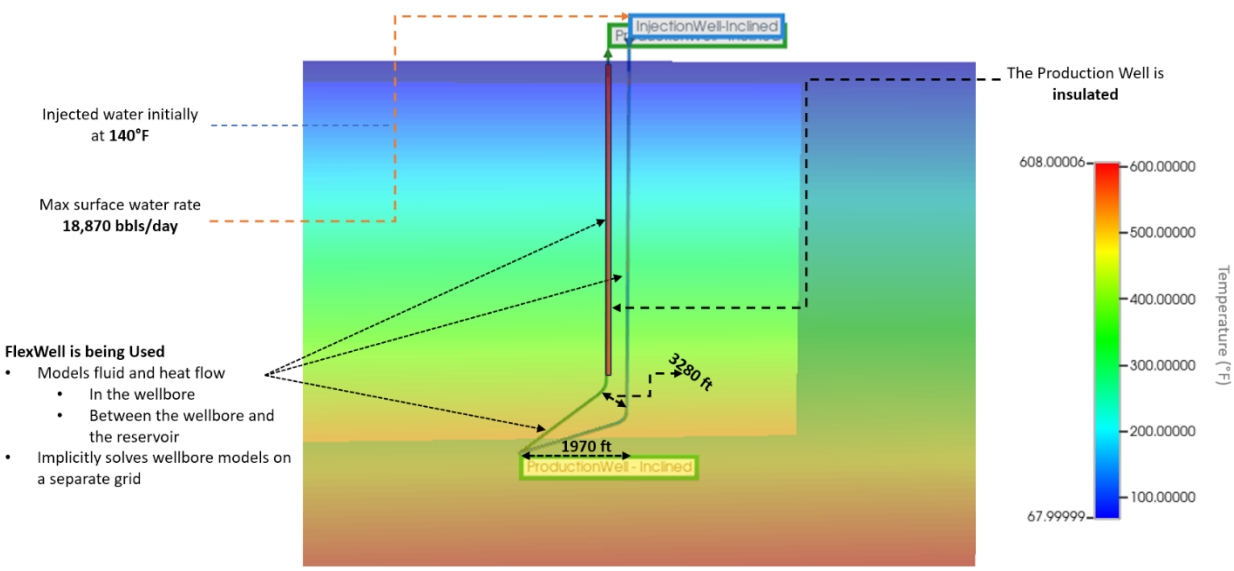

Figure 3.4: Inclined V-Shaped Closed Loop Well Model Description Geometric Configuration

The Inc V-Shaped model is characterized by its unique geometry that includes two wells spaced 1000 meters apart on the surface. Each well descends vertically before diverging into an inclined section that extends 600 meters laterally and reaches a depth of 860 meters, culminating at a bottom hole location at 6100 meters with a reservoir temperature of 300°C.

This geometric design is carefully crafted to maximize the thermal contact surface area between the heat transfer fluid and the surrounding reservoir rock, thereby increasing the system's overall heat recovery capacity.

Well Configurations and Operational Parameters

Within this system and similarly to the U-Shaped Model, the injection well introduces water at a temperature of 60°C. The maximum surface water rate is capped at 3000 m^3/day. This elevated flow rate is integral to the system's design, ensuring a substantial volume of fluid is heated by the geothermal reservoir, thus optimizing energy production.

The production well is also insulated to minimize thermal losses during fluid transport to the surface. Insulation is a critical component of this model, as it retains the heat within the produced fluid, which is crucial for assessing the effectiveness of thermal insulation in contrast to non-insulated systems.

D. Well Creation for the PIP Model:

The Pipe-in-Pipe (PIP) Closed Loop System introduces an advanced method for maximizing thermal efficiency in extracting geothermal energy from HDR reservoirs. It features a distinctive dual-pipe configuration, enhancing the heat exchange between the heat transfer fluid and the reservoir rock (Figure 3.5).

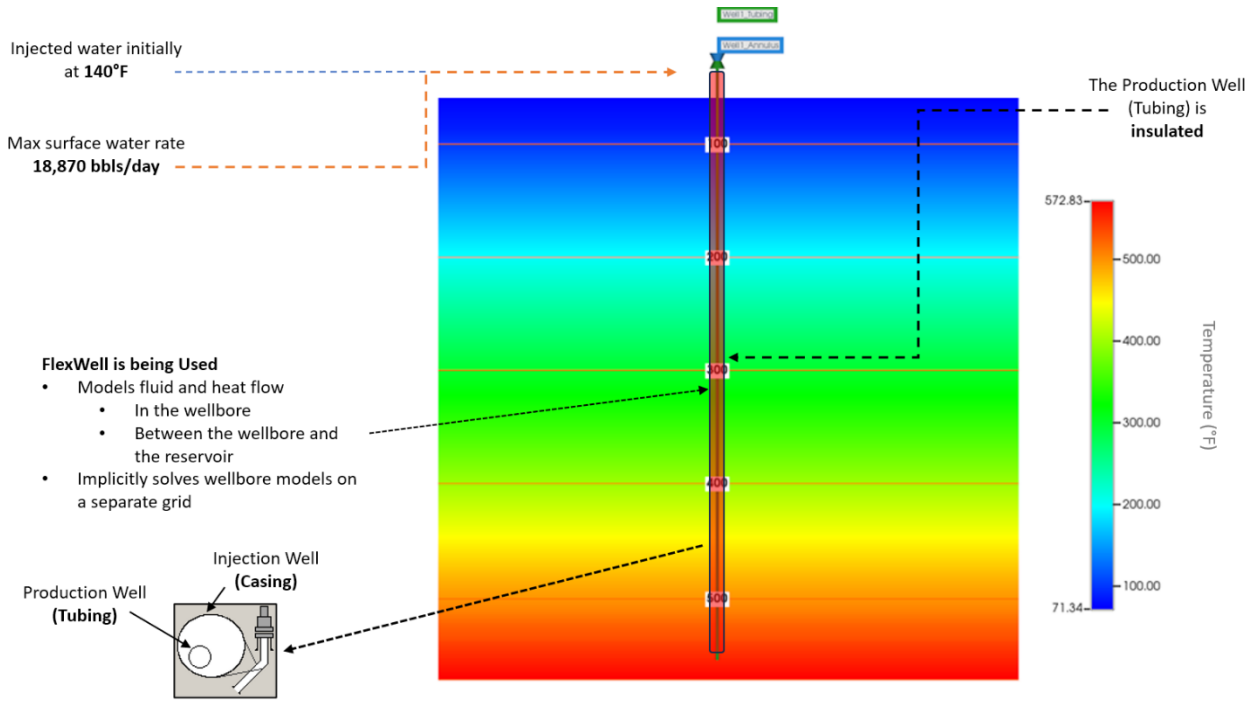

Figure 3.5: Pipe-in-Pipe Closed Loop Well Model Description

For the PIP configuration, two primary wells are constructed without the need for an additional layering well. This setup includes:

1. "Casing" Well: Serves as the outer section of the PIP configuration, designed to facilitate thermal convection and enhance system efficiency. The well's trajectory is meticulously aligned with refined grid blocks for accurate modeling. Notably, the "Casing" is classified as an injection well, with specifications including a maximum surface water rate of 3000 m^3/day (Table 3.9). The well's radius is set at 0.14 m (Table 3.11).
2. "Tubing" Well: Mirrors the "Casing" well's operational parameters, functioning as a producer with the same fluid flow rate and a minimum bottom hole pressure (BHP) of 5900 kPa (Table 3.9). This design choice reflects averaged parameters from leading case

studies, optimizing the model for realistic simulation scenarios. The injector well's radius is defined at 0.076 m (Table 3.11).

Fluid Dynamics: The injected fluid, freshwater, is characterized by specific properties including a temperature of 60°C, a steam quality of 0, and a pressure of 6875 kPa, ensuring compatibility with the geothermal reservoir conditions and the system's operational demands (Table 3.10).

The following tables summarize the operational parameters and fluid characteristics within the PIP model:

Table 3.9: Operational Parameters for 'Casing' and 'Tubing' Wells

Constraint	**Parameter**	**"Casing" Well Value**	**"Tubing" Well Value**
OPERATE	STW surface water rate	MAX 3000 m^3/day	MAX 3000 m^3/day
OPERATE	BHP bottom hole pressure	-	MIN 5900 kPa

Table 3.10: Fluid Injection Parameters

Parameter	**Value**
Temperature	60 °C
Steam Quality	0
Pressure	6875 kPa

These configurations and parameters lay the groundwork for a comprehensive simulation of the PIP model, aiming to accurately assess the thermal efficiency and operational viability of this innovative geothermal system design.

FlexWell Configuration and Implementation

This section delineates the methodology employed to simulate the Pipe-in-Pipe (PIP) configuration using the FlexWell system, a crucial component in modeling the dynamic interactions within this complex geothermal well structure.

Creation of Perforations for FlexWell

Initially, the perforation intervals for the constructed wells are meticulously defined, with locations spanning from UBA (67,28,1) to (67,28,77). Specifically:

- The "Casing" well is configured with all perforation intervals sealed, except for the final interval at K = 77, which remains open to facilitate fluid movement.
- The " Tubing" well's last perforation interval, also at I = 76, is uniquely left open, ensuring unimpeded fluid dynamics within the intended path. This configuration elucidates how the "Casing" and "Tubing" serve as the structural periphery of the conceptual annular section, with the concentric tubing embodying the central tubular component.

Following the establishment of perforations, the FlexWell feature is activated to integrate the wells into a cohesive model. The initial step involves selecting the "Casing" well, adopting default casing properties and setting a consistent diameter.

Table 3.11: Perforation-Related Well Radius Specifications

Well	**Radius (m)**
Casing	0.14
Tubing	0.076

Subsequent steps incorporate the "Tubing" well through the "Add Tubing" option, aligning insulation properties with standard wall attributes. The "Tubing" well is similarly added,

necessitating the specification of isolation materials to achieve the intended thermal insulation efficiency.

Table 3.12: Casing and Insulation Parameters for Pipe Components

Property	**Value (J/(m³·°C) or J/(m·day·°C))**
Wall Heat Capacity	3.63e+06
Wall Heat Conductivity	3.888e+06
Insulation Heat Capacity	3,283
Insulation Heat Conductivity	16,800

The final modeling stage involves specifying well diameters to account for inner diameters, pipe thickness, tubing insulation, and cementation (Table 3.13).

Table 3.13: Well Wall Diameter Specifications

Well	**Inner Diameter (ID) (m)**	**Outer Diameter (OD) (m)**
Tubing	0.076	0.089
Tubing Insulation	0.089	0.102
Casing	0.14	0.152
Cement (Annulus)	0.152	0.178

Upon defining all necessary parameters within the FlexWell model, the simulation is fully equipped to represent the thermal and fluid dynamics of the Pipe-in-Pipe geothermal system configuration, paving the way for an in-depth analysis of its performance characteristics.

E. Well Creation for EGS Model:

The Enhanced Geothermal System (EGS) model is a forward-thinking approach in the field of geothermal energy, designed to amplify heat extraction by introducing engineered hydraulic fractures to increase reservoir permeability and create extensive pathways for heat transfer (Figure 3.6).

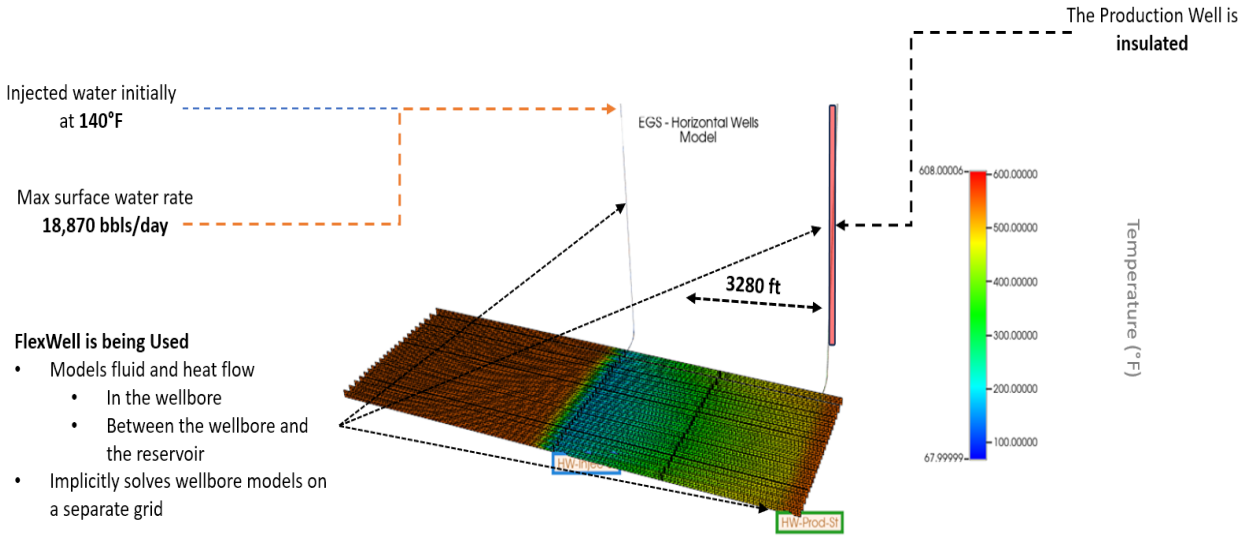

Figure 3.6: EGS Well Model Description

The EGS configuration employs a similar approach to well construction as seen in the U-Shaped and PIP models but is uniquely tailored for the Enhanced Geothermal System to optimize geothermal energy extraction. This configuration includes:

- Injector Well: Functions as the entry point for the working fluid into the geothermal system, designed to inject water at a specified rate and temperature to absorb heat from the surrounding rock. Its trajectory is meticulously planned within the reservoir grid, extending from UBA (47, 12, 1) at the surface to UBA (47, 12, 77) at the heel, and finally to UBA (47, 36, 77) to cover the horizontal section. The trajectory ensures accurate representation within the refined grid blocks, enhancing the simulation's fidelity. The injector well is specified with a maximum surface water rate of 3000 m^3/day and a radius of 0.14 m.
- Producer Well: The counterpart to the injector, this well is responsible for extracting the heated fluid from the geothermal reservoir. It follows a parallel trajectory to the injector

well, designed to efficiently capture and bring the heated fluid to the surface for energy production, extending from UBA (87, 12, 1) at the surface to UBA (87, 12, 77) at the heel, and finally to UBA (87, 36, 77). Similar operational parameters are applied to the producer well, with a focus on maximizing the retrieval of heated fluid.

Fluid Dynamics:

Freshwater serves as the working fluid, characterized by a temperature of 60°C, steam quality of 0, and a pressure of 6875 kPa. These properties are critical for ensuring the fluid's effective heat absorption and compatibility with the EGS operational demands.

FlexWell Configuration for EGS:

The FlexWell system is pivotal for accurately modeling the EGS configuration, facilitating the simulation of complex fluid and thermal interactions within the geothermal reservoir. Initial steps involve defining the perforation intervals for both the injector and producer wells, ensuring proper fluid flow and heat exchange:

- Injector Well: All perforation intervals are configured along its trajectory, with specifications aligning with the grid blocks to ensure precise modeling of fluid injection.
- Producer Well: Similarly, the producer well's perforations are strategically placed to optimize the extraction of heated fluid, mirroring the injector well's specifications for consistency.

The FlexWell feature integrates these components into a cohesive simulation model, capturing the dynamic behavior of the EGS system. Well diameters are calculated based on the specified radii, ensuring accurate representation of the well structures within the simulation.

Operational Parameters:

The operational parameters for the EGS model, including fluid injection conditions and well specifications, are summarized in tables similar to those provided for the PIP and U-Shaped configurations. These parameters lay the foundation for a comprehensive simulation of the EGS model, aiming to assess its thermal efficiency and operational viability in a high-temperature geothermal context.

F. Enhanced Geothermal System (EGS) Inclined Model Description

The Inclined version of the Enhanced Geothermal Open Loop model is a strategic adaptation within enhanced geothermal systems, employing a distinctive inclined configuration. This approach is not primarily driven by the aim to intensify heat extraction efficiency; instead, it emerges as a pragmatic solution to overcome technical drilling challenges encountered in accessing deep-seated geothermal resources.

The inclined design facilitates drilling operations when vertical drilling is not feasible or poses significant risks, such as in areas with complex geological structures or where straight drilling paths are obstructed.

Geometric Configuration

In the EGS - Inc model, the wells penetrate vertically down to a true vertical depth of 6100 meters, situating them within a high-temperature zone that promises an abundance of geothermal energy.

Post reaching this depth, the wells extend horizontally for 1000 meters. This horizontal expanse, stationed at the bottom of the geothermal gradient, is designed to traverse through the hottest parts of the HDR formation, thereby ensuring maximum thermal interaction and energy transfer (Figure 3.7).

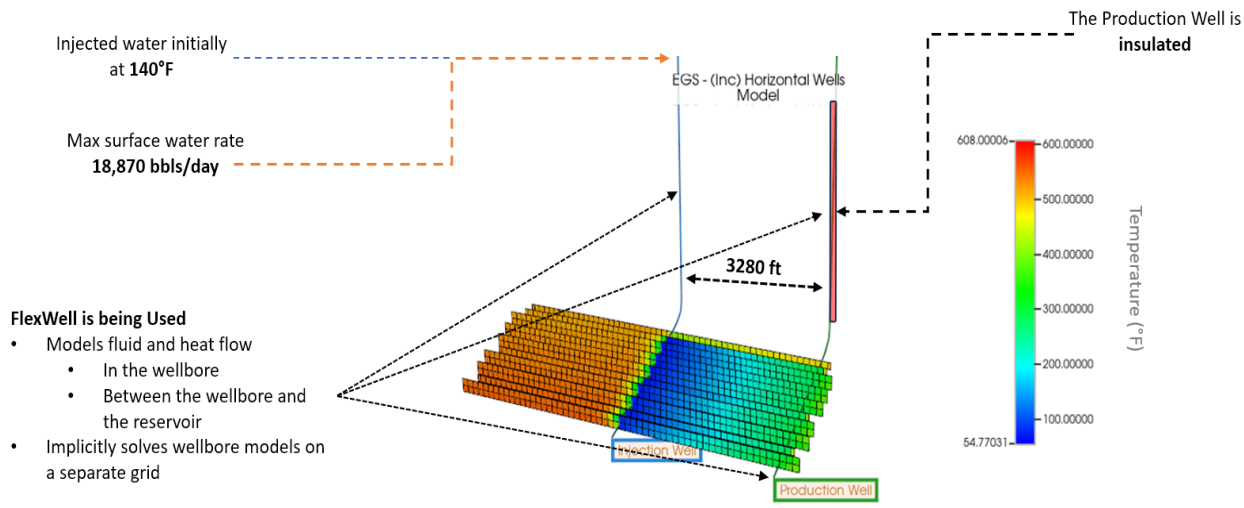

Figure 3.7: Inclined EGS Well Model Description

Well Configurations and Operational Parameters

Mirroring the previous EGS model, this inclined system employs a maximum surface water rate of 3000 m³/day and injects water at 140°F (60°C). The choice of injection temperature is strategically set to optimize thermal uptake by the fluid while maintaining a fluidity that permits extensive circulation through the induced fractures.

A key feature of the EGS - Inc model is the utilization of insulation in the production well to prevent heat loss. This aspect is crucial, given the extensive lateral reach of the wells at such profound depths, as it ensures that the thermal energy harnessed from the reservoir is not compromised on its journey to the surface.

Hydraulic Fracturing and Reservoir Stimulation

The model advocates for an aggressive reservoir stimulation strategy, incorporating multiple stages of hydraulic fracturing to enhance the permeability of the rock matrix. This

strategy is critical in creating an extensive network of interconnected fractures, which not only facilitates the flow of geothermal fluids but also significantly increases the effective surface area for heat exchange.

3.2.8 Integration of Empirical Data and Theoretical Models

In order to establish a robust foundation for our simulation models, we have systematically incorporated key parameters and findings from an array of seminal papers within the geothermal energy domain. These sources have been instrumental in shaping the theoretical and empirical underpinnings of our research:

A. *Thermal Parameters and Geothermal System Comparisons:*

Drawing on the work of Frash, Meng, and K C (2024), our simulation integrates critical thermal parameters such as the rock and cement thermal conductivities and specific heat capacities. These parameters are pivotal in modeling the thermal dynamics of the reservoir and the interaction between geothermal fluids and reservoir formations. Additionally, Frash et al.'s comparative analysis of various geothermal systems offers invaluable insights into optimizing our model's design and operational parameters to simulate advanced, enhanced, and caged geothermal systems effectively (Frash, Meng, and K C 2024).

B. *Casing Material Properties:*

The research conducted by Won et al. (2016) provides essential data on the thermal and mechanical properties of casing materials, including specific heat capacity and thermal conductivity. These properties are crucial for accurately simulating the thermal and mechanical stability of geothermal wells, particularly in the context of the heat exchange processes and the integrity of well structures under operational stresses.

C. EGS Model Validation:

The report by Norbeck and Latimer (2023) on the commercial-scale demonstration of enhanced geothermal systems (EGS) offers a real case scenario that serves as a benchmark for our simulations. Their report provides a proven framework for assessing the performance of EGS deployments, which we aim to further explore and adapt in the context of our research objectives. As shown in the figure below, our CMG model matches the data coming from Norbeck and Latimer's study with a 3% deviation between the temperature obtained at the production well surface (Figure 3.8). This ensures that our model is working smoothly and can be utilized for modeling other EGS Scenarios.

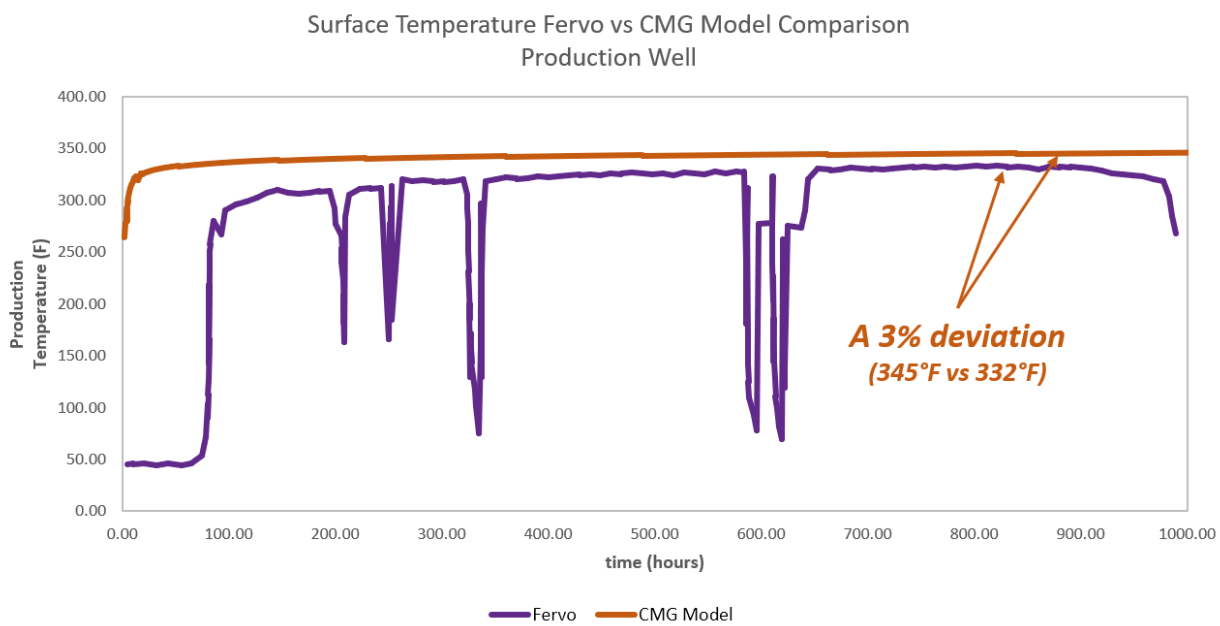

Figure 3.8: Fervo vs CMG Model (Surface Temperature Comparison)

To further demonstrate the model validation, both injection and production wells were evaluated and compared with the data obtained from Norbeck and Latimer's work. Figure 3.9 illustrates the different validation over temperature, pressure, and flow rate at surface conditions

for both injection and production wells. The models match very well and demonstrate that they can be further developed for our study.

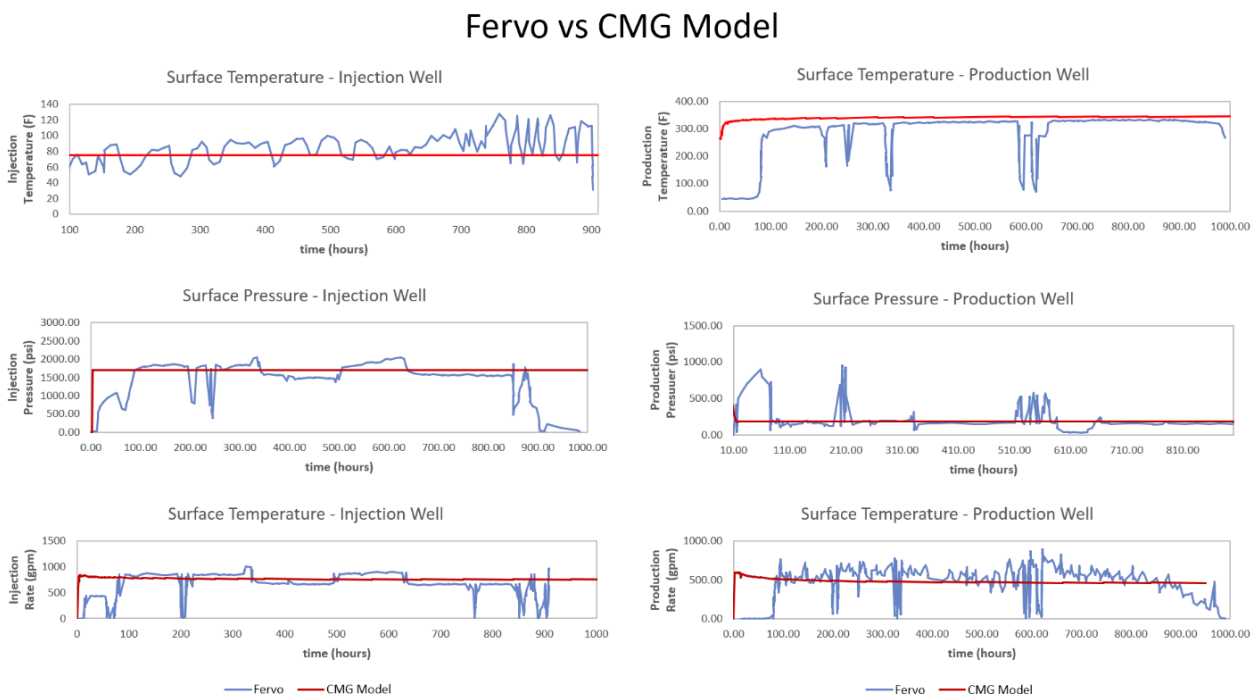

Figure 3.9: Fervo vs CMG Model (Injection and production Wells Comparison)

D. U-Shaped Model Validation:

Incorporating Kaveh Amini's work within our institution (Amini, personal communication), our study seeks to validate and refine the U-shaped model concept for geothermal energy extraction. Amini's work, with its focus on innovative reservoir configurations and operational strategies, provides a critical reference point for our simulations, offering both a methodological guide and empirical data for enhancing our model's accuracy and effectiveness. Our CMG model aligns very well with Amini's results, showing only a 3% difference (Figure 3.10).

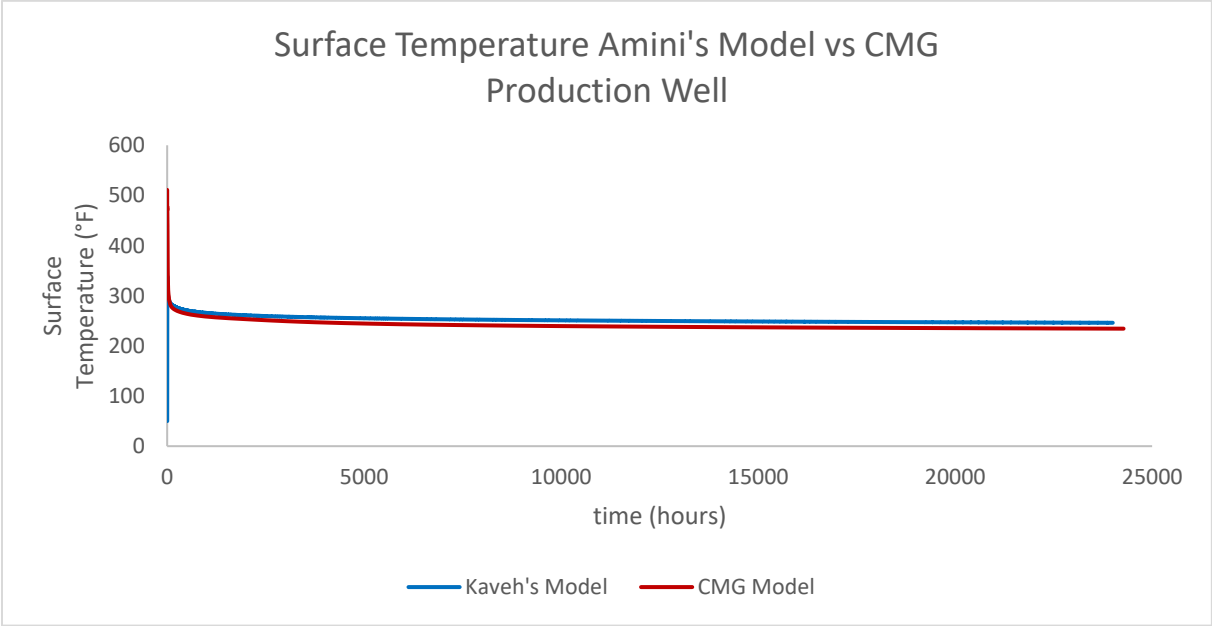

Figure 3.10: Amini's Model vs CMG Model (Surface Temperature Comparison)

CHAPTER 4
RESULTS

This section provides a comprehensive analysis of the simulation results obtained from the study of different closed-loop geothermal well configurations over a simulation period of 80 years. The models evaluated include U-Shaped Closed Loop Wells, V-Shaped Closed Loop Wells, Inclined V-Shaped Closed Loop Wells, Pipe-in-Pipe (PIP) Closed Loop Wells, Enhanced Geothermal System (EGS) Wells, and Inclined Enhanced Geothermal System (EGS) Wells. The primary metric for comparison is the temperature achieved after 20 years of operation, reflecting the system's efficiency in harnessing geothermal energy.

4.1 Long-Term Performance Analysis of U-Shaped Geothermal Well Models

4.1.1 Base Model

The U-Shaped Closed Loop Wells model has shown good performance in extracting heat from the deepest formations of the Wattenberg formation reservoir model. As shown in Figure 4.1, the injected water takes advantage of all the heat trapped throughout the formation beds surrounding the injection and production wells. The greater contribution comes from the lateral well connecting the injection and production wells, where this lateral well absorbs heat from the highest reachable depth (6100 m) with the highest temperature recorded (300°C). The lateral section has increased contact between the wells and the targeted formation, making it an excellent configuration in Closed-loop systems.

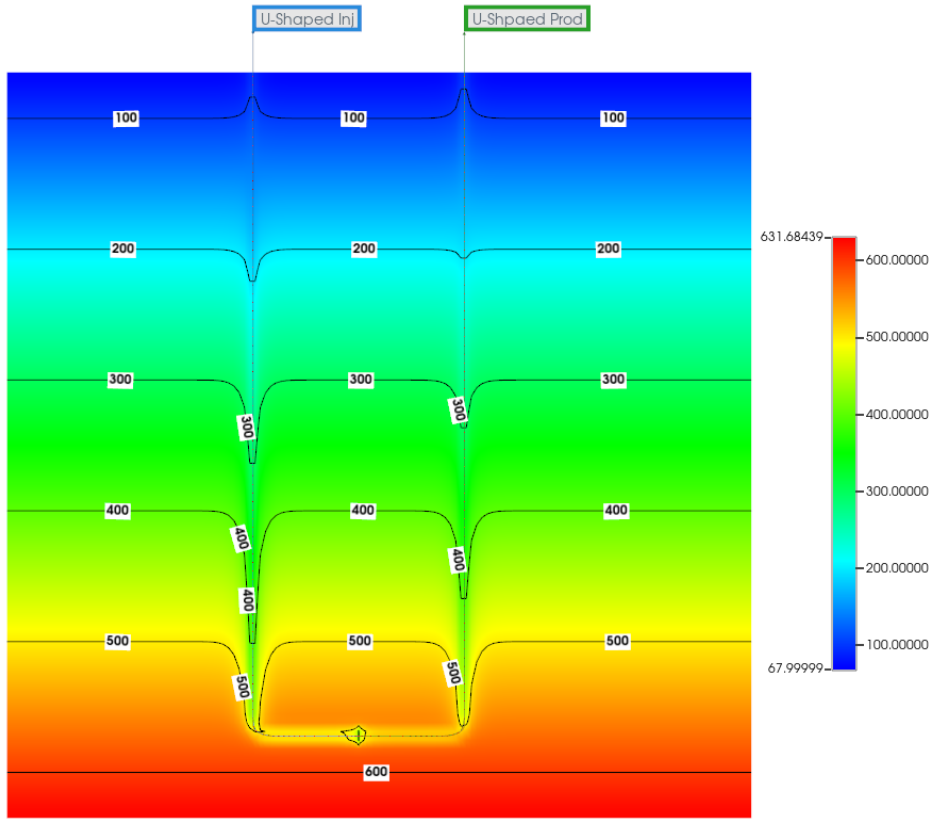

Figure 4.1: U-Shaped Closed Loop Wells Reservoir Model (After 80 years)

After 20 years of simulation, the model exhibited a final temperature of 182°F (Figure 4.2). This temperature value will be examined relative to the injected fluid's temperature (140°C) to facilitate a comprehensive interpretation of the amount of heat gained from these configurations.

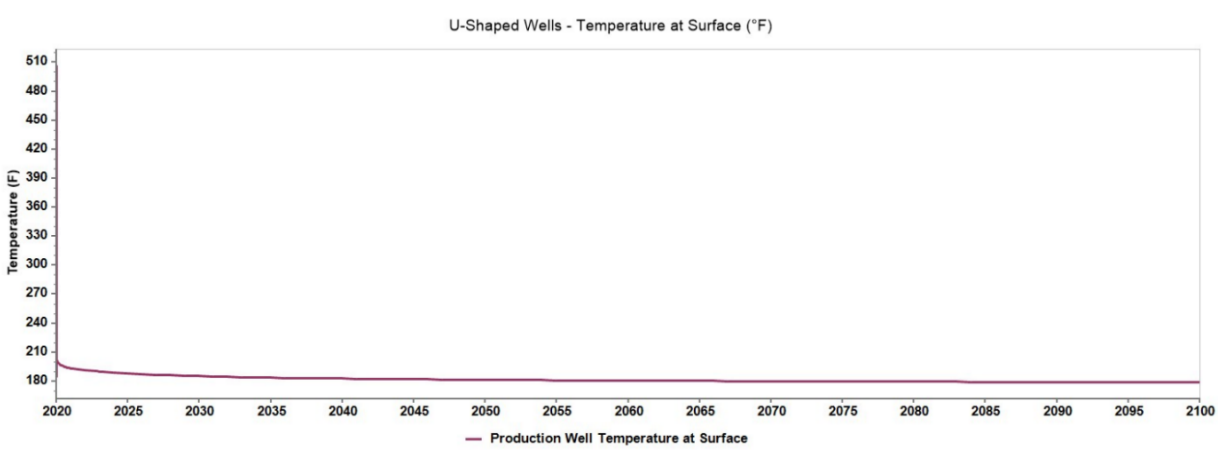

Figure 4.2: U-Shaped (Base Model) – Temperature (°F) vs Time (years)

In the evaluation of temperature profiles for the U-Shaped well model, the importance of depth becomes clear, particularly in how it influences temperature dissipation and gradients within the well. As shown in Figure 4.3, a slight decrease in temperature is observed at shallower depths adjacent to the surface. This can be attributed to the temperature gradient that exists within the earth's subsurface; despite the injected water having a temperature of 140°F, the temperature at these shallower depths falls slightly below the injection temperature due to cooler surrounding rock formations. As the well extends deeper into the subsurface, the temperature naturally increases according to the geothermal gradient, reflecting the expected increment in ambient temperatures with depth.

This nuanced observation complements the overarching analysis of thermal dynamics in the U-Shaped model. It's evident that both the injection and production wells' temperature profiles intersect at bottom-hole depth, signifying a point where the heat extraction mechanism is optimized and there is uniformity in the bottom hole temperature of both wells. This confluence suggests an efficient heat transfer process, yet less facilitated through the casing walls rather than direct contact between the water and the reservoir formation.

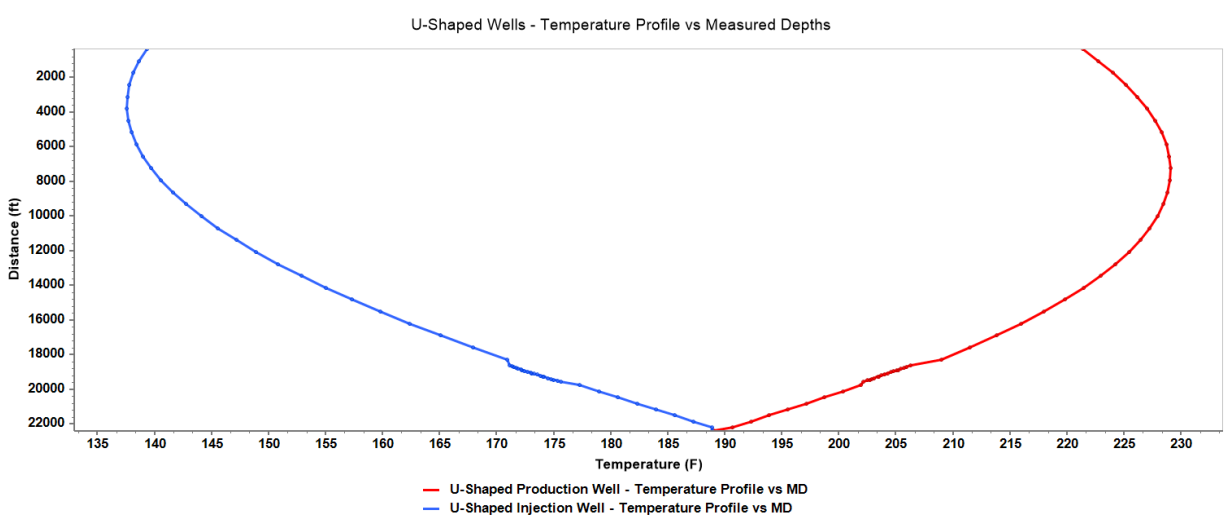

Figure 4.3: U-Shaped (Base Model) – Temperature Profile (°F) vs Depth (ft)

It is essential to point out that in our system, we only have water as the working fluid. The P-h Diagram for water up to 250 MPa shown in Figure 4.4 illustrates the thermodynamic properties of water under a variety of conditions, confirming that within our U-Shaped Model, the fluid remains in the liquid phase throughout the operational, which includes both injection and production surface as well as bottom hole scenarios.

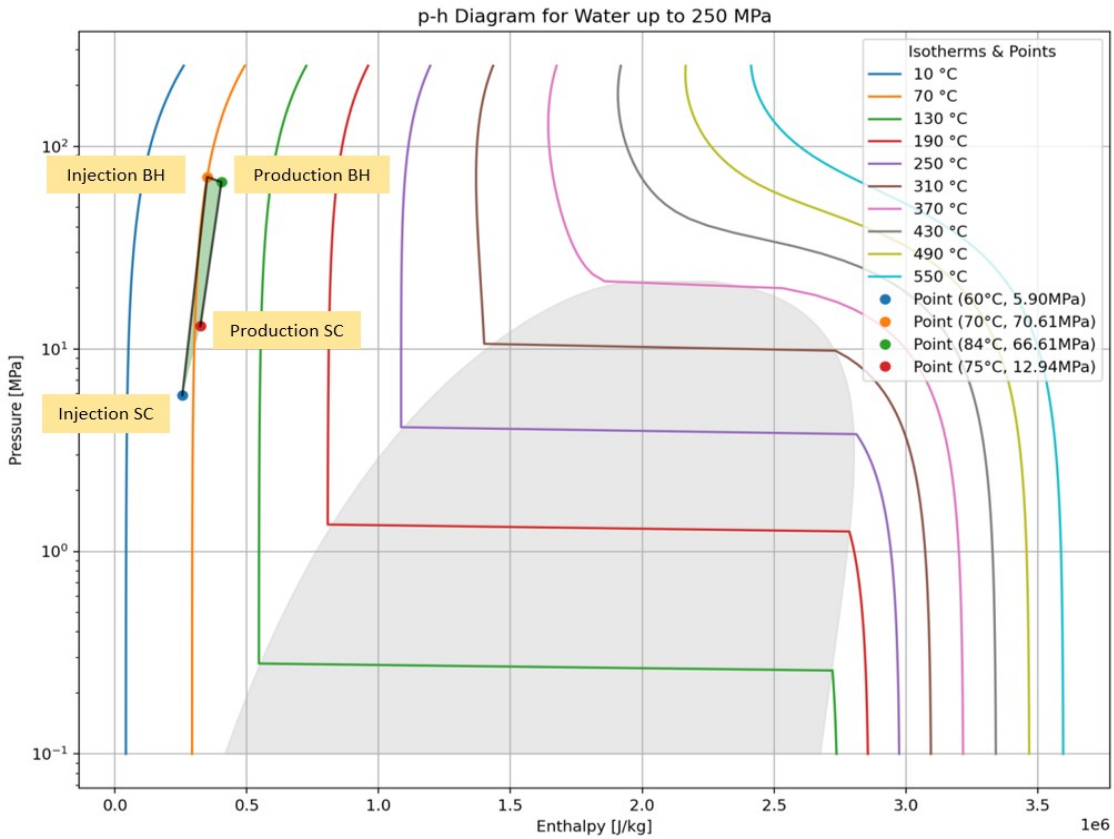

Figure 4.4: U-Shaped (Base Model) – P-h Diagram for Water up to 250 MPa

The U-Shaped Closed Loop Wells model demonstrates solid baseline efficiency, attributed to its straightforward design which balances heat extraction with simplicity of construction and operational feasibility. Despite its simplicity, the U-shaped configuration effectively maintains high temperatures over extended periods while sustaining stable

temperature and pressure profiles across different formations. This suggests it is a reliable option for geothermal energy extraction (Figure 4.5).

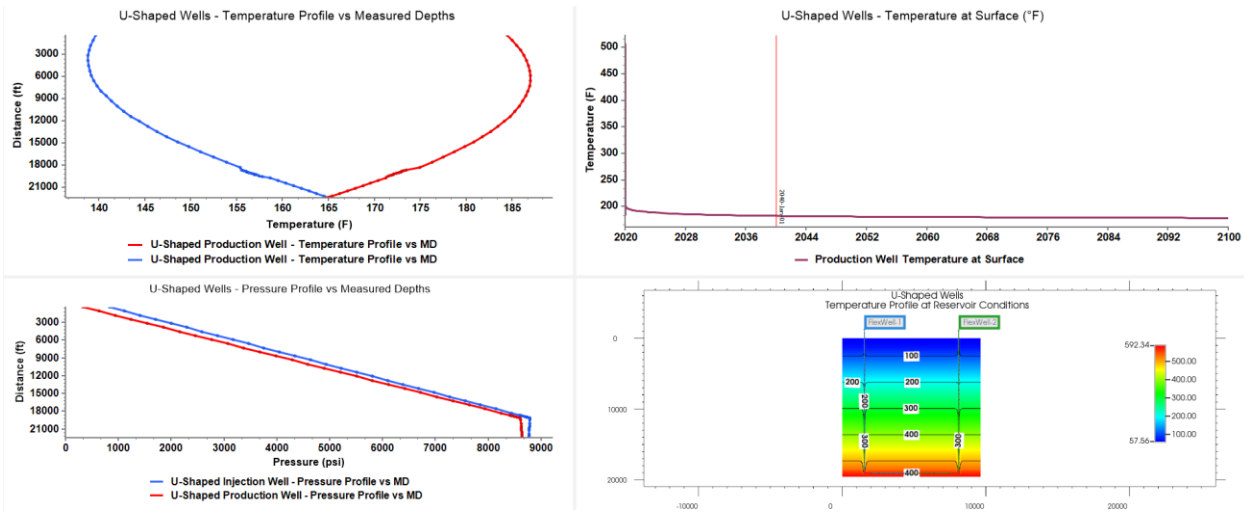

Figure 4.5: Thermal and Pressure Dynamics in U-Shaped Well Systems: Profiles and Projections

4.1.2 Fractured Models

To simulate introducing a highly conductive material into the reservoir, the thermal conductivity of the reservoir water was artificially increased from 53,500 J/(m·day·°C) to 6.48e+06 J/(m·day·°C). This increase in conductivity aims to mimic the effect of adding a material like copper to the reservoir, possibly through hydraulic fracturing. With the well perforations closed, this setup maintains a controlled environment, minimizing the increased reservoir conductivity's impact on the circulating water's temperature. This scenario represents intact well integrity, preventing exchange between the well water and the reservoir.

When the well perforations are open, it signifies a potential for interaction between the well water and the reservoir, allowing the high conductivity of the reservoir water to more directly impact the well's thermal profile. The increased conductivity could facilitate more efficient heat transfer between the well water and the surrounding environment, leading to a

noticeable temperature rise in the model. After 20 years of simulation, the model exhibited a final temperature of 189°F (Figure 4.6). This temperature is analyzed relative to the injected fluid's temperature (140°C) for a deeper understanding of the heat gained from these configurations. The inclusion of a highly conductive material in the reservoir has slightly influenced the thermal performance of the U-shaped closed loop wells system.

A. U-Shaped Well (Fractures Closed with Highly Conductive Material)

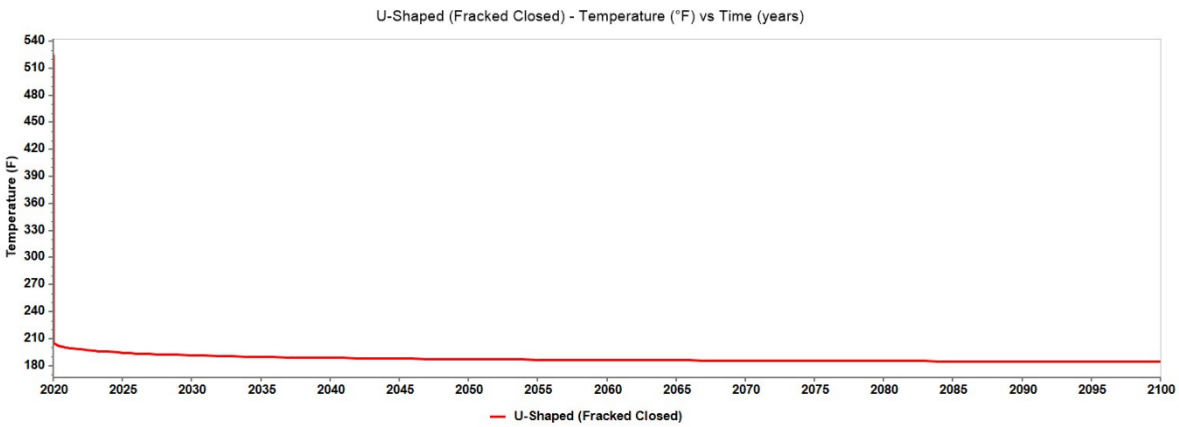

Figure 4.6: U-Shaped (Fracked - Closed) – Temperature (°F) vs Time (years)

With perforations closed, the conductive material appears effective in evenly distributing heat, maintaining a nearly constant temperature with only a 3% deviation. This suggests that the closed fractures, combined with the conductive material, create a barrier to heat flux, thus preserving the well's temperature within a narrow range. This could be advantageous in applications where temperature stability is crucial over time.

B. U-Shaped Well (Fractures Opened with Highly Conductive Material)

Opening the perforations in the presence of highly conductive material shows a stark contrast in thermal behavior compared to the closed configuration. As illustrated in Figure 4.7,

the model exhibits a significant temperature increase, surging by about 23% to reach approximately 225°F.

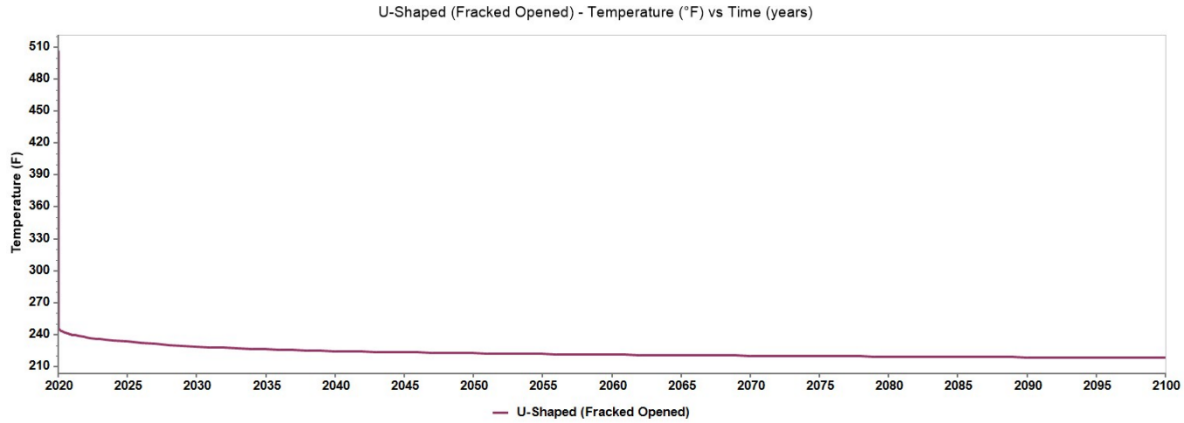

Figure 4.7: U-Shaped (Fracked - Opened) – Temperature (°F) vs Time (years)

This substantial shift underscores the open fractures' influence on the system's thermal dynamics, where the enlarged contact surface and enhanced fluid movement bolster heat transfer processes. This can be particularly beneficial in operations requiring increased temperatures, suggesting that strategic management of fracture states can significantly alter heat distribution and could be utilized to augment processes such as thermal recovery in reservoirs.

4.1.3 U-Shaped Wells Models Comparison

In summary, introducing a highly conductive material into the reservoir shows a minimal impact on the U-shaped closed well system, maintaining a stable average temperature of 189°F over 20 years. In contrast, the opened fracture model reveals a notable temperature increase to an average of 225°F, indicating that open fractures significantly enhance heat transfer, which could be advantageous for thermal recovery processes (Figure 4.8).

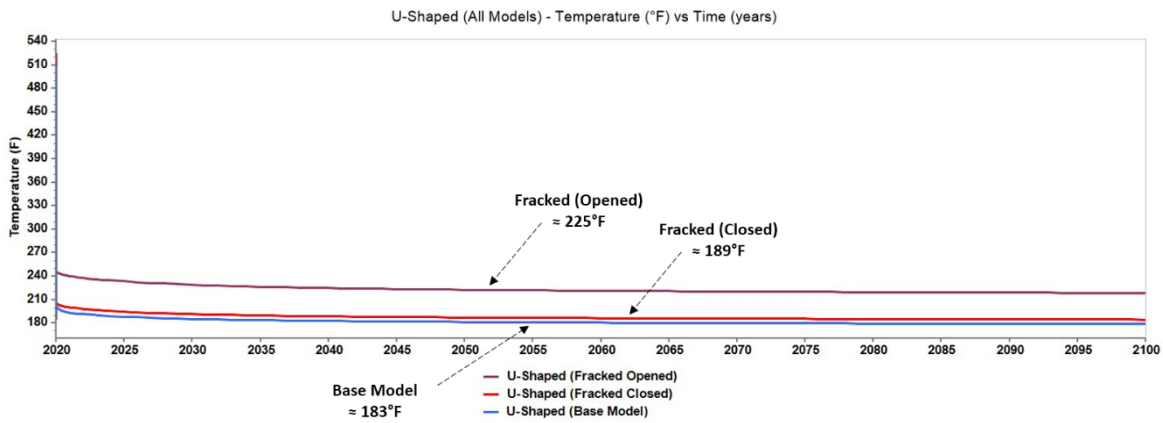

Figure 4.8: Temperature (°F) vs Time (years) – U-Shaped (All Models) Comparison

4.2 Long-Term Performance Analysis of Pipe-in-Pipe Geothermal Well Models

The Pipe-in-Pipe Closed Loop Well model has demonstrated poor performance in extracting heat from the deepest formations of the Wattenberg formation reservoir model. As shown in Figure 4.9, the injected water ineffectively utilizes the heat trapped throughout the formation beds surrounding the injection well.

This poor performance is attributed to the lack of a lateral well that significantly contributes to absorbing heat from the highest reachable depth (6100 m), with the highest temperature recorded (300°C). Moreover, the reduced space available for water flow within each well significantly affects performance.

The design, where the production well is concentric within the injection well, also greatly diminishes heat transfer. Unlike the U-Shaped configuration, where the injection well can still access heat at shallower depths, the absence of a lateral section and the inner placement of the injection well in the Pipe-in-Pipe system substantially reduce the contact area between the wells and the targeted formation, resulting in a less effective configuration in Closed-loop systems.

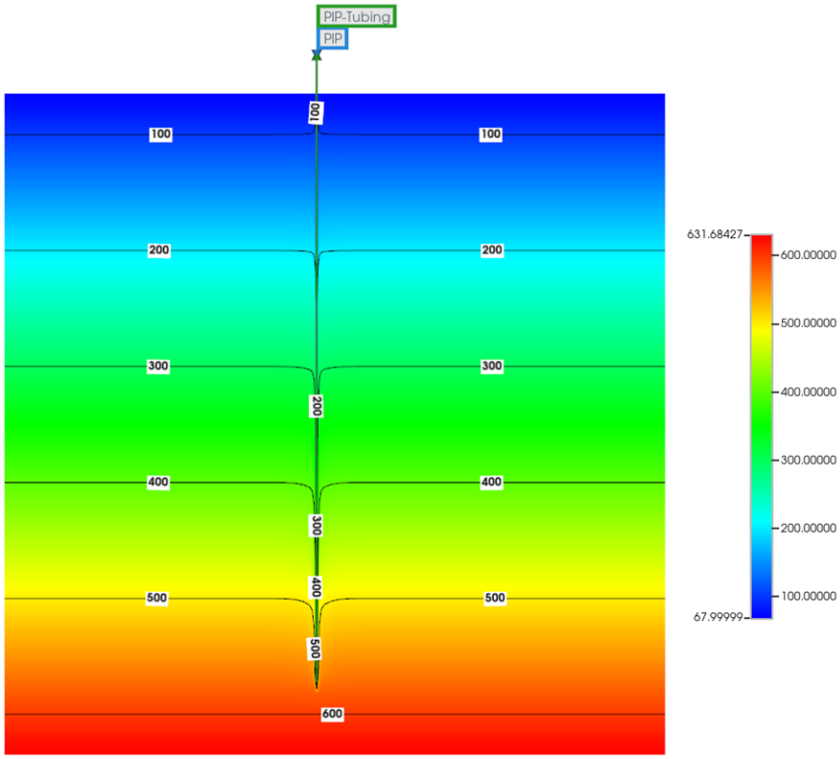

Figure 4.9: Pipe-in-Pipe Well Closed Loop Well Reservoir Model (After 80 years)

After 20 years of simulation, this model exhibited a final temperature of 143°F (Figure 4.10). This temperature value will be analyzed relative to the injected fluid's temperature (140°C) to facilitate a thorough interpretation of the amount of heat gained from these configurations.

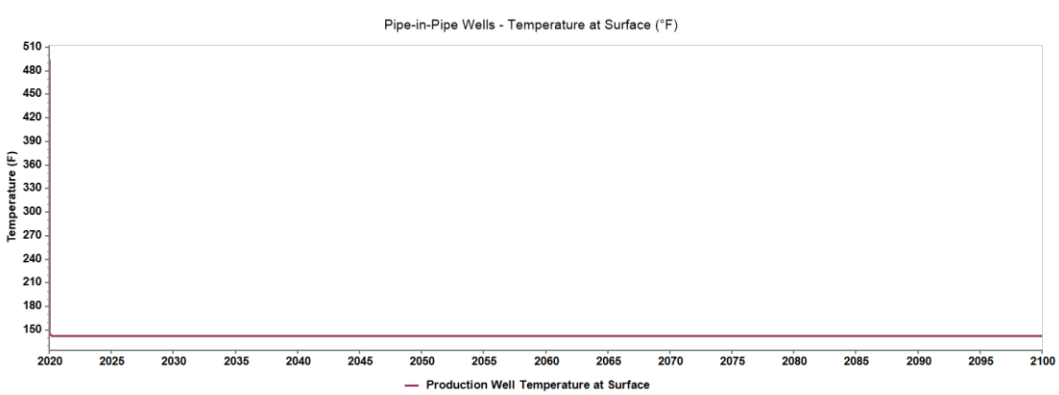

Figure 4.10: Pipe-in-Pipe Well – Temperature (°F) vs Time (years)

Evaluating the temperature profile across different wells and depths is crucial to understanding where temperature dissipation occurs most and how the temperature increases from one well to another. As illustrated in Figure 4.11, a slight decrease in temperature is observed at shallower depths adjacent to the surface and the temperature profiles of both wells intersect at one point, demonstrating the Pipe-in-Pipe (PIP) model's mechanism for extracting heat, where there is no difference in the bottom hole temperature of either well. However, the temperature profile in the production well significantly illustrates the impact of the concentric tubing design on heat extraction, as it shows a lower temperature profile compared to the U-Shaped model.

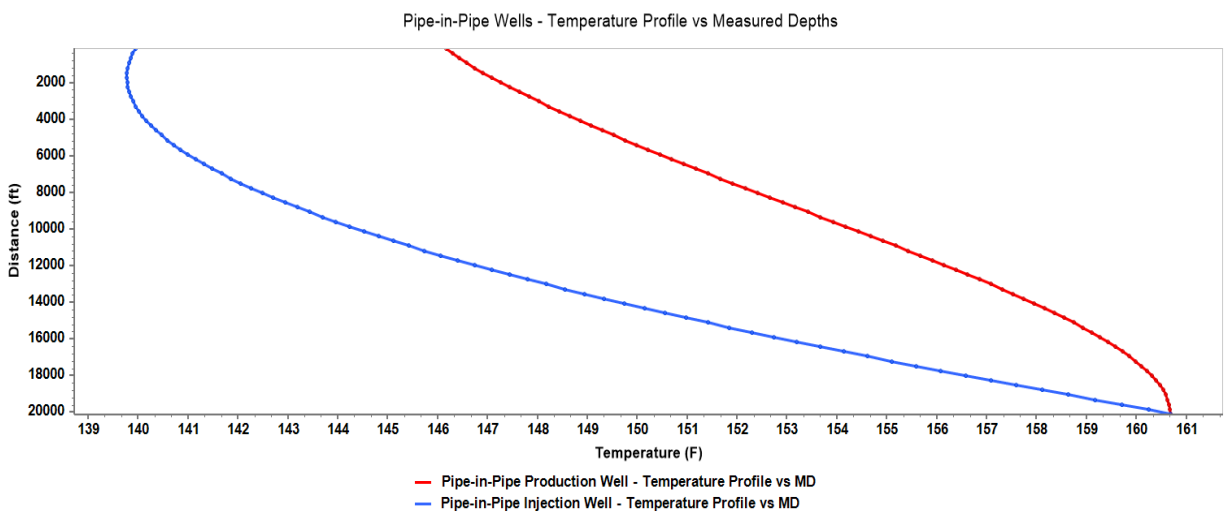

Figure 4.11: Pipe-in-Pipe Well – Temperature Profile (°F) vs Depth (ft)

In line with the working fluid strategy of our previous configuration, the Pipe-In-Pipe system exclusively utilizes water as the working fluid. The P-h Diagram for water up to 250 MPa (Figure 4.12) outlines the water's thermodynamic properties under various conditions and affirms that, within the Pipe-In-Pipe Model, the water remains in the liquid phase throughout all operational states.

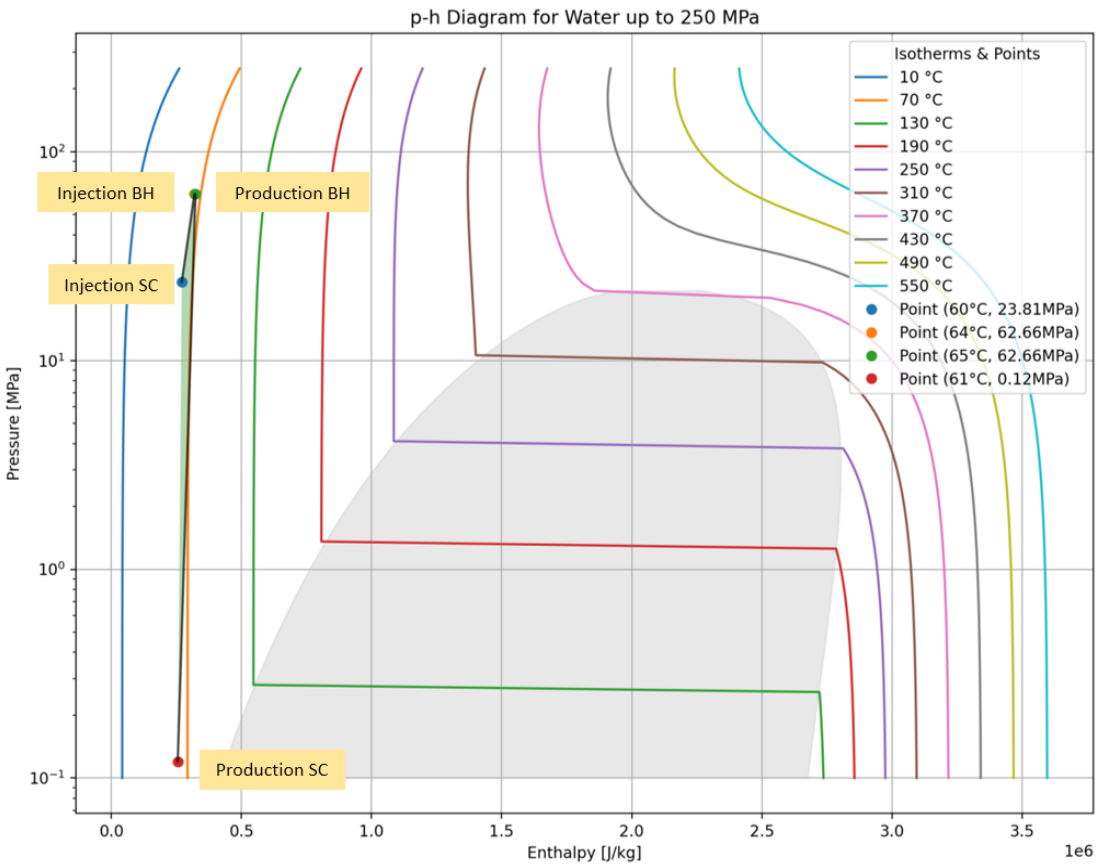

Figure 4.12: Pipe-In-Pipe Model – P-h Diagram for Water up to 250 MPa

The Pipe-in-Pipe (PIP) Closed Loop Well model exhibits weaker performance compared to the U-Shaped model, primarily due to the inherent challenges of its design, which include the potential for reduced heat exchange efficiency due to the double-pipe configuration. The results suggest that, although innovative, the PIP system may require further optimization to improve its thermal performance and compete with single-pipe configurations (Figure 4.13).

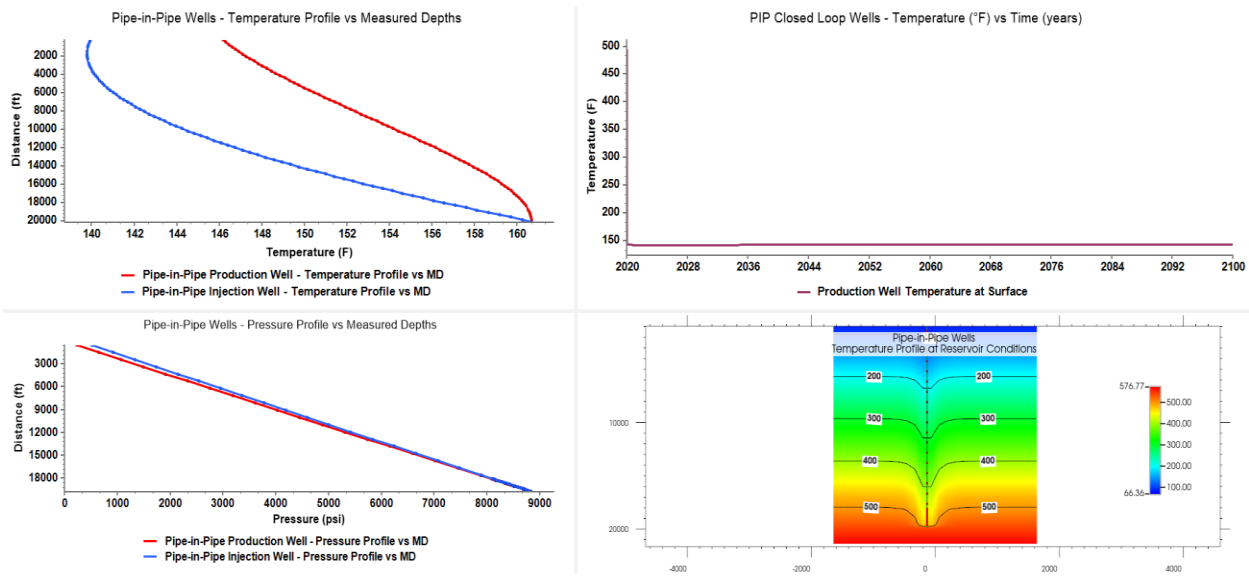

Figure 4.13: Thermal and Pressure Dynamics in Pipe-in-Pipe Well Systems: Profiles and Projections

4.3 Long-Term Performance Analysis of V-Shaped Geothermal Well Models

The V-Shaped Closed Loop Wells model has demonstrated excellent performance in extracting heat from the deepest formations of the Wattenberg formation reservoir model. As shown in Figure 4.14, the injected water efficiently utilizes all the heat trapped throughout the formation beds surrounding the injection and production wells.

The most significant contribution comes from the lateral well connecting the injection and production wells, where this lateral well absorbs heat from the highest reachable depth (6100 m), with the highest temperature recorded (300°C). The increased lateral section, compared to the U-Shaped Base Model, has further enhanced the contact between the wells and the targeted formation, making it an excellent configuration in Closed-loop systems.

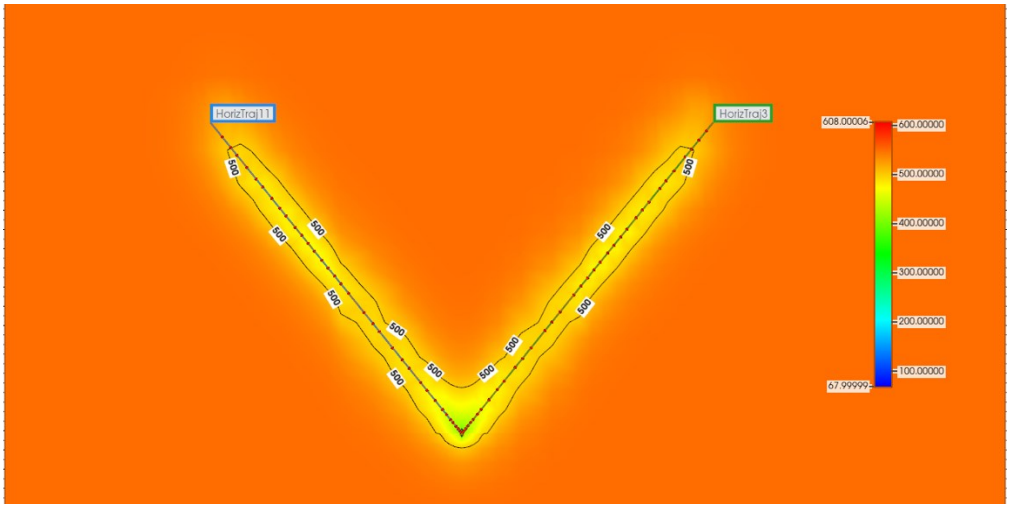

Figure 4.14: V-Shaped Closed Loop Wells Reservoir Model (After 80 years)

After 20 years of simulation, this model exhibited a final temperature of 185°F (Figure 4.15). This temperature value will be analyzed in relation to the injected fluid's temperature (140°C) to provide a clear interpretation of the amount of heat gained from these configurations.

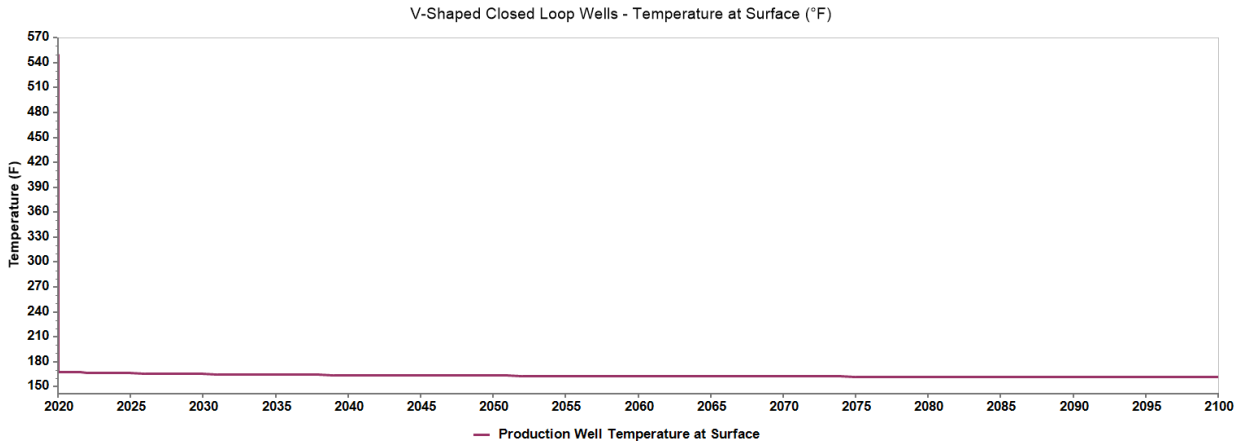

Figure 4.15: V-Shaped Wells – Temperature (°F) vs Time (years)

Evaluating the temperature profile across various wells at different depths is crucial for understanding where temperature dissipation primarily occurs and how the temperature increases from one well to another. As illustrated in Figure 4.16, a slight decrease in temperature is observed at shallower depths adjacent to the surface and the temperature profiles of both wells intersect at one point, demonstrating the efficiency of the V-Shaped model in extracting heat, with no significant difference in the bottom hole temperature of either well. This indicates that there is no direct contact between the water and the reservoir formation, thus all heat transfer occurs through the casing walls, a characteristic very similar to the U-Shaped configuration.

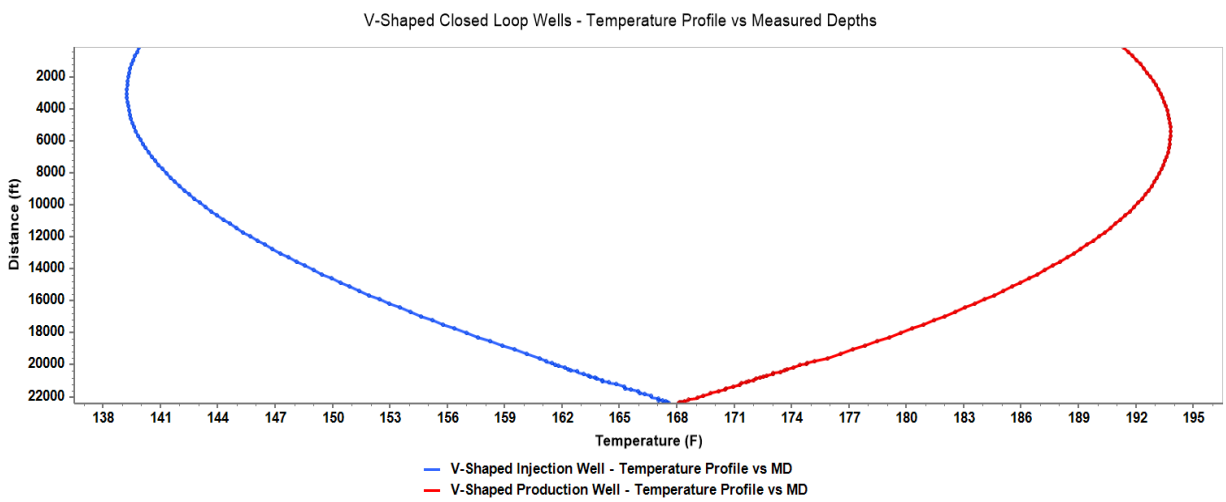

Figure 4.16: V-Shaped Wells – Temperature Profile (°F) vs Depth (ft)

Consistent with our previously discussed models, the V-Shaped system also exclusively uses water as the working fluid. The P-h Diagram for water up to 250 MPa (Figure 4.17) displays the water's thermodynamic properties and confirms that in the V-Shaped Model, water consistently stays in the liquid phase across all operational states.

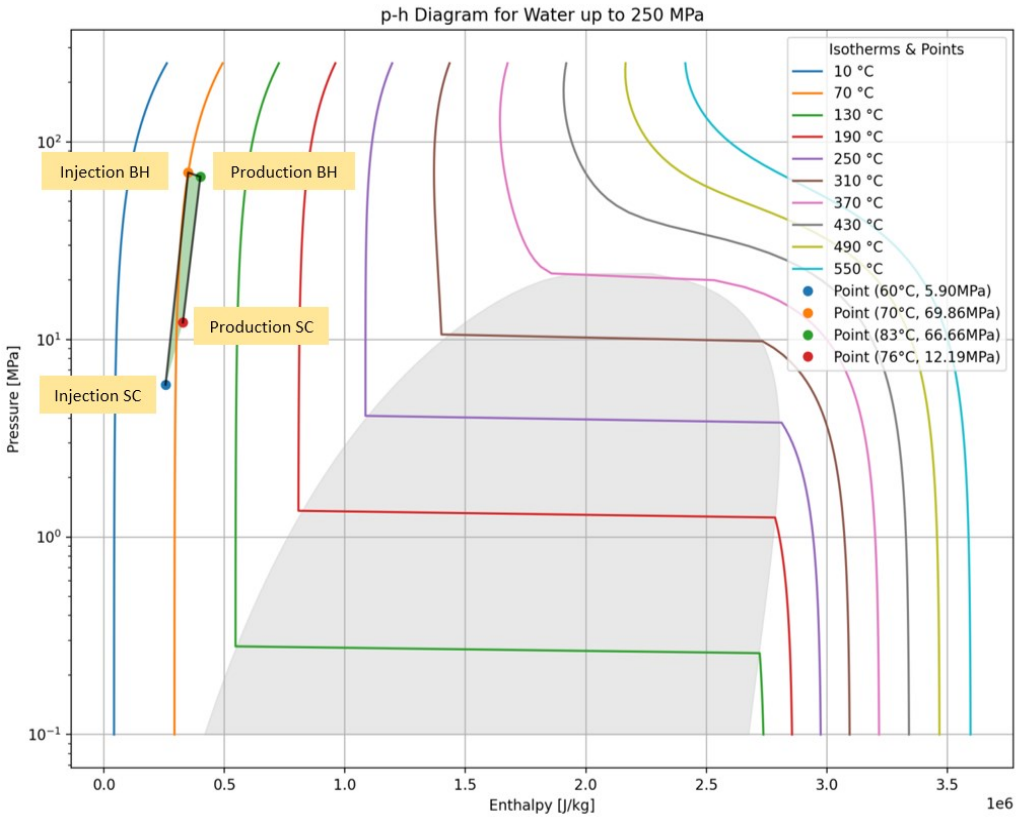

Figure 4.17: V-Shaped Model – P-h Diagram for Water up to 250 MPa

The V-Shaped Closed Loop Wells model exhibits solid baseline efficiency, with a slightly improved outcome compared to the U-Shaped model. The increase in temperature can be attributed to the V-shaped design's enhanced ability to access deeper geothermal reservoirs effectively, tapping into higher thermal gradients. The advantage of this design lies in its extended surface area in contact with the hot rock, facilitating more efficient heat transfer. The V-shaped configuration is effective in maintaining high temperatures over an extended period while sustaining stable temperature and pressure profiles across different formations, indicating it is a reliable option for geothermal energy extraction (Figure 4.18).

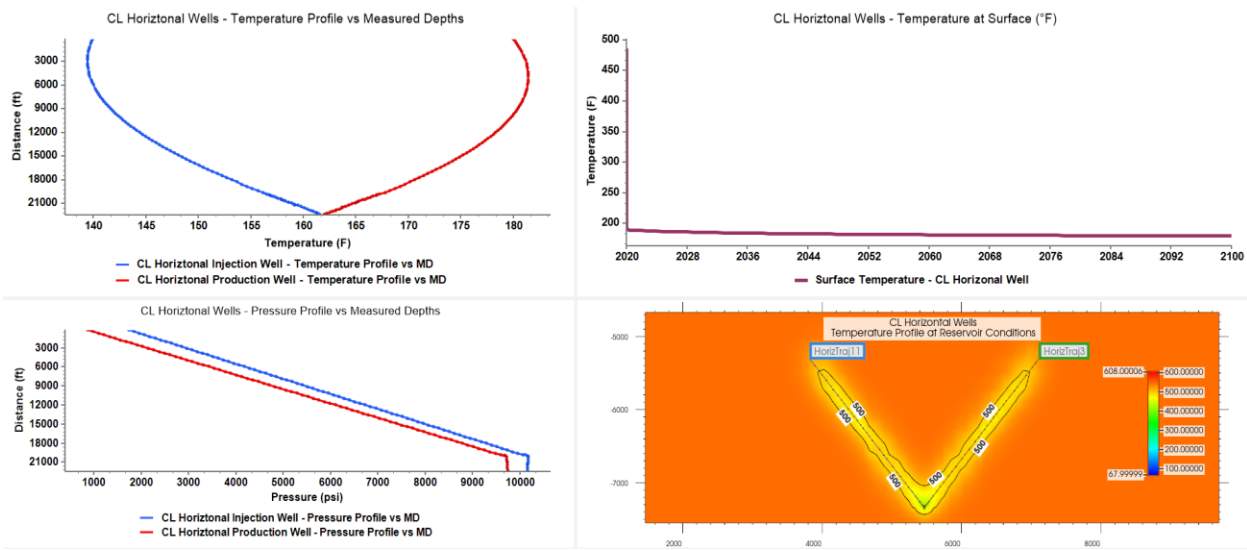

Figure 4.18: Thermal and Pressure Dynamics in V-Shaped Wells Systems: Profiles and Projections

4.4 Long-Term Performance Analysis of Inclined V-Shaped Geothermal Well Models

The Inclined V-Shaped Closed Loop Wells model has shown good performance in extracting heat from the deepest formations of the Wattenberg formation reservoir model, albeit with lower temperatures compared to the U-Shaped and V-Shaped models. As shown in Figure 4.19, the injected water takes advantage of all the heat trapped throughout the formation beds surrounding the injection and production wells. However, the contribution from the lateral well connecting the injection and production wells is lower, where this lateral well absorbs heat from the highest reachable depth (6100 m), with the highest temperature recorded (300°C). Compared to the U-Shaped Base Model, the lateral section in this model has reduced the contact between the wells and the targeted formation at 6100 m, making it a less favored configuration in Closed-loop systems.

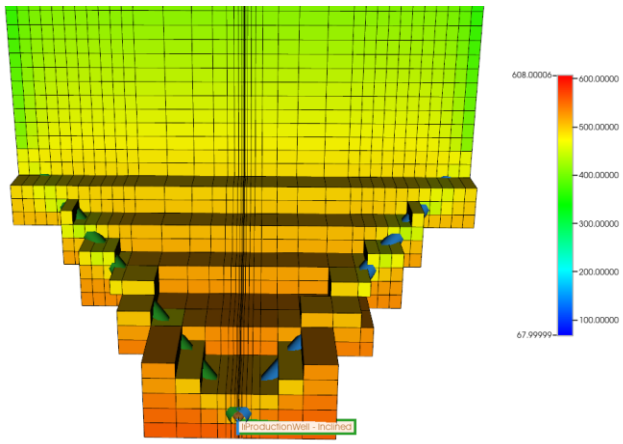

Figure 4.19: Inclined V-Shaped Closed Loop Wells Reservoir Model (After 80 years)

After 20 years of simulation, this model exhibited a final temperature of 179°F (Figure 4.20). This temperature value will be analyzed in relation to the injected fluid's temperature (140°C) to provide a comprehensive interpretation of the amount of heat gained from these configurations.

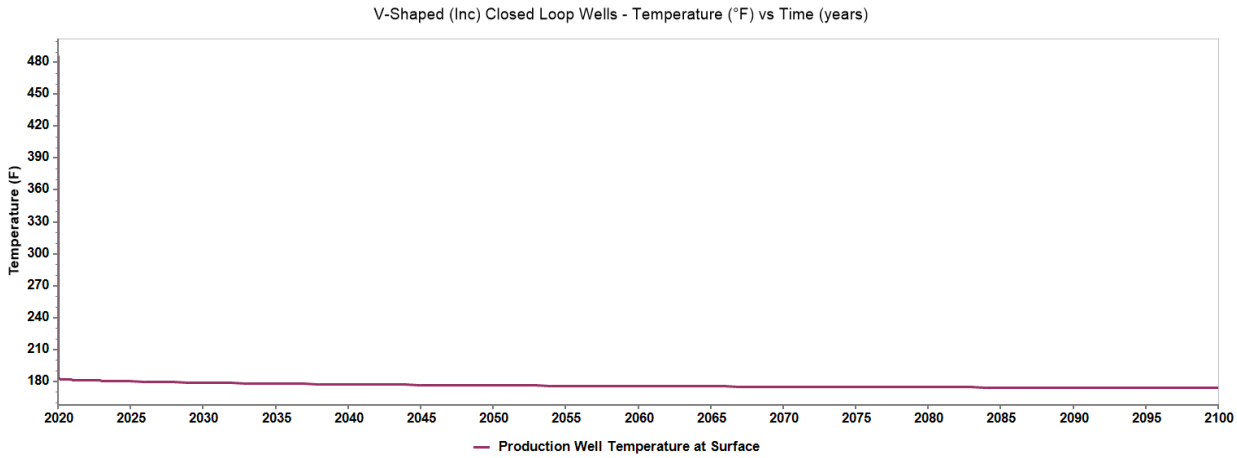

Figure 4.20: Inclined V-Shaped Wells – Temperature (°F) vs Time (years)

Evaluating the temperature profile across various wells at different depths is crucial to understanding where temperature dissipation primarily occurs and how temperature increases

from one well to another. As illustrated in Figure 4.21, a slight decrease in temperature is observed at shallower depths adjacent to the surface and the temperature profiles of both wells intersect at one point, demonstrating the Inclined V-Shaped model's efficiency in extracting heat, with no significant difference in the bottom hole temperature of either well, akin to the U-Shape and V-Shape models.

However, a disturbance in the temperature profiles in the wellbore area indicates an unsteady increase in temperature, attributable to the inclination of the wellbore configuration. This shows that the temperature across the wellbore area is not as stable as in other Closed-loop models.

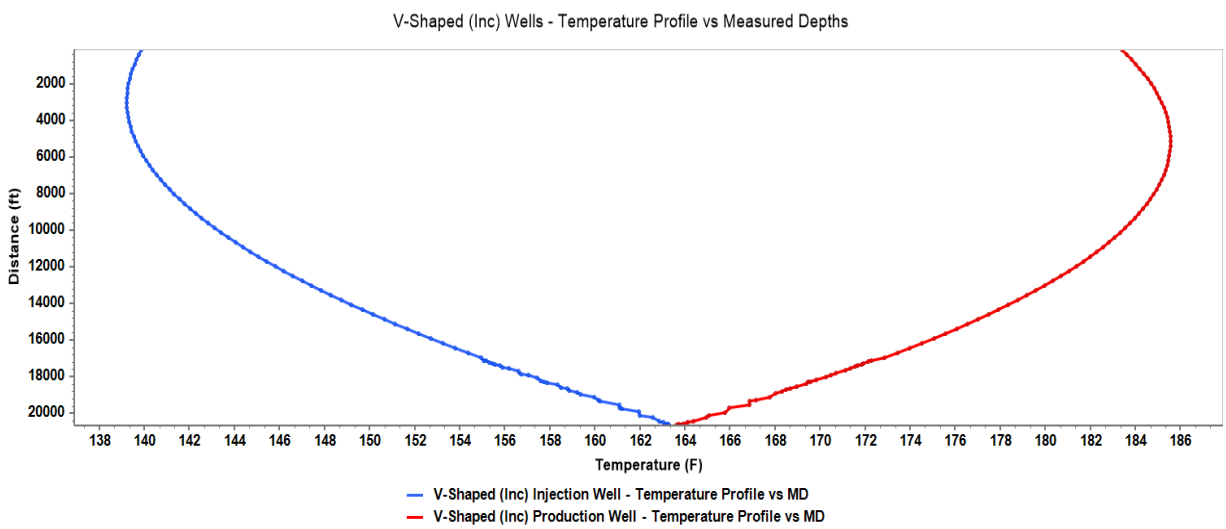

Figure 4.21: Inclined V-Shaped Wells – Temperature Profile (°F) vs Depth (ft)

In line with the working fluid strategy of our previous configurations, the Inclined V-Shaped system similarly relies on water as its sole operational medium. The accompanying P-h Diagram, up to pressures of 250 MPa (Figure 4.22), showcases the range of water's thermodynamic states and upholds that within the unique geometry of the Inclined V-Shaped

Model, the water is maintained in its liquid form throughout the entirety of the operational parameters.

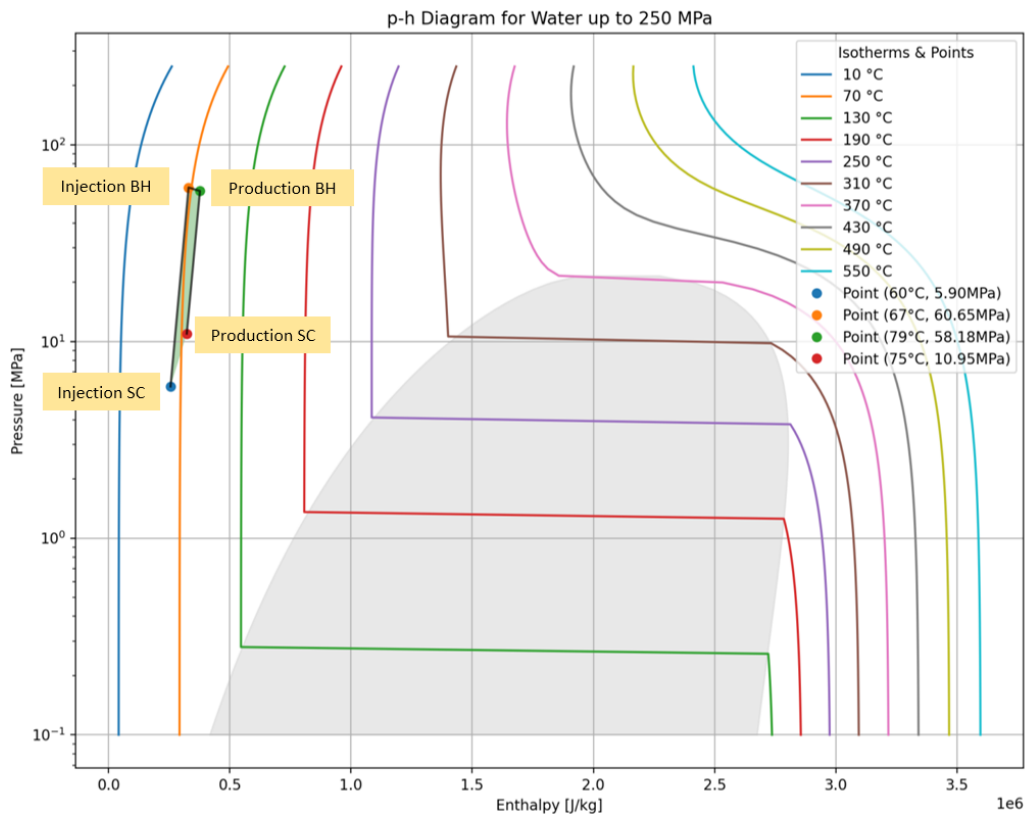

Figure 4.22: Inclined V-Shaped Model – P-h Diagram for Water up to 250 MPa

The Inclined V-Shaped Closed Loop Wells model shows good baseline efficiency, albeit with a slightly regressed outcome. The temperature decrease compared to the U-Shaped and V-Shape models can be attributed to the Inclined V-shaped design's less effective access to deeper geothermal reservoirs, resulting in lower thermal gradients.

The inclination is designed to overcome drilling challenges, but it introduces complexities that marginally reduce thermal efficiency. This performance highlights the trade-

offs in adjusting well configurations to address technical constraints, where the inclination may lead to increased thermal losses compared to vertical configurations.

Although less effective in maintaining high temperatures over an extended period, the Inclined V-shaped configuration still provides stable temperature and pressure profiles across different formations, suggesting it is a reliable option for geothermal energy extraction (Figure 4.23).

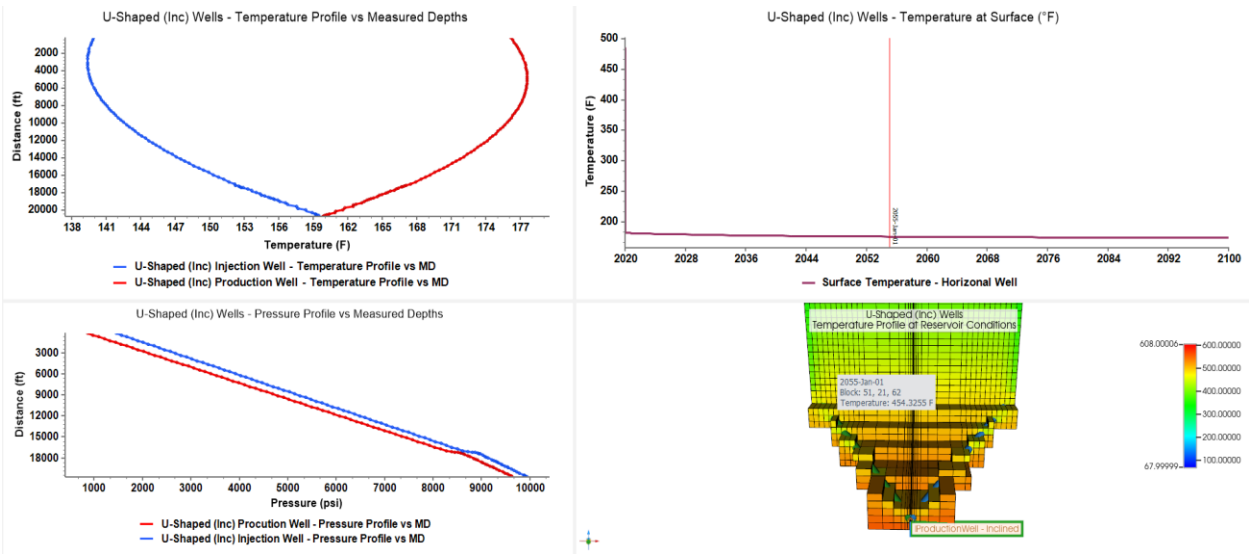

Figure 4.23: Thermal and Pressure Dynamics in V-Shaped Wells Systems: Profiles and Projections

4.5 Long-Term Performance Analysis of EGS Well Models

The Enhanced Geothermal System (EGS) Wells model has demonstrated remarkable performance in extracting heat from the deepest formations of the Wattenberg formation reservoir model. As shown in Figure 4.24, the injected water efficiently utilizes the heat trapped throughout the formation beds surrounding the injection and production wells, including the fractures induced by hydraulic fracturing.

The major contribution comes from the fractures connecting the injection and production wells, where these extended fractures, with high contact areas, absorb heat from the highest reachable depth (6100 m), with the highest temperature recorded (300°C). These extended fractures have significantly increased the contact between the injected fluid and the targeted formation, making it an excellent configuration compared to Closed-loop systems.

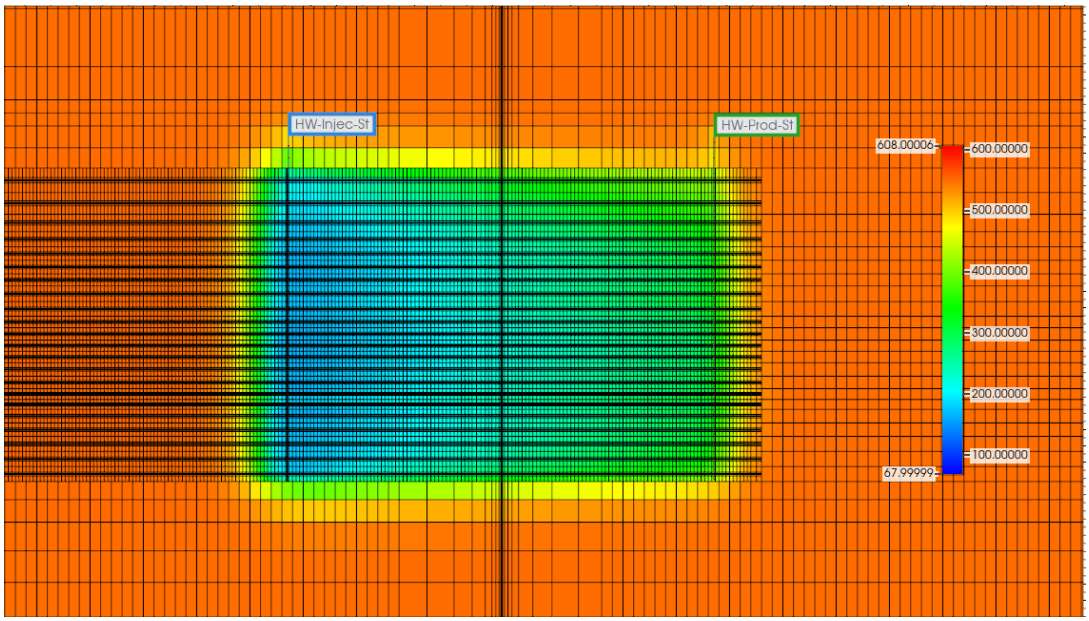

Figure 4.24: EGS Well Reservoir Model (After 80 years)

After 20 years of simulation, this model exhibited a final temperature of 446°F (Figure 4.25). This temperature value will be analyzed in relation to the injected fluid's temperature (140°C) to provide a clear interpretation of the amount of heat gained from these configurations.

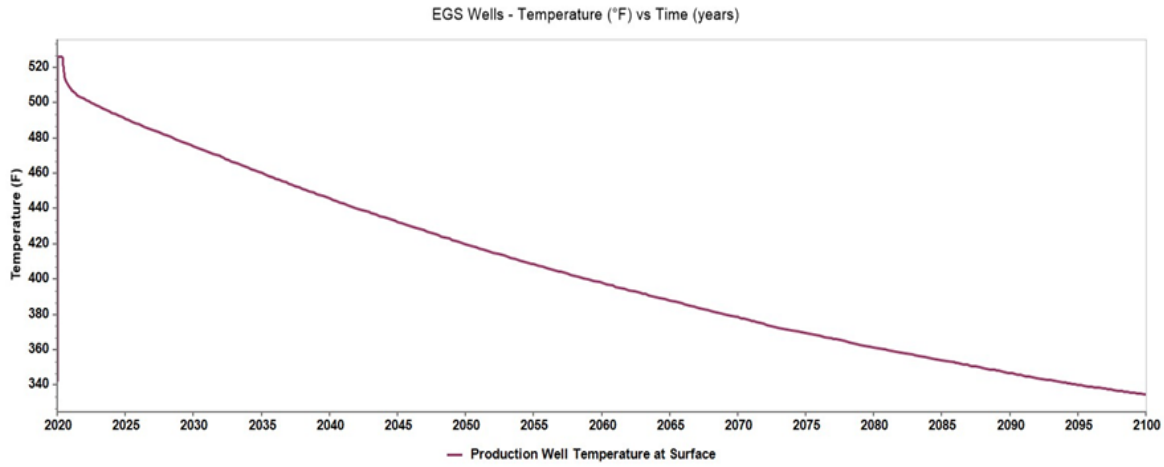

Figure 4.25: EGS Wells – Temperature (°F) vs Time (years)

Evaluating the temperature profile across various wells at different depths is crucial for understanding where temperature dissipation occurs predominantly and how the temperature increases from one well to another. As illustrated in Figure 4.26, the temperature profile of both wells shows a significant gap between them, demonstrating the EGS model's effectiveness in extracting heat, with a large margin difference between the bottom hole temperature of each well, unlike in Closed-Loop models. This indicates good contact between the injected water and the reservoir formation, resulting in very high temperature production at the surface.

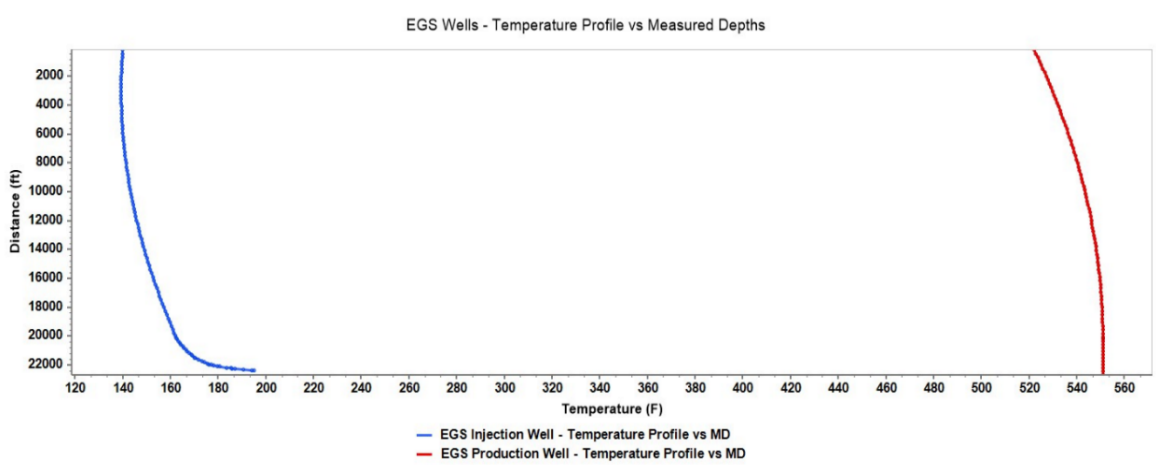

Figure 4.26: EGS Wells – Temperature Profile (°F) vs Depth (ft)

Building upon the fluid strategies of our prior designs, the Enhanced Geothermal System (EGS) employs water as the exclusive thermal medium. The expanded P-h Diagram for water up to 250 MPa (Figure 4.27) not only confirms this uniformity but also reflects a wider operational window afforded by the EGS model's robust geometry. It affirms that within this model, water reliably remains in its liquid phase across a broader range of thermodynamic conditions, underscoring the system's versatility.

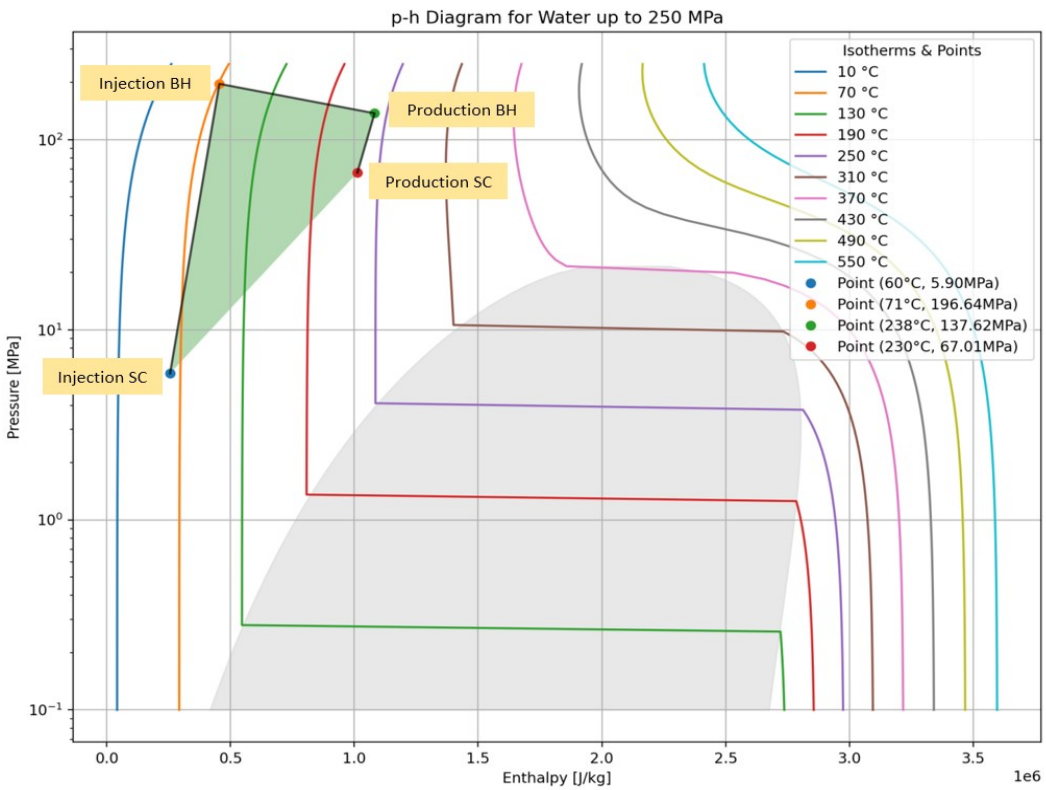

Figure 4.27: EGS Model – P-h Diagram for Water up to 250 MPa

The EGS Wells model exhibits exceptional efficiency, thanks to its advanced design that improves heat extraction through hydraulic fracturing. This superior performance stems from the EGS model's ability to increase reservoir permeability via hydraulic fracturing, facilitating a more extensive and effective heat extraction process.

It maintains stable temperature and pressure profiles across various formations, indicating it is a reliable option for geothermal energy extraction (Figure 4.28). The high temperatures achieved highlight the potential of EGS technologies in accessing and utilizing deeper and hotter geothermal resources.

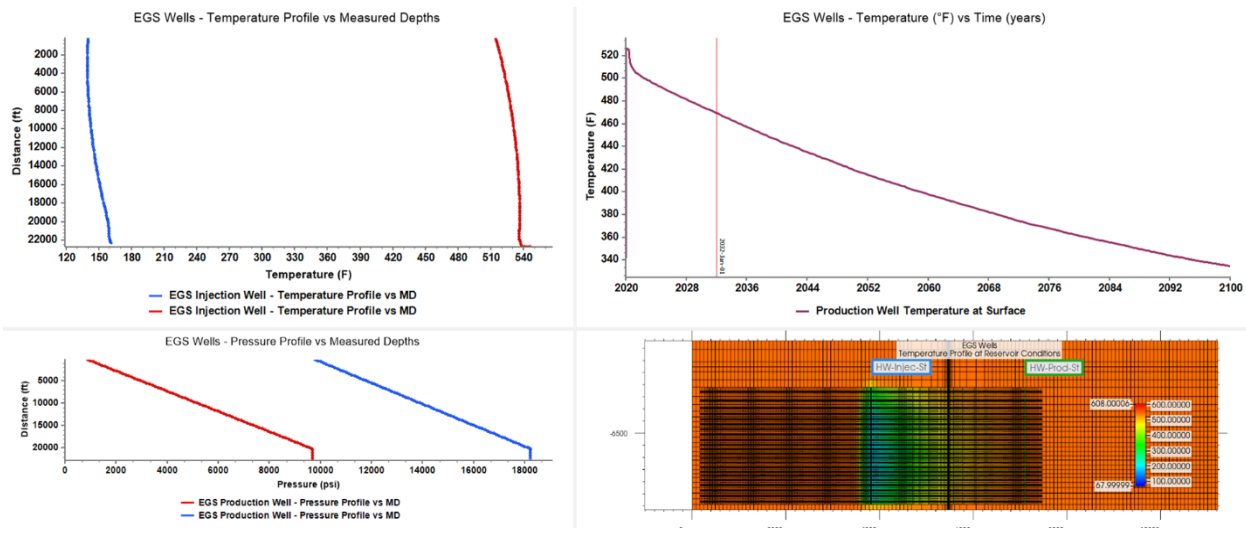

Figure 4.28: Thermal and Pressure Dynamics in EGS Wells Systems: Profiles and Projections

4.6 Long-Term Performance Analysis of Inclined EGS Well Models

The Inclined EGS Wells model has shown remarkable performance in extracting heat from the deepest formations of the Wattenberg formation reservoir model, although at lower temperatures compared to the EGS model. As shown in Figure 4.29, the injected water effectively utilizes all the heat trapped throughout the formation beds surrounding the injection and production wells, including fractures induced by hydraulic fracturing.

The most significant contribution is from the fractures connecting the injection and production wells, where these extended fractures, with high contact areas, absorb heat from the highest reachable depth (6100 m), with the highest temperature recorded (300°C). These extended fractures have significantly increased the contact between the injected fluid and the

targeted formation, making it an excellent configuration compared to Closed-loop systems, but less favorable when compared with the EGS model.

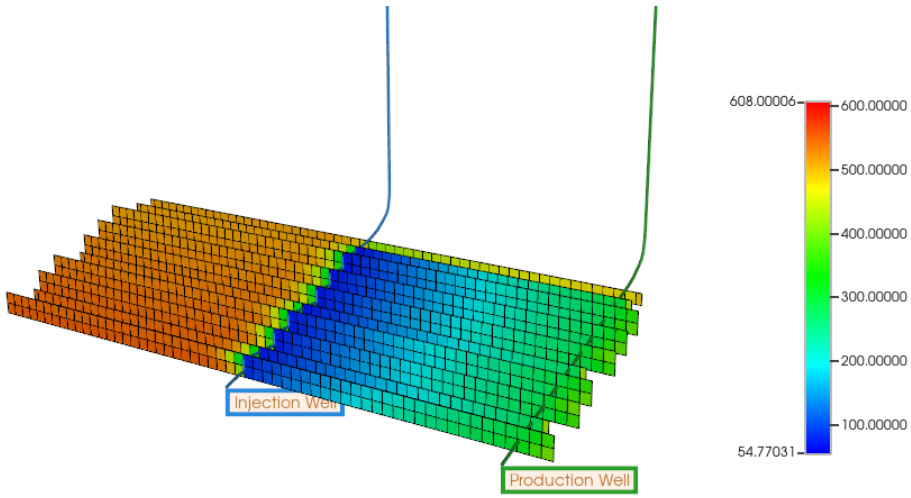

Figure 4.29: Inclined EGS Well Reservoir Model (After 80 years)

After 20 years of simulation, this model exhibited a final temperature of 425°F (Figure 4.30). This temperature value will be analyzed in relation to the injected fluid's temperature (140°C) to provide a comprehensive interpretation of the amount of heat gained from these configurations.

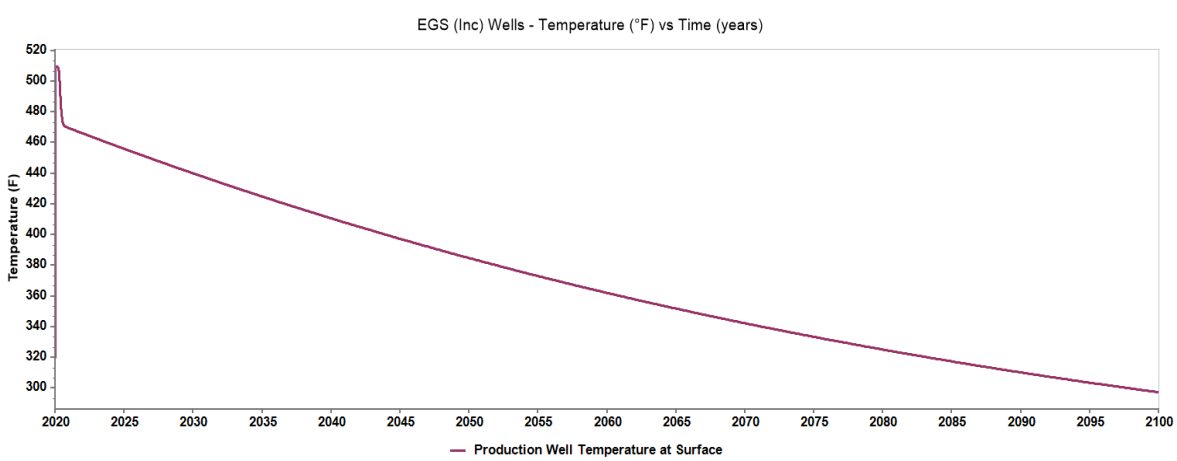

Figure 4.30: EGS Wells – Temperature (°F) vs Time (years)

Evaluating the temperature profile across different wells at various depths is crucial for understanding where temperature dissipation occurs predominantly and how much the temperature increases from one well to another. As depicted in Figure 4.31, the temperature profiles of the geothermal wells converge at the bottom. This convergence occurs because the fractures do not extend to the well's tip, resulting in an undisturbed section where the temperature remains constant. Notably, a significant disparity is observed between the temperature profiles of the two wells, highlighting the effectiveness of the Enhanced Geothermal System (EGS) model in heat extraction. This is evidenced by the substantial difference in the bottom hole temperature of each well, in contrast to the results typically seen in Closed-Loop geothermal systems.

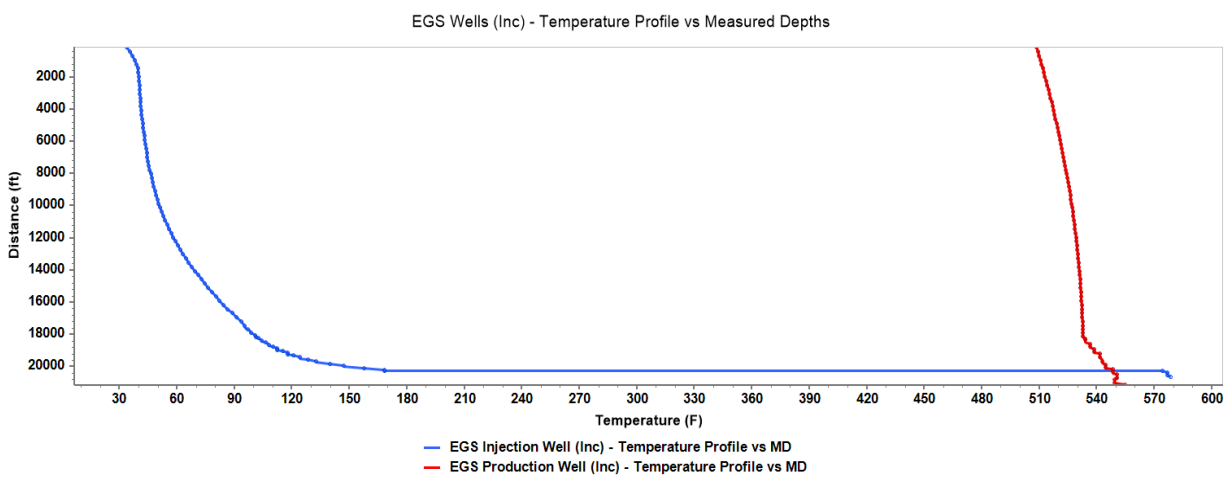

Figure 4.31: Inclined EGS Wells – Temperature Profile (°F) vs Depth (ft)

Compared to the EGS model, a disturbance in the temperature profiles in the wellbore area is noticeable, indicating an unsteady increase in temperature due to the inclination of the wellbore configuration. This suggests that the temperature is not steady across the wellbore area;

however, there is effective contact between the injected water and the reservoir formation, resulting in very high temperature production at the surface.

Building upon the fluid strategies of our prior designs, the Inclined Enhanced Geothermal System (Inclined EGS) employs water as the exclusive thermal medium. The expanded P-h Diagram for water up to 250 MPa (Figure 4.32) not only confirms this uniformity but also reflects a wider operational window afforded by the Inclined EGS model's robust geometry. It affirms that within this model, water reliably remains in its liquid phase across a broader range of thermodynamic conditions, underscoring the system's versatility.

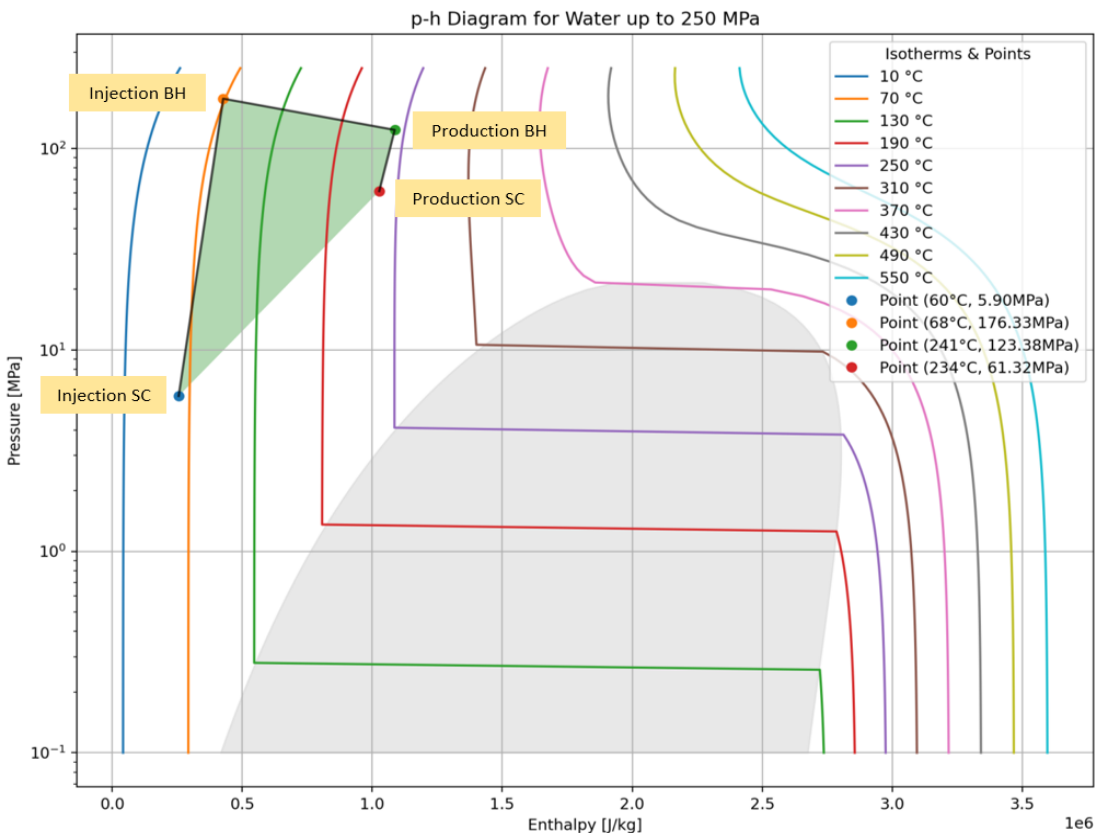

Figure 4.32: Inclined EGS Model – P-h Diagram for Water up to 250 MPa

The Inclined EGS Wells model exhibits exceptional efficiency, credited to its advanced design that improves heat extraction through hydraulic fracturing. Although its performance is

lower than the standard EGS model, the superior efficiency of the Inclined EGS model stems from its capacity to enhance reservoir permeability via hydraulic fracturing. This allows for a comprehensive and effective heat extraction process while maintaining stable temperature and pressure profiles across various formations. It presents another reliable option for geothermal energy extraction (Figure 4.33).

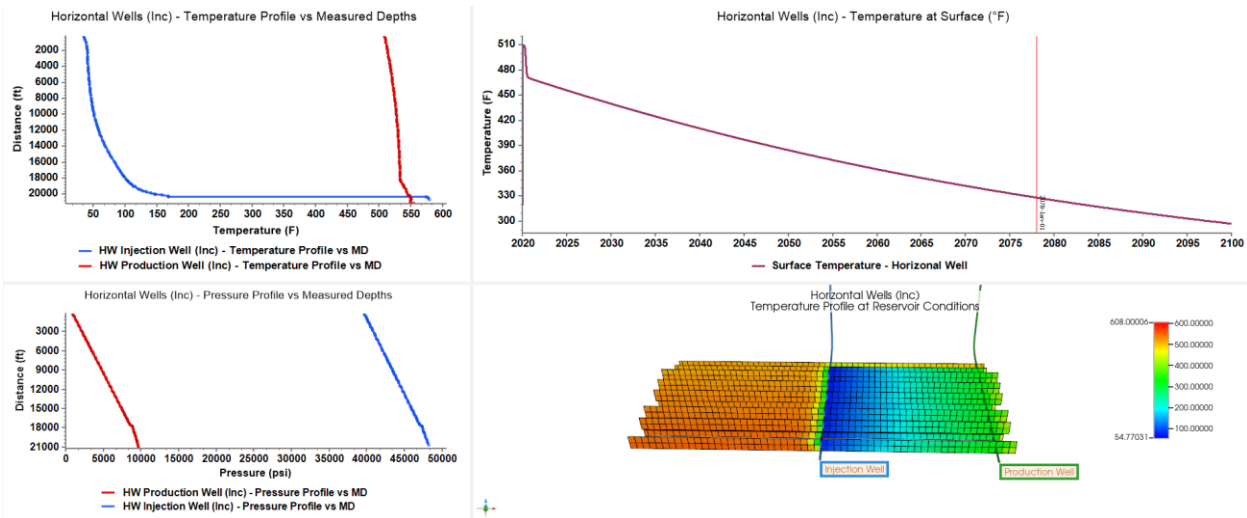

Figure 4.33: Thermal and Pressure Dynamics in Inclined EGS Wells Systems: Profiles and Projections

The inclined design, akin to the Inclined V-Shaped model, is a strategic choice to navigate drilling obstacles. Although its efficiency is reduced compared to the non-inclined counterpart, this model demonstrates the feasibility and potential effectiveness of inclined designs in exploiting geothermal energy under challenging conditions.

4.7 Comparison of Closed-Loop Systems

The following plot illustrates the temperature outcomes after 20 years for the U-Shaped, V-Shaped, Inclined V-Shaped, and PIP Closed Loop Wells (Figure 4.34).

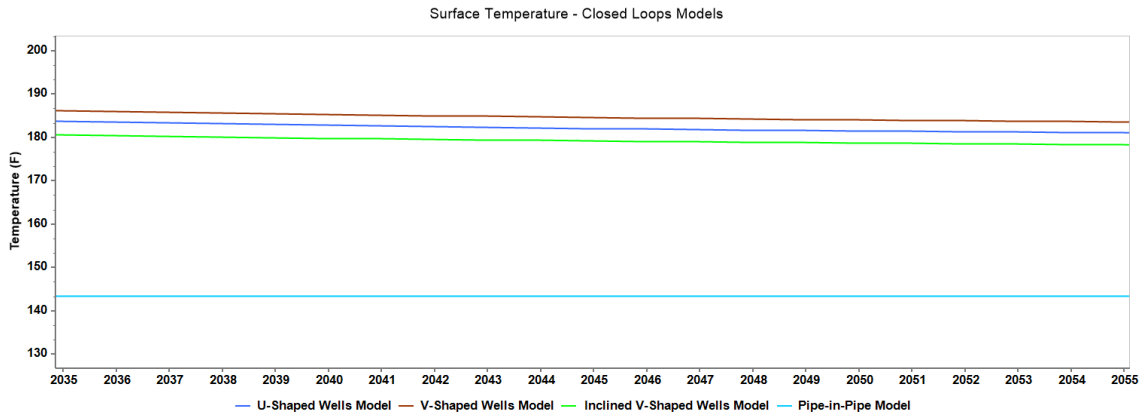

Figure 4.34: Temperature Comparison of Closed-Loop Well Configurations after 20 Years

This visual representation highlights the relatively narrow temperature range within which the closed-loop systems operate, underscoring the V-Shaped model's slight thermal advantage. The plot clarifies the trade-offs between system simplicity and efficiency, where even minor design adjustments can lead to measurable differences in performance.

4.8 Comparison of EGS Systems

The following plot focuses on the performance of the EGS and Inclined EGS Wells, showcasing their significantly higher temperatures compared to the closed-loop systems (Figure 4.35).

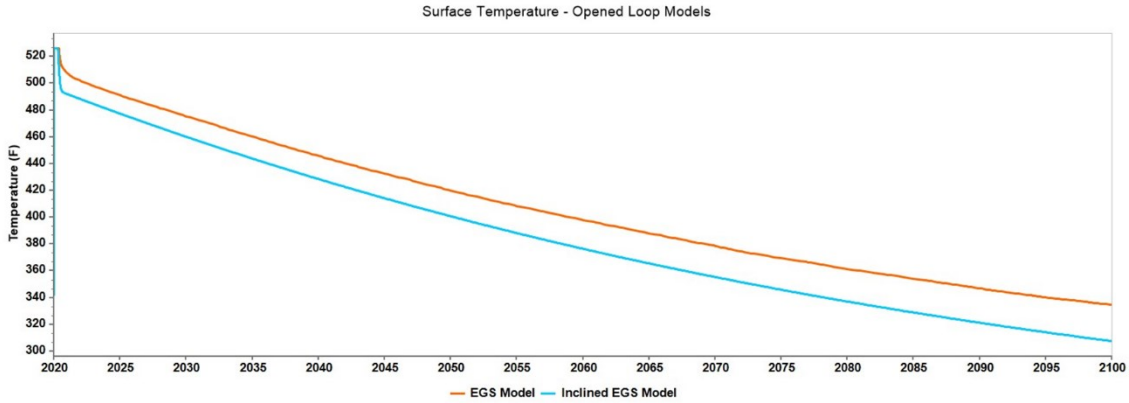

Figure 4.35: Temperature Outcomes of EGS and Inclined EGS Wells after 20 Years

By comparing these two models directly, the plot reveals the impact of inclining the wells to circumvent drilling challenges, a necessity that slightly compromises the system's thermal efficiency. Despite this, both EGS configurations far exceed the thermal performance of their closed-loop counterparts, affirming the potential of EGS technology in exploiting deeper geothermal resources.

4.9 Overall Performance Comparison

The following plot consolidates the temperature data for all models, providing a comprehensive overview of the study's findings (Figure 4.36).

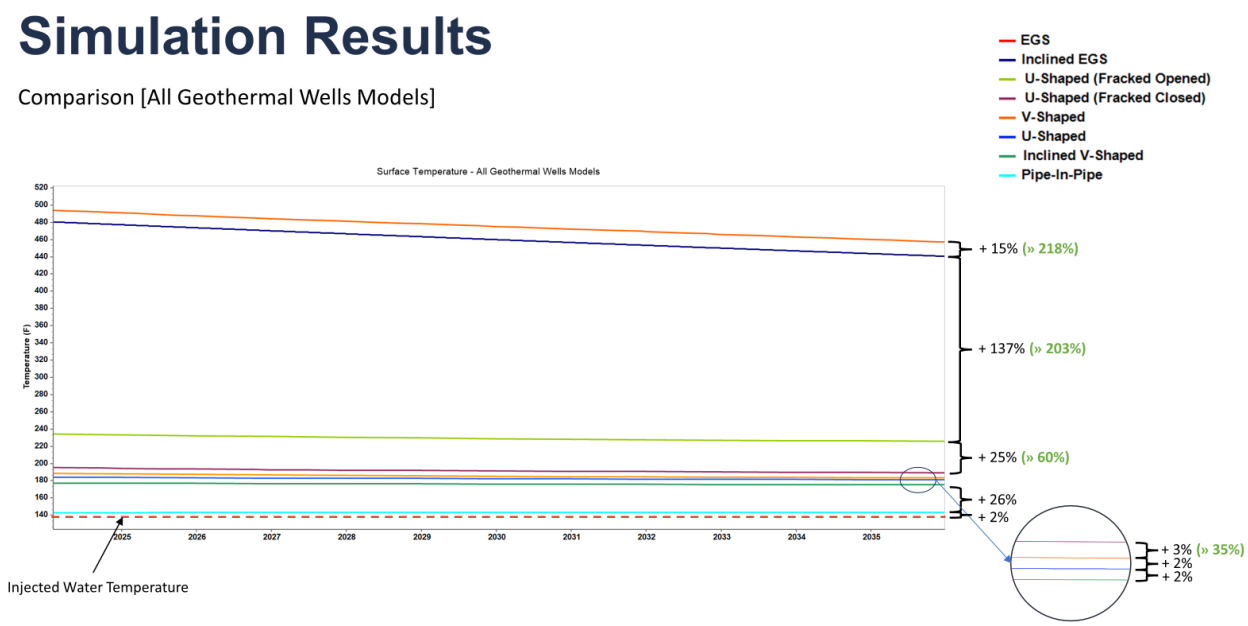

Figure 4.36: Overall Temperature Comparison of All Geothermal Well Configurations after 20 Years

This aggregate view facilitates a direct comparison across all models, highlighting the stark contrast between the closed-loop and EGS systems. It serves as a potent visual summary of the research findings, illustrating the wide spectrum of performance across the different geothermal well configurations studied.

The delta temperature (ΔT) values extracted from the well models, when assessed against the injected water temperature of 140°F, display varying levels of thermal efficiency among the different configurations. The U-Shaped, V-Shaped, and Inclined V-Shaped models offer moderate temperature gains between +39°F and +45°F.

Notably, the U-Shaped Fracked High-Conductivity models further differentiate themselves with the incorporation of fracturing processes. The U-Shaped (Fracked Closed) configuration enhances this performance slightly to +49°F, while the introduction of high-conductivity materials in the U-Shaped (Fracked Opened) model markedly improves the temperature gain to +85°F. This methodological improvement in the U-Shaped configurations underscores the efficacy of targeted modifications in closed-loop systems.

Conversely, the Pipe-in-Pipe model exhibits a marginal increase of +3°F, pointing to its comparatively limited thermal efficiency and suggesting a higher susceptibility to thermal losses. In sharp contrast, the EGS models, both standard and inclined, show exceptional thermal gains of +306°F and +285°F, respectively.

These substantial temperature increments underscore the EGS models' advanced capacity for high-temperature capture and their significant potential in the realm of geothermal energy exploitation. This comparative analysis not only reaffirms the superior performance of EGS systems but also illustrates the tangible benefits of enhancing closed-loop systems through fracturing and material innovation (Table 4.1).

Table 4.1: Well Models Temperature Performance Comparison

Well Model	Surface Temperature (°F)	ΔT (°F)
Pipe-in-Pipe	143	+3
Inclined V-Shaped	179	+39
U-Shaped	182	+42
V-Shaped	185	+45
U-Shaped (Fracked Closed)	189	+49
U-Shaped (Fracked Opened)	225	+85
Inclined EGS	425	+285
EGS	446	+306

The analysis of the simulation results reveals significant variations in temperature performance across different geothermal well configurations. While traditional closed-loop systems offer a range of efficiencies, EGS technologies demonstrate a superior capability in harnessing high-temperature geothermal resources.

However, the choice of system design must consider various factors, including geological conditions, technical challenges, and cost-effectiveness. The insights derived from this analysis contribute to a deeper understanding of the potential and limitations of various geothermal energy extraction techniques, guiding future research and development efforts in this promising renewable energy sector.

CHAPTER 5
CONCLUSION

This thesis conducts a thorough numerical modeling investigation of various geothermal well configurations within the Wattenberg formation of the DJ Basin, with a focus on evaluating their thermal efficiency and potential for electricity generation. These configurations range from traditional Closed-Loop Geothermal (CLG) setups, such as pipe-in-pipe and U-shaped designs, to more innovative systems, including a hybrid model that combines closed-loop concepts with open-loop features through induced hydraulic fracturing and the injection of high-conductivity materials. The CLG models evaluated include the conventional Pipe-in-Pipe, U-Shaped, V-Shaped, and Inclined V-Shaped designs. In contrast, the EGS category comprises the standard EGS and an Inclined EGS configuration. These models, each with their unique operational dynamics, were assessed for their ability to transfer heat from the hot geothermal reservoir rocks to the working fluid that remains isolated from direct contact with the rock formations. By simulating the working fluid's interaction with the reservoir rock, primarily via heat conduction, this study provides a detailed assessment of heat transfer mechanisms across diverse well designs.

Utilizing the advanced capabilities of CMG-STARS thermal reservoir simulation software, the models were meticulously calibrated and validated against existing analytical and field results to establish their accuracy. The software's advanced capabilities allowed for the accurate reproduction of the results from leading studies in the field, with minor deviations that underscore its precision and reliability.

For the EGS configurations, our research drew from the pivotal work of Norbeck and Latimer (2023), who set a commercial-scale benchmark for EGS efficacy. By comparing our

CMG-STARS simulations with the real-world data from their study, we achieved a remarkable correlation, with a mere 3% deviation in surface temperature measurements at the production well. This validation establishes the robustness of our CMG model and affirms its potential for broader application in EGS scenarios.

In the realm of CLG configurations, particularly the U-Shaped models, our study engaged with the work of Kaveh Amini from our institution. Amini's innovative approach to reservoir configurations and operational methodologies provided a solid foundation for our simulations. The comparative analysis revealed a close match with Amini's findings, with a minor 3% difference in surface temperature, underscoring the veracity of our CMG simulations. This validation not only reinforces the credibility of our U-Shaped model simulations but also signifies the advancement of our understanding in optimizing geothermal extraction techniques.

Our research within the DJ Basin's Wattenberg formation has provided a comprehensive evaluation of thermal efficiencies across the diverse array of geothermal well configurations. By comparing the delta temperature (ΔT) values against a baseline injected water temperature of 140°F, the study has distinguished clear performance disparities among the different models. The Closed-Loop Geothermal (CLG) systems in the DJ Basin's Wattenberg formation, encompassing U-Shaped, V-Shaped, and Inclined V-Shaped configurations, have demonstrated moderate thermal performance. The Inclined V-Shaped model, while only slightly underperforming the U-Shaped and V-Shaped models by 2% and 4% respectively, suggests that if CLG systems were to be considered, the Inclined V-Shaped could be a more favorable choice due to drilling efficiencies. Yet, it's crucial to understand that despite the drilling advantages, these CLG models do not fulfill the higher thermal requirements needed for electricity generation in this region.

A noteworthy enhancement within the CLG systems was achieved through the novel introduction of a Hybrid system, which integrates the principles of closed-loop systems with the strategic induction of hydraulic fractures filled with highly conductive materials. This advancement has notably improved the performance of U-Shaped models, with the Fracked High-Conductivity variants registering significant increases in ΔT values. The U-Shaped (Fracked Closed) and U-Shaped (Fracked Opened) models showed increases of +49°F and +85°F respectively, highlighting the effectiveness of targeted enhancements in thermal conductivity within closed-loop systems. The dynamics of fractures in these Hybrid systems have had a positive impact on outcomes, with opened fractures in particular significantly enhancing U-shaped model performance, evidenced by a 30% increase in surface temperature.

Expanding upon the closed-loop models, our investigation also encompassed Enhanced Geothermal Systems (EGS) configurations. Both the standard EGS and the Inclined EGS exhibited remarkable ΔT values of +306°F and +285°F, respectively, illustrating an exceptional capacity for heat extraction that could be advantageous in deeper and more geologically complex reservoirs. These opened-loop models are highly suitable for electricity generation within the DJ Basin's Wattenberg formation. Although the inclined EGS configuration offered decent outcomes, they did not surpass the EGS's ability to reach deep formation temperatures.

The superior performance of these EGS models, however, comes with the challenge of adapting to the intricate geological formations within the DJ Basin. Their implementation requires a detailed scientific and technical approach to ensure that their pronounced thermal gains are effectively translated into sustainable energy output. The efficient EGS model, while promising, poses technical challenges including fracture closure and fluid loss, which strongly advise the conduction of detailed microseismic studies to fully understand their impact.

CHAPTER 6
FUTURE IMPLICATIONS

The findings of this research pave the way for several promising avenues in the advancement of geothermal energy extraction technologies. The future implications drawn from the study are multifaceted and suggest a strategic roadmap for the evolution of this renewable energy source.

1. Advanced Open-Fracture Stimulation Methods: Given the significant impact of open fractures on thermal efficiency, developing sophisticated methods to stimulate open-fracture networks could revolutionize energy capture in geothermal systems.
2. Cost-Benefit Analysis of EGS: The economic viability of EGS technologies, particularly in complex formations like the DJ Basin, requires a detailed analysis of the investment versus the output over time. This will encompass not only the initial capital expenditure but also operational costs, lifespan, and potential subsidies or incentives for renewable energy projects.
3. Supercritical Fluids in Geothermal Extraction: Investigating the use of supercritical fluids could unlock new potentials in geothermal energy production. These fluids have unique properties that can significantly increase energy extraction efficiency, but they require robust containment and control methods to be viable.
4. Machine Learning for Reservoir Performance Prediction: Machine learning offers a powerful tool for predicting geothermal reservoir performance. By leveraging large datasets and advanced algorithms, predictive models can be developed to optimize well placement, extraction rates, and system design, leading to smarter, more efficient geothermal energy production.

REFERENCES

Abdelrahman K, Ekwok SE, Ulem CA, Eldosouky AM, Al-Otaibi N, Hazaea BY, Hazaea SA, Andráš P, Akpan AE. 2023. Exploratory Mapping of the Geothermal Anomalies in the Neoproterozoic Arabian Shield, Saudi Arabia, Using Magnetic Data. *Minerals*, **13**(5), 694. https://doi.org/10.3390/min13050694.

Algieri A, Šebo J. 2017. Energetic Investigation of Organic Rankine Cycles (ORCs) for the Exploitation of Low-Temperature Geothermal Sources – A Possible Application in Slovakia. *Procedia Computer Science*, **109**(January), 833–40. https://doi.org/10.1016/j.procs.2017.05.348.

Altun AF, Kilic M. 2020. Thermodynamic Performance Evaluation of a Geothermal ORC Power Plant. *Renewable Energy*, **148**(April), 261–74. https://doi.org/10.1016/j.renene.2019.12.034.

Amini, S. (2023). Personal communication. [Discussion on the modeling approach for U-shaped geothermal wells, February 5, 2024].

Andrés S, Santillán D, Mosquera JC, Cueto-Felgueroso L. 2022. Hydraulic Stimulation of Geothermal Reservoirs: Numerical Simulation of Induced Seismicity and Thermal Decline. *Water*, **14**(22), 3697. https://doi.org/10.3390/w14223697.

Axelsson G. 2010. Sustainable Geothermal Energy Utilization. *International Review of Applied Sciences and Engineering*, **1**(1–2), 21–30. https://doi.org/10.1556/irase.1.2010.1-2.4.

Beckers KF, Lukawski MZ, Anderson BJ, Moore MC, Tester JW. 2014. Levelized Costs of Electricity and Direct-Use Heat from Enhanced Geothermal Systems. *Journal of Renewable and Sustainable Energy*, **6**(1), 013141. https://doi.org/10.1063/1.4865575.

Briola S, Gabbrielli R, Bischi A. 2019. Off-Design Performance Analysis of a Novel Hybrid Binary Geothermal-Biomass Power Plant in Extreme Environmental Conditions. *Energy Conversion and Management*, **195**(September), 210–25. https://doi.org/10.1016/j.enconman.2019.05.008.

Bu X, Jiang K, Li H. 2019. Performance of Geothermal Single Well for Intermittent Heating. *Energy*, **186**(November), 115858. https://doi.org/10.1016/j.energy.2019.115858.

Chen G, Jiao JJ, Jiang C, Luo X. 2024. Surrogate-Assisted Level-Based Learning Evolutionary Search for Geothermal Heat Extraction Optimization. *Renewable and Sustainable Energy Reviews*, **189**(January), 113860. https://doi.org/10.1016/j.rser.2023.113860.

Cheng Y, Zhang Y, Yu Z, Hu Z, Ma Y, Yang Y. 2021. Experimental and Numerical Studies on Hydraulic Fracturing Characteristics with Different Injection Flow Rates in Granite Geothermal Reservoir. *Energy Science & Engineering*, **9**(1), 142–68. https://doi.org/10.1002/ese3.816.

Clauser C. 2006. The Earth's Thermal Regime. In *Renewable Energy*, Heinloth K (ed.), 3C:493–548. Springer Berlin Heidelberg. https://doi.org/10.1007/10858992_17.

Colorado Geological Survey, Department of Natural Resources. 2010. Interpretive Geothermal Gradient Map of Colorado. *Colorado Geological Survey*. https://coloradogeologicalsurvey.org/publications/interpretive-geothermal-gradient-map-colorado.

Computer Modelling Group Ltd. 2024. STARS. https://www.cmgl.ca/solutions/software/stars/.

Coskun C, Oktay Z, Dincer I. 2011. Performance Evaluations of a Geothermal Power Plant. *Applied Thermal Engineering*, **31**(17), 4074–82. https://doi.org/10.1016/j.applthermaleng.2011.08.013.

Cremer GM. 1981. Hot Dry Rock Geothermal Energy Development Program. Annual Report, Fiscal Year 1980. LA-8855-HDR, *Los Alamos National Lab*. (LANL), Los Alamos, NM (United States). https://doi.org/10.2172/6073244.

Cui G, Ren S, Zhang L, Ezekiel J, Enechukwu C, Wang Y, Zhang R. 2017. Geothermal Exploitation from Hot Dry Rocks via Recycling Heat Transmission Fluid in a Horizontal Well. *Energy*, **128**(June), 366–77. https://doi.org/10.1016/j.energy.2017.04.027.

De Souza R, Casisi M, Micheli D, Reini M. 2021. A Review of Small–Medium Combined Heat and Power (CHP) Technologies and Their Role within the 100% Renewable Energy Systems Scenario. *Energies*, **14**(17), 5338. https://doi.org/10.3390/en14175338.

DiPippo R. 2016. Chapter 8 - Binary Cycle Power Plants. In *Geothermal Power Plants* (Fourth Edition), Ronald DiPippo (ed.), 193–239. Oxford: Butterworth-Heinemann. https://doi.org/10.1016/B978-0-08-100879-9.00008-2.

EnvGeo EGS, Inc. 2020. Publications. *EnvGeo* (blog). https://envgeo.com/publications/.

Erkan K, Holdmann G, Benoit W, Blackwell D. 2008. Understanding the Chena Hot Springs, Alaska, Geothermal System Using Temperature and Pressure Data from Exploration Boreholes. *Geothermics*, **37**(6), 565–85. https://doi.org/10.1016/j.geothermics.2008.09.001.

Fournier RO. 1999. Hydrothermal Processes Related to Movement of Fluid from Plastic into Brittle Rock in the Magmatic-Epithermal Environment. *Economic Geology*, **94**(8), 1193–1211. https://doi.org/10.2113/gsecongeo.94.8.1193.

Frash LP, Meng M, K C BJ. 2024. Greenfield Reservoir Engineering for the Wattenberg Field with Comparison of Advanced, Enhanced, and Caged Geothermal Systems. Presented at the 49th Workshop on Geothermal Reservoir Engineering, Stanford University, Stanford, California, 12–14 February. SGP-TR-227.

Glassley WE. 2010. Geothermal Energy: Renewable Energy and the Environment. Boca Raton: CRC Press. https://doi.org/10.1201/EBK1420075700.

Gunatilake T. 2023. Dynamics between Earthquakes, Volcanic Eruptions, and Geothermal Energy Exploitation in Japan. *Scientific Reports*, **13**(1), 4625. https://doi.org/10.1038/s41598-023-31627-3.

Hoteit H, He X, Yan B, Vahrenkamp V. 2023. Uncertainty Quantification and Optimization Method Applied to Time-Continuous Geothermal Energy Extraction. *Geothermics*, **110**(May), 102675. https://doi.org/10.1016/j.geothermics.2023.102675.

Hu B, Guo J, Yang Y, Shao Y. 2022. Experimental Study on Horizontal Tube Spray Falling Film Evaporator in a Low Temperature Geothermal Binary Cycle Power System. *Energy Reports*, **8**(June), 187–93. https://doi.org/10.1016/j.egyr.2022.01.092.

Huang W, Cao W, Jiang F. 2018. A Single-Well Geothermal System for Hot Dry Rock Geothermal Energy Exploitation. *Energy*, **162**(August), 630. https://doi.org/10.1016/j.energy.2018.08.055.

Ibrahim TK, Basrawi F, Awad OI, Abdullah AN, Najafi G, Mamat R, Hagos FY. 2017. Thermal Performance of Gas Turbine Power Plant Based on Exergy Analysis. *Applied Thermal Engineering*, **115**(March), 977–85. https://doi.org/10.1016/j.applthermaleng.2017.01.032.

Jiang H, Guo L, Kang F, Wang F, Cao Y, Sun Z, Shi M. 2023. Geothermal Characteristics and Productivity Potential of a Super-Thick Shallow Granite-Type Enhanced Geothermal System: A Case Study in Wendeng Geothermal Field, China. *Sustainability*, **15**(February), 3551. https://doi.org/10.3390/su15043551.

Kazemi AR, Mahbaz SB, Dehghani-Sanij AR, Dusseault MB, Fraser R. 2019. Performance Evaluation of an Enhanced Geothermal System in the Western Canada Sedimentary Basin. *Renewable and Sustainable Energy Reviews*, **113**(October), 109278. https://doi.org/10.1016/j.rser.2019.109278.

Lei Z, Zhang Y, Zhang S, Fu L, Hu Z, Yu Z, Li L, Zhou J. 2020. Electricity Generation from a Three-Horizontal-Well Enhanced Geothermal System in the Qiabuqia Geothermal Field, China: Slickwater Fracturing Treatments for Different Reservoir Scenarios. *Renewable Energy*, **145**(January), 65–83. https://doi.org/10.1016/j.renene.2019.06.024.

Liu C, Gao T, Zhu J, Xu J. 2016. Performance Optimization and Economic Analysis of Geothermal Power Generation by Subcritical and Supercritical Organic Rankine Cycles. In *American Society of Mechanical Engineers Digital Collection*. https://doi.org/10.1115/GT2016-56821.

Majer EL, Baria R, Stark M, Oates S, Bommer J, Smith B, Asanuma H. 2007. Induced Seismicity Associated with Enhanced Geothermal Systems. *Geothermics*, **36**(3), 185–222. https://doi.org/10.1016/j.geothermics.2007.03.003.

Manente G, Da Lio L, Lazzaretto A. 2016. Influence of Axial Turbine Efficiency Maps on the Performance of Subcritical and Supercritical Organic Rankine Cycle Systems. *Energy*, **107**(July), 761–72. https://doi.org/10.1016/j.energy.2016.04.063.

Massachusetts Institute of Technology (ed). 2006. The Future of Geothermal Energy: Impact of Enhanced Geothermal Systems (EGS) on the United States in the 21st Century: An Assessment. Cambridge, Mass.: *Massachusetts Institute of Technology*.

Mines G. 2016. Binary Geothermal Energy Conversion Systems: Basic Rankine, Dual–Pressure, and Dual–Fluid Cycles. In *Geothermal Power Generation*, Ronald DiPippo (ed.), 353–89. Woodhead Publishing. https://doi.org/10.1016/B978-0-08-100337-4.00013-9.

Montesdeoca-Martínez F, Velázquez-Medina S. 2023. Geothermal Energy Exploitation in an Island-Based 100% Renewables Strategy. Case Study of Tenerife (Spain). *Journal of Cleaner Production*, **426**(November), 139139. https://doi.org/10.1016/j.jclepro.2023.139139.

Morrone P, Algieri A. 2020. Integrated Geothermal Energy Systems for Small-Scale Combined Heat and Power Production: Energy and Economic Investigation. *Applied Sciences*, **10**(19), 6639. https://doi.org/10.3390/app10196639.

Moska R, Labus K, Kasza P, Moska A. 2023. Geothermal Potential of Hot Dry Rock in South-East Baltic Basin Countries—A Review. *Energies*, **16**(4), 1662. https://doi.org/10.3390/en16041662.

Nasruddin N, Saputra ID, Mentari T, Bardow A, Marcelina O, Berlin S. 2020. Exergy, Exergoeconomic, and Exergoenvironmental Optimization of the Geothermal Binary Cycle Power Plant at Ampallas, West Sulawesi, Indonesia. *Thermal Science and Engineering Progress*, **19**(October), 100625. https://doi.org/10.1016/j.tsep.2020.100625.

Nondy J, Gogoi TK. 2021. Exergoeconomic Investigation and Multi-Objective Optimization of Different ORC Configurations for Waste Heat Recovery: A Comparative Study. *Energy Conversion and Management*, **245**(October), 114593. https://doi.org/10.1016/j.enconman.2021.114593.

Norbeck JH, Latimer T. 2023. Commercial-Scale Demonstration of a First-of-a-Kind Enhanced Geothermal System. *EarthArXiv*. https://eartharxiv.org/repository/view/5704 (preprint; published July 18, 2023).

Panchuk K. 2019. Earth's Interior Heat. https://openpress.usask.ca/physicalgeology/chapter/3-3-earths-interior-heat/. (accessed 5 November 2023).

Pratama H, Saptadji N. 2021. Study of Production-Injection Strategies for Sustainable Production in Geothermal Reservoir Two-Phase by Numerical Simulation. *Indonesian Journal on Geoscience*, **8**(April), 25–38.

Robson SG, Banta ER. 1987. Geology and Hydrology of the Deep Bedrock Aquifers in Eastern Colorado. *Water-Resources Investigations Report*, **85**–4240. U.S. Geological Survey. https://doi.org/10.3133/wri854240.

Simmons SF, Allis RG, Kirby SM, Moore JN, Fischer TP. 2021. Interpretation of Hydrothermal Conditions, Production-Injection Induced Effects, and Evidence for Enhanced

Geothermal System-Type Heat Exchange in Response to >30 Years of Production at Roosevelt Hot Springs, Utah, USA. *Geosphere*, **17**(6), 1997–2026. https://doi.org/10.1130/GES02348.1.

Song X, Shi Y, Li G, Shen Z, Hu X, Lyu Z, Zheng R, Wang G. 2018. Numerical Analysis of the Heat Production Performance of a Closed Loop Geothermal System. *Renewable Energy*, **120**(May), 365–78. https://doi.org/10.1016/j.renene.2017.12.065.

Song X, Shi Y, Li G, Yang R, Wang G, Zheng R, Li J, Lyu Z. 2018. Numerical Simulation of Heat Extraction Performance in Enhanced Geothermal System with Multilateral Wells. *Applied Energy*, **218**(May), 325–37. https://doi.org/10.1016/j.apenergy.2018.02.172.

Sun F, Yao Y, Li G, Li X. 2018. Geothermal Energy Development by Circulating CO2 in a U-Shaped Closed Loop Geothermal System. *Energy Conversion and Management*, **174**(October), 971–82. https://doi.org/10.1016/j.enconman.2018.08.094.

Sun ZX, Zhang X, Xu Y, Yao J, Wang HX, Lv S, Sun ZL, Huang Y, Cai MY, Huang X. 2017. Numerical Simulation of the Heat Extraction in EGS with Thermal-Hydraulic-Mechanical Coupling Method Based on Discrete Fractures Model. *Energy*, **120**(February), 20–33. https://doi.org/10.1016/j.energy.2016.10.046.

Vivas C, Salehi S, Nygaard R, Rehg D. 2023. Scalable Geothermal Energy Potential from Sedimentary Basins and Leveraging Oil and Gas Industry Experience: Case Studies from Texas Gulf Coast. In *OnePetro*. https://doi.org/10.4043/32381-MS.

Wang G, Song X, Shi Y, Zheng R, Li J, Li Z. 2020. Production Performance of a Novel Open Loop Geothermal System in a Horizontal Well. *Energy Conversion and Management*, **206**(February), 112478. https://doi.org/10.1016/j.enconman.2020.112478.

Won J, Choi HJ, Lee H, Choi H. 2016. Numerical Investigation on the Effect of Cementing Properties on the Thermal and Mechanical Stability of Geothermal Wells. *Energies*, **9**(12), 1016. https://doi.org/10.3390/en9121016.

Xiao D, Chen W, Li L, Gao R, Yang R, Tang H, Li G. 2022. Techno-Economic Coupling Model of U-Shaped Closed-Loop Geothermal System. *Geothermics*, **105**(November), 102540. https://doi.org/10.1016/j.geothermics.2022.102540.

Xu T, Zhao Y, Zhao J, Zhang L, Liu S, Liu Z, Feng B, Feng G, Yue G. 2021. Heat Extraction Performance and Optimization for a Doublet-Well Geothermal System in Dezhou, China. *Energy Exploration & Exploitation*, **40**(September), 014459872110435. https://doi.org/10.1177/01445987211043578.

Ye H, Wu X, Guo G, Li D, Jiang Y. 2022. A Novel Wellbore-Wall Heating Method without External Energy Injection for Natural Gas Hydrate Production—A Heat Transfer Device. *Journal of Marine Science and Engineering*, **10**(6), 799. https://doi.org/10.3390/jmse10060799.

Zhai HX, An Q, Shi L. 2014. Preliminary Study on Mixture Working Fluids Design for Low Temperature Geothermal Binary Organic Rankine Cycle. *Journal of Engineering Thermophysics*, **35**(August), 1498–1502.

Zhang C, Feng Q, Zhang L, Qin S, Jiang G, Hu J, Hu S, Huang R, Zhang H. 2022. Characteristics of Radiogenic Heat Production of Widely Distributed Granitoids in Western Sichuan, Southeast Tibetan Plateau. *Lithosphere*, **2022**(1), 4165618. https://doi.org/10.2113/2022/4165618.

Zhang Y, Yu C, Li G, Guo X, Wang G, Shi Y, Peng C, Tan Y. 2019. Performance Analysis of a Downhole Coaxial Heat Exchanger Geothermal System with Various Working Fluids. *Applied Thermal Engineering*, **163**(December), 114317. https://doi.org/10.1016/j.applthermaleng.2019.114317.

Zhu J, Cui Z, Feng B, Ren H, Liu X. 2023. Numerical Simulation of Geothermal Reservoir Reconstruction and Heat Extraction System Productivity Evaluation. *Energies*, **16**(1), 127. https://doi.org/10.3390/en16010127.

APPENDIX A

U-SHAPE CASE .DAT CODE

The following is the code used by CMG-STARS to read and run the U-Shaped model evaluated in Chapter 3. The .dat file shown in this appendix is for the U-Shaped configuration:

```
WPRN FLEXWELL GRID 1
INUNIT SI
WSRF WELL 1
WSRF GRID 1
OUTPRN WELL ALL
OUTSRF GRID PRES TEMP
OUTSRF FLEXLAYER ALL
** ***************************************************************************
** Definition of fundamental cartesian grid
** ***************************************************************************
GRID VARI 141 59 86
KDIR DOWN
DI IVAR
 33*25 23.45849 26.54151 9*25 24.49771 25.50229 11*25 65.34148 60.70843
 45.15225 30.72313 15.49412 9.455536 7.353459 4.220635 1.744516 0.5337693
 1.929242 4.338603 8.275842 9.484993 15.19955 33.58041 45.02962 62.02818
 54.40624 65*25
DJ JVAR
 176.1509 195.1326 180.95 171.1689 142.8038 161.14 136.7701 113.4248
 105.1153 95.86959 54.23617 27.39765 25.25799 13.34987 9.483962 7.421422
 3.828545 6.518665 9.517457 10.4837 22.00102 34.03863 52.70155 50.58076
 53.319 57.23955 64.08638 86.99856 71.46339 70.47914 84.68485 40.83618
 34.14172 45.68966 52.04939 57.07023 74.9779 57.99526 64.52908 68.01714
 76.80607 93.124 108.0698 115.7344 111.9021 104.2376 119.5666 119.1834
 96.95626 126.8479 100.7885 111.9021 93.50723 104.2376 93.124 115.0915
 3*80
DK ALL
 715434*80
DTOP
 8319*0
**  0 = null block, 1 = active block
NULL CON          1
*PLNRFRAC_TEMPLATE 'Planar Template'
   *PLNR_REFINE *INTO  7 7 3
   *BWHLEN 1100
   *IDIR
   *INNERWIDTH 0.6096
```

```
   *WF1 0.001
   *K_CENT 50000
   *KH_TYPE LINEAR
   *KH_TIP 50000 50000
   *KV_TYPE LINEAR
   *KV_TIP 50000 50000
   *HEIGHTUP 50
   *HEIGHTDOWN 50
   *POR MATRIX *FZ 0.0016
*END_TEMPLATE
POR CON         0.01
*MOD
  67:67 17:17 1:1   = 0.996
  67:67 17:17 77:77   = 0.996
  67:67 17:17 1:1   = 0.01
PERMI CON        1E-06
*MOD
  67:67 17:17 1:1   = 10000
  67:67 17:17 77:77   = 10000
  67:67 17:17 1:1   = 1e-06
PERMJ  EQUALSI
PERMK  EQUALSI
**  0 = pinched block, 1 = active block
PINCHOUTARRAY CON            1
*NFZG-ALIGN ON
END-GRID
ROCKTYPE 1
CPOR 4.35e-7
ROCKCP 2667500 0
THCONR 252720
THCONW 53500
** Model and number of components
MODEL 1 1 1 1
COMPNAME 'H2O'
CMM
0
PCRIT
0
TCRIT
0
MASSDEN
1000
AVISC
0.0047352
BVISC
1515.7
```

```
ROCKFLUID
RPT 1 WATWET
**      Sw      krw     krow
SWT

0       0       1
1       1       0
**      Sl      krg     krog
SLT

0       1       0
1       0       1
INITIAL
VERTICAL OFF

INITREGION 1
REFPRES 5820
REFDEPTH 5820
PRES KVAR
 800 1600 2400 3200 4000 4800 5600 6400 7200 8000 8800 9600 10400 11200
 12000 12800 13600 14400 15200 16000 16800 17600 18400 19200 20000
 20800 21600 22400 23200 24000 24800 25600 26400 27200 28000 28800
 29600 30400 31200 32000 32800 33600 34400 35200 36000 36800 37600
 38400 39200 40000 40800 41600 42400 43200 44000 44800 45600 46400
 47200 48000 48800 49600 50400 51200 52000 52800 53600 54400 55200
 56000 56800 57600 58400 59200 60000 60800 61600 62400 63200 64000
 64800 65600 66400 67200 68000 68800
TEMP KVAR
 20 23.6842 27.3684 31.0526 34.7368 38.4211 42.1053 45.7895 49.4737
 53.1579 56.8421 60.5263 64.2105 67.8947 71.5789 75.2632 78.9474 82.6316
 86.3158 90 93.6842 97.3684 101.053 104.737 108.421 112.105 115.789
 119.474 123.158 126.842 130.526 134.211 137.895 141.579 145.263 148.947
 152.632 156.316 160 163.684 167.368 171.053 174.737 178.421 182.105
 185.789 189.474 193.158 196.842 200.526 204.211 207.895 211.579 215.263
 218.947 222.632 226.316 230 233.684 237.368 241.053 244.737 248.421
 252.105 255.789 259.474 263.158 266.842 270.526 274.211 277.895 281.579
 285.263 288.947 292.632 296.316 300 303.684 307.368 311.053 314.737
 318.421 322.105 325.789 329.474 333.158
NUMERICAL
AUTOTUNE ON
RUN
DATE 2020 1 1
DTWELL 0.1
**
WELL  'U-Shaped Inj'
INJECTOR MOBWEIGHT IMPLICIT 'U-Shaped Inj'
```

```
INCOMP  WATER  1.0
TINJW  60.0
QUAL  0.0
PINJW  6875.0
OPERATE  MAX  STW  3000.0  CONT
**        rad  geofac  wfrac  skin
GEOMETRY  K  0.0762  0.249  1.0  0.0
  PERF_FLX     GEOA  'U-Shaped Inj'
** UBA              ff        Status  Connection
   47 17 1        1.0  CLOSED  FLOW-FROM  'SURFACE'  REFLAYER
   47 17 2        1.0  CLOSED  FLOW-FROM  1
   47 17 3        1.0  CLOSED  FLOW-FROM  2
   47 17 4        1.0  CLOSED  FLOW-FROM  3
   47 17 5        1.0  CLOSED  FLOW-FROM  4
   47 17 6        1.0  CLOSED  FLOW-FROM  5
   47 17 7        1.0  CLOSED  FLOW-FROM  6
   47 17 8        1.0  CLOSED  FLOW-FROM  7
   47 17 9        1.0  CLOSED  FLOW-FROM  8
   47 17 10        1.0  CLOSED  FLOW-FROM  9
   47 17 11        1.0  CLOSED  FLOW-FROM  10
   47 17 12        1.0  CLOSED  FLOW-FROM  11
   47 17 13        1.0  CLOSED  FLOW-FROM  12
   47 17 14        1.0  CLOSED  FLOW-FROM  13
   47 17 15        1.0  CLOSED  FLOW-FROM  14
   47 17 16        1.0  CLOSED  FLOW-FROM  15
   47 17 17        1.0  CLOSED  FLOW-FROM  16
   47 17 18        1.0  CLOSED  FLOW-FROM  17
   47 17 19        1.0  CLOSED  FLOW-FROM  18
   47 17 20        1.0  CLOSED  FLOW-FROM  19
   47 17 21        1.0  CLOSED  FLOW-FROM  20
   47 17 22        1.0  CLOSED  FLOW-FROM  21
   47 17 23        1.0  CLOSED  FLOW-FROM  22
   47 17 24        1.0  CLOSED  FLOW-FROM  23
   47 17 25        1.0  CLOSED  FLOW-FROM  24
   47 17 26        1.0  CLOSED  FLOW-FROM  25
   47 17 27        1.0  CLOSED  FLOW-FROM  26
   47 17 28        1.0  CLOSED  FLOW-FROM  27
   47 17 29        1.0  CLOSED  FLOW-FROM  28
   47 17 30        1.0  CLOSED  FLOW-FROM  29
   47 17 31        1.0  CLOSED  FLOW-FROM  30
   47 17 32        1.0  CLOSED  FLOW-FROM  31
   47 17 33        1.0  CLOSED  FLOW-FROM  32
   47 17 34        1.0  CLOSED  FLOW-FROM  33
   47 17 35        1.0  CLOSED  FLOW-FROM  34
   47 17 36        1.0  CLOSED  FLOW-FROM  35
   47 17 37        1.0  CLOSED  FLOW-FROM  36
```

47 17 38	1.0	CLOSED	FLOW-FROM	37
47 17 39	1.0	CLOSED	FLOW-FROM	38
47 17 40	1.0	CLOSED	FLOW-FROM	39
47 17 41	1.0	CLOSED	FLOW-FROM	40
47 17 42	1.0	CLOSED	FLOW-FROM	41
47 17 43	1.0	CLOSED	FLOW-FROM	42
47 17 44	1.0	CLOSED	FLOW-FROM	43
47 17 45	1.0	CLOSED	FLOW-FROM	44
47 17 46	1.0	CLOSED	FLOW-FROM	45
47 17 47	1.0	CLOSED	FLOW-FROM	46
47 17 48	1.0	CLOSED	FLOW-FROM	47
47 17 49	1.0	CLOSED	FLOW-FROM	48
47 17 50	1.0	CLOSED	FLOW-FROM	49
47 17 51	1.0	CLOSED	FLOW-FROM	50
47 17 52	1.0	CLOSED	FLOW-FROM	51
47 17 53	1.0	CLOSED	FLOW-FROM	52
47 17 54	1.0	CLOSED	FLOW-FROM	53
47 17 55	1.0	CLOSED	FLOW-FROM	54
47 17 56	1.0	CLOSED	FLOW-FROM	55
47 17 57	1.0	CLOSED	FLOW-FROM	56
47 17 58	1.0	CLOSED	FLOW-FROM	57
47 17 59	1.0	CLOSED	FLOW-FROM	58
47 17 60	1.0	CLOSED	FLOW-FROM	59
47 17 61	1.0	CLOSED	FLOW-FROM	60
47 17 62	1.0	CLOSED	FLOW-FROM	61
47 17 63	1.0	CLOSED	FLOW-FROM	62
47 17 64	1.0	CLOSED	FLOW-FROM	63
47 17 65	1.0	CLOSED	FLOW-FROM	64
47 17 66	1.0	CLOSED	FLOW-FROM	65
47 17 67	1.0	CLOSED	FLOW-FROM	66
47 17 68	1.0	CLOSED	FLOW-FROM	67
47 17 69	1.0	CLOSED	FLOW-FROM	68
47 17 70	1.0	CLOSED	FLOW-FROM	69
47 17 71	1.0	CLOSED	FLOW-FROM	70
47 17 72	1.0	CLOSED	FLOW-FROM	71
47 17 73	1.0	CLOSED	FLOW-FROM	72
47 17 74	1.0	CLOSED	FLOW-FROM	73
47 17 75	1.0	CLOSED	FLOW-FROM	74
47 17 76	1.0	CLOSED	FLOW-FROM	75
48 17 76	1.0	CLOSED	FLOW-FROM	76
48 17 77	1.0	CLOSED	FLOW-FROM	77
49 17 77	1.0	CLOSED	FLOW-FROM	78
50 17 77	1.0	CLOSED	FLOW-FROM	79
51 17 77	1.0	CLOSED	FLOW-FROM	80
52 17 77	1.0	CLOSED	FLOW-FROM	81
53 17 77	1.0	CLOSED	FLOW-FROM	82

```
   54 17 77        1.0  CLOSED  FLOW-FROM  83
   55 17 77        1.0  CLOSED  FLOW-FROM  84
   56 17 77        1.0  CLOSED  FLOW-FROM  85
   57 17 77        1.0  CLOSED  FLOW-FROM  86
   58 17 77        1.0  CLOSED  FLOW-FROM  87
   59 17 77        1.0  CLOSED  FLOW-FROM  88
   60 17 77        1.0  CLOSED  FLOW-FROM  89
   61 17 77        1.0  CLOSED  FLOW-FROM  90
   62 17 77        1.0  CLOSED  FLOW-FROM  91
   63 17 77        1.0  CLOSED  FLOW-FROM  92
   64 17 77        1.0  CLOSED  FLOW-FROM  93
   65 17 77        1.0  CLOSED  FLOW-FROM  94
   66 17 77        1.0  CLOSED  FLOW-FROM  95
   67 17 77        1.0  OPEN    FLOW-FROM  96
LAYERXYZ  'U-Shaped Inj'
** perf geometric data: UBA, block entry(x,y,z) block exit(x,y,z), length
   47 17 1   1165.470000  1617.370000  0.000000  1165.470000  1617.370000  80.000000
80.000000
   47 17 2   1165.470000  1617.370000  80.000000  1165.470000  1617.370000  160.000000
80.000000
   47 17 3   1165.470000  1617.370000  160.000000  1165.470000  1617.370000  240.000000
80.000000
   47 17 4   1165.470000  1617.370000  240.000000  1165.470000  1617.370000  320.000000
80.000000
   47 17 5   1165.470000  1617.370000  320.000000  1165.470000  1617.370000  400.000000
80.000000
   47 17 6   1165.470000  1617.370000  400.000000  1165.470000  1617.370000  480.000000
80.000000
   47 17 7   1165.470000  1617.370000  480.000000  1165.470000  1617.370000  560.000000
80.000000
   47 17 8   1165.470000  1617.370000  560.000000  1165.470000  1617.370000  640.000000
80.000000
   47 17 9   1165.470000  1617.370000  640.000000  1165.470000  1617.370000  720.000000
80.000000
   47 17 10  1165.470000  1617.370000  720.000000  1165.470000  1617.370000  800.000000
80.000000
   47 17 11  1165.470000  1617.370000  800.000000  1165.470000  1617.370000  880.000000
80.000000
   47 17 12  1165.470000  1617.370000  880.000000  1165.470000  1617.370000  960.000000
80.000000
   47 17 13  1165.470000  1617.370000  960.000000  1165.470000  1617.370000  1040.000000
80.000000
   47 17 14  1165.470000  1617.370000  1040.000000  1165.470000  1617.370000  1120.000000
80.000000
   47 17 15  1165.470000  1617.370000  1120.000000  1165.470000  1617.370000  1200.000000
80.000000
```

47 17 16 1165.470000 1617.370000 1200.000000 1165.470000 1617.370000 1280.000000
80.000000
47 17 17 1165.470000 1617.370000 1280.000000 1165.470000 1617.370000 1360.000000
80.000000
47 17 18 1165.470000 1617.370000 1360.000000 1165.470000 1617.370000 1440.000000
80.000000
47 17 19 1165.470000 1617.370000 1440.000000 1165.470000 1617.370000 1520.000000
80.000000
47 17 20 1165.470000 1617.370000 1520.000000 1165.470000 1617.370000 1600.000000
80.000000
47 17 21 1165.470000 1617.370000 1600.000000 1165.470000 1617.370000 1680.000000
80.000000
47 17 22 1165.470000 1617.370000 1680.000000 1165.470000 1617.370000 1760.000000
80.000000
47 17 23 1165.470000 1617.370000 1760.000000 1165.470000 1617.370000 1840.000000
80.000000
47 17 24 1165.470000 1617.370000 1840.000000 1165.470000 1617.370000 1920.000000
80.000000
47 17 25 1165.470000 1617.370000 1920.000000 1165.470000 1617.370000 2000.000000
80.000000
47 17 26 1165.470000 1617.370000 2000.000000 1165.470000 1617.370000 2080.000000
80.000000
47 17 27 1165.470000 1617.370000 2080.000000 1165.470000 1617.370000 2160.000000
80.000000
47 17 28 1165.470000 1617.370000 2160.000000 1165.470000 1617.370000 2240.000000
80.000000
47 17 29 1165.470000 1617.370000 2240.000000 1165.470000 1617.370000 2320.000000
80.000000
47 17 30 1165.470000 1617.370000 2320.000000 1165.470000 1617.370000 2400.000000
80.000000
47 17 31 1165.470000 1617.370000 2400.000000 1165.470000 1617.370000 2480.000000
80.000000
47 17 32 1165.470000 1617.370000 2480.000000 1165.470000 1617.370000 2560.000000
80.000000
47 17 33 1165.470000 1617.370000 2560.000000 1165.470000 1617.370000 2640.000000
80.000000
47 17 34 1165.470000 1617.370000 2640.000000 1165.470000 1617.370000 2720.000000
80.000000
47 17 35 1165.470000 1617.370000 2720.000000 1165.470000 1617.370000 2800.000000
80.000000
47 17 36 1165.470000 1617.370000 2800.000000 1165.470000 1617.370000 2880.000000
80.000000
47 17 37 1165.470000 1617.370000 2880.000000 1165.470000 1617.370000 2960.000000
80.000000
47 17 38 1165.470000 1617.370000 2960.000000 1165.470000 1617.370000 3040.000000
80.000000

47 17 39 1165.470000 1617.370000 3040.000000 1165.470000 1617.370000 3120.000000 80.000000
47 17 40 1165.470000 1617.370000 3120.000000 1165.470000 1617.370000 3200.000000 80.000000
47 17 41 1165.470000 1617.370000 3200.000000 1165.470000 1617.370000 3280.000000 80.000000
47 17 42 1165.470000 1617.370000 3280.000000 1165.470000 1617.370000 3360.000000 80.000000
47 17 43 1165.470000 1617.370000 3360.000000 1165.470000 1617.370000 3440.000000 80.000000
47 17 44 1165.470000 1617.370000 3440.000000 1165.470000 1617.370000 3520.000000 80.000000
47 17 45 1165.470000 1617.370000 3520.000000 1165.470000 1617.370000 3600.000000 80.000000
47 17 46 1165.470000 1617.370000 3600.000000 1165.470000 1617.370000 3680.000000 80.000000
47 17 47 1165.470000 1617.370000 3680.000000 1165.470000 1617.370000 3760.000000 80.000000
47 17 48 1165.470000 1617.370000 3760.000000 1165.470000 1617.370000 3840.000000 80.000000
47 17 49 1165.470000 1617.370000 3840.000000 1165.470000 1617.370000 3920.000000 80.000000
47 17 50 1165.470000 1617.370000 3920.000000 1165.470000 1617.370000 4000.000000 80.000000
47 17 51 1165.470000 1617.370000 4000.000000 1165.470000 1617.370000 4080.000000 80.000000
47 17 52 1165.470000 1617.370000 4080.000000 1165.470000 1617.370000 4160.000000 80.000000
47 17 53 1165.470000 1617.370000 4160.000000 1165.470000 1617.370000 4240.000000 80.000000
47 17 54 1165.470000 1617.370000 4240.000000 1165.470000 1617.370000 4320.000000 80.000000
47 17 55 1165.470000 1617.370000 4320.000000 1165.470000 1617.370000 4400.000000 80.000000
47 17 56 1165.470000 1617.370000 4400.000000 1165.470000 1617.370000 4480.000000 80.000000
47 17 57 1165.470000 1617.370000 4480.000000 1165.470000 1617.370000 4560.000000 80.000000
47 17 58 1165.470000 1617.370000 4560.000000 1165.470000 1617.370000 4640.000000 80.000000
47 17 59 1165.470000 1617.370000 4640.000000 1165.470000 1617.370000 4720.000000 80.000000
47 17 60 1165.470000 1617.370000 4720.000000 1165.470000 1617.370000 4800.000000 80.000000
47 17 61 1165.470000 1617.370000 4800.000000 1165.470000 1617.370000 4880.000000 80.000000

47 17 62 1165.470000 1617.370000 4880.000000 1165.470000 1617.370000 4960.000000
80.000000
47 17 63 1165.470000 1617.370000 4960.000000 1165.470000 1617.370000 5040.000000
80.000000
47 17 64 1165.470000 1617.370000 5040.000000 1165.470000 1617.370000 5120.000000
80.000000
47 17 65 1165.470000 1617.370000 5120.000000 1165.470000 1617.370000 5200.000000
80.000000
47 17 66 1165.470000 1617.370000 5200.000000 1165.470000 1617.370000 5280.000000
80.000000
47 17 67 1165.470000 1617.370000 5280.000000 1165.470000 1617.370000 5360.000000
80.000000
47 17 68 1165.470000 1617.370000 5360.000000 1165.470000 1617.370000 5440.000000
80.000000
47 17 69 1165.470000 1617.370000 5440.000000 1165.470000 1617.370000 5520.000000
80.000000
47 17 70 1165.470000 1617.370000 5520.000000 1165.470000 1617.370000 5600.000000
80.000000
47 17 71 1165.470000 1617.370000 5600.000000 1165.470000 1617.370000 5680.000000
80.000000
47 17 72 1165.470000 1617.370000 5680.000000 1165.470000 1617.370000 5760.000000
80.000000
47 17 73 1165.470000 1617.370000 5760.000000 1165.470000 1617.370000 5840.000000
80.000000
47 17 74 1165.470000 1617.370000 5840.000000 1165.495913 1617.370000 5920.837096
80.000018
47 17 75 1165.495913 1617.370000 5920.837096 1165.615382 1617.370000 6000.000000
80.000081
47 17 76 1165.615382 1617.370000 6004.696414 1175.374318 1617.370000 6066.488764
33.014219
48 17 76 1175.374318 1617.370000 6066.488764 1183.703971 1617.370000 6080.671288
8.329653
48 17 77 1183.703971 1617.370000 6080.671288 1200.564363 1617.370000 6099.121687
16.860392
49 17 77 1200.564363 1617.370000 6099.121687 1225.307472 1617.370000 6114.668491
24.743109
50 17 77 1225.307472 1617.370000 6114.668491 1250.022316 1617.370000 6121.557449
24.714845
51 17 77 1250.022316 1617.370000 6121.557449 1275.000000 1617.370000 6123.110000
24.977684
52 17 77 1275.000000 1617.370000 6123.110000 1300.000000 1617.370000 6123.110000
25.000000
53 17 77 1300.000000 1617.370000 6123.110000 1325.000000 1617.370000 6123.110000
25.000000
54 17 77 1325.000000 1617.370000 6123.110000 1350.000000 1617.370000 6123.110000
25.000000

```
   55 17 77  1350.000000  1617.370000  6123.110000  1375.000000  1617.370000  6123.110000
25.000000
   56 17 77  1375.000000  1617.370000  6123.110000  1400.000000  1617.370000  6123.110000
25.000000
   57 17 77  1400.000000  1617.370000  6123.110000  1425.000000  1617.370000  6123.110000
25.000000
   58 17 77  1425.000000  1617.370000  6123.110000  1490.341476  1617.370000  6123.110000
65.341476
   59 17 77  1490.341476  1617.370000  6123.110000  1551.049908  1617.370000  6123.110000
60.708431
   60 17 77  1551.049908  1617.370000  6123.110000  1596.202156  1617.370000  6123.110000
45.152248
   61 17 77  1596.202156  1617.370000  6123.110000  1626.925285  1617.370000  6123.110000
30.723129
   62 17 77  1626.925285  1617.370000  6123.110000  1642.419405  1617.370000  6123.110000
15.494120
   63 17 77  1642.419405  1617.370000  6123.110000  1651.874941  1617.370000  6123.110000
9.455536
   64 17 77  1651.874941  1617.370000  6123.110000  1659.228400  1617.370000  6123.110000
7.353459
   65 17 77  1659.228400  1617.370000  6123.110000  1663.449035  1617.370000  6123.110000
4.220635
   66 17 77  1663.449035  1617.370000  6123.110000  1665.193551  1617.370000  6123.110000
1.744516
   67 17 77  1665.193551  1617.370000  6123.110000  1665.727320  1617.370000  6123.110000
0.533769

FLX_WELLBORE 'FlexWell-InjectionWell' ATTACHTO 'U-Shaped Inj'
SOLID_BLOCK OFF
SEGREGATION ON
ANNULUS ATTACHTO 'U-Shaped Inj'
TUBULARS VARIABLE
**ID        OD        CEMENT OD        DEVICE
  0.14        0.152        0.178
  0.14        0.152        0.178
  0.14        0.152        0.178
  0.14        0.152        0.178
  0.14        0.152        0.178
  0.14        0.152        0.178
  0.14        0.152        0.178
  0.14        0.152        0.178
  0.14        0.152        0.178
  0.14        0.152        0.178
  0.14        0.152        0.178
  0.14        0.152        0.178
  0.14        0.152        0.178
```

0.14	0.152	0.178
0.14	0.152	0.178
0.14	0.152	0.178
0.14	0.152	0.178
0.14	0.152	0.178
0.14	0.152	0.178
0.14	0.152	0.178
0.14	0.152	0.178
0.14	0.152	0.178
0.14	0.152	0.178
0.14	0.152	0.178
0.14	0.152	0.178
0.14	0.152	0.178
0.14	0.152	0.178
0.14	0.152	0.178
0.14	0.152	0.178
0.14	0.152	0.178
0.14	0.152	0.178
0.14	0.152	0.178
0.14	0.152	0.178
0.14	0.152	0.178
0.14	0.152	0.178
0.14	0.152	0.178
0.14	0.152	0.178
0.14	0.152	0.178
0.14	0.152	0.178
0.14	0.152	0.178
0.14	0.152	0.178
0.14	0.152	0.178
0.14	0.152	0.178
0.14	0.152	0.178
0.14	0.152	0.178
0.14	0.152	0.178
0.14	0.152	0.178
0.14	0.152	0.178
0.14	0.152	0.178
0.14	0.152	0.178
0.14	0.152	0.178
0.14	0.152	0.178
0.14	0.152	0.178
0.14	0.152	0.178
0.14	0.152	0.178
0.14	0.152	0.178
0.14	0.152	0.178
0.14	0.152	0.178
0.14	0.152	0.178

```
 0.14        0.152        0.178
 0.14        0.152        0.178
 0.14        0.152        0.178
 0.14        0.152        0.178
 0.14        0.152        0.178
 0.14        0.152        0.178
 0.14        0.152        0.178
 0.14        0.152        0.178
 0.14        0.152        0.178
 0.14        0.152        0.178
 0.14        0.152        0.178
 0.14        0.152        0.178
 0.14        0.152        0.178
 0.14        0.152        0.178
 0.14        0.152        0.178
 0.14        0.152        0.178
 0.14        0.152        0.178
 0.14        0.152        0.178
 0.14        0.152        0.178
 0.14        0.152        0.178
 0.14        0.152        0.178
 0.14        0.152        0.178
 0.14        0.152        0.178
 0.14        0.152        0.178
 0.14        0.152        0.178
 0.14        0.152        0.178
 0.14        0.152        0.178
 0.14        0.152        0.178
 0.14        0.152        0.178
 0.14        0.152        0.178
 0.14        0.152        0.178
 0.14        0.152        0.178
 0.14        0.152        0.178
 0.14        0.152        0.178
 0.14        0.152        0.178
 0.14        0.152        0.178
 0.14        0.152        0.178
 0.14        0.152        0.178
 0.14        0.152        0.178
 0.14        0.152        0.178
 0.14        0.152        0.178
 0.14        0.152        0.178
WALL_CP  3.61288e+06
WALL_HCN 6.48e+06
CEMENT_HEAT_PROP 2e+06 172800
REL_ROUGH 0.0001
MAX_NUSSELT 10000


**
```

```
**
WELL  'U-Shaped Prod'
PRODUCER 'U-Shaped Prod'
OPERATE  MAX  STW  3000.0  CONT
OPERATE  MIN  BHP  5900.0  CONT
**        rad  geofac  wfrac  skin
GEOMETRY  K  0.0762  0.249  1.0  0.0
  PERF_FLX     GEOA  'U-Shaped Prod'
** UBA              ff        Status  Connection
   87 17 1        1.0  CLOSED  FLOW-TO  'SURFACE'  REFLAYER
   87 17 2        1.0  CLOSED  FLOW-TO  1
   87 17 3        1.0  CLOSED  FLOW-TO  2
   87 17 4        1.0  CLOSED  FLOW-TO  3
   87 17 5        1.0  CLOSED  FLOW-TO  4
   87 17 6        1.0  CLOSED  FLOW-TO  5
   87 17 7        1.0  CLOSED  FLOW-TO  6
   87 17 8        1.0  CLOSED  FLOW-TO  7
   87 17 9        1.0  CLOSED  FLOW-TO  8
   87 17 10        1.0  CLOSED  FLOW-TO  9
   87 17 11        1.0  CLOSED  FLOW-TO  10
   87 17 12        1.0  CLOSED  FLOW-TO  11
   87 17 13        1.0  CLOSED  FLOW-TO  12
   87 17 14        1.0  CLOSED  FLOW-TO  13
   87 17 15        1.0  CLOSED  FLOW-TO  14
   87 17 16        1.0  CLOSED  FLOW-TO  15
   87 17 17        1.0  CLOSED  FLOW-TO  16
   87 17 18        1.0  CLOSED  FLOW-TO  17
   87 17 19        1.0  CLOSED  FLOW-TO  18
   87 17 20        1.0  CLOSED  FLOW-TO  19
   87 17 21        1.0  CLOSED  FLOW-TO  20
   87 17 22        1.0  CLOSED  FLOW-TO  21
   87 17 23        1.0  CLOSED  FLOW-TO  22
   87 17 24        1.0  CLOSED  FLOW-TO  23
   87 17 25        1.0  CLOSED  FLOW-TO  24
   87 17 26        1.0  CLOSED  FLOW-TO  25
   87 17 27        1.0  CLOSED  FLOW-TO  26
   87 17 28        1.0  CLOSED  FLOW-TO  27
   87 17 29        1.0  CLOSED  FLOW-TO  28
   87 17 30        1.0  CLOSED  FLOW-TO  29
   87 17 31        1.0  CLOSED  FLOW-TO  30
   87 17 32        1.0  CLOSED  FLOW-TO  31
   87 17 33        1.0  CLOSED  FLOW-TO  32
   87 17 34        1.0  CLOSED  FLOW-TO  33
   87 17 35        1.0  CLOSED  FLOW-TO  34
   87 17 36        1.0  CLOSED  FLOW-TO  35
   87 17 37        1.0  CLOSED  FLOW-TO  36
```

87 17 38	1.0	CLOSED	FLOW-TO	37
87 17 39	1.0	CLOSED	FLOW-TO	38
87 17 40	1.0	CLOSED	FLOW-TO	39
87 17 41	1.0	CLOSED	FLOW-TO	40
87 17 42	1.0	CLOSED	FLOW-TO	41
87 17 43	1.0	CLOSED	FLOW-TO	42
87 17 44	1.0	CLOSED	FLOW-TO	43
87 17 45	1.0	CLOSED	FLOW-TO	44
87 17 46	1.0	CLOSED	FLOW-TO	45
87 17 47	1.0	CLOSED	FLOW-TO	46
87 17 48	1.0	CLOSED	FLOW-TO	47
87 17 49	1.0	CLOSED	FLOW-TO	48
87 17 50	1.0	CLOSED	FLOW-TO	49
87 17 51	1.0	CLOSED	FLOW-TO	50
87 17 52	1.0	CLOSED	FLOW-TO	51
87 17 53	1.0	CLOSED	FLOW-TO	52
87 17 54	1.0	CLOSED	FLOW-TO	53
87 17 55	1.0	CLOSED	FLOW-TO	54
87 17 56	1.0	CLOSED	FLOW-TO	55
87 17 57	1.0	CLOSED	FLOW-TO	56
87 17 58	1.0	CLOSED	FLOW-TO	57
87 17 59	1.0	CLOSED	FLOW-TO	58
87 17 60	1.0	CLOSED	FLOW-TO	59
87 17 61	1.0	CLOSED	FLOW-TO	60
87 17 62	1.0	CLOSED	FLOW-TO	61
87 17 63	1.0	CLOSED	FLOW-TO	62
87 17 64	1.0	CLOSED	FLOW-TO	63
87 17 65	1.0	CLOSED	FLOW-TO	64
87 17 66	1.0	CLOSED	FLOW-TO	65
87 17 67	1.0	CLOSED	FLOW-TO	66
87 17 68	1.0	CLOSED	FLOW-TO	67
87 17 69	1.0	CLOSED	FLOW-TO	68
87 17 70	1.0	CLOSED	FLOW-TO	69
87 17 71	1.0	CLOSED	FLOW-TO	70
87 17 72	1.0	CLOSED	FLOW-TO	71
87 17 73	1.0	CLOSED	FLOW-TO	72
87 17 74	1.0	CLOSED	FLOW-TO	73
87 17 75	1.0	CLOSED	FLOW-TO	74
87 17 76	1.0	CLOSED	FLOW-TO	75
86 17 76	1.0	CLOSED	FLOW-TO	76
86 17 77	1.0	CLOSED	FLOW-TO	77
85 17 77	1.0	CLOSED	FLOW-TO	78
84 17 77	1.0	CLOSED	FLOW-TO	79
83 17 77	1.0	CLOSED	FLOW-TO	80
82 17 77	1.0	CLOSED	FLOW-TO	81
81 17 77	1.0	CLOSED	FLOW-TO	82

```
   80 17 77        1.0  CLOSED  FLOW-TO  83
   79 17 77        1.0  CLOSED  FLOW-TO  84
   78 17 77        1.0  CLOSED  FLOW-TO  85
   77 17 77        1.0  CLOSED  FLOW-TO  86
   76 17 77        1.0  CLOSED  FLOW-TO  87
   75 17 77        1.0  CLOSED  FLOW-TO  88
   74 17 77        1.0  CLOSED  FLOW-TO  89
   73 17 77        1.0  CLOSED  FLOW-TO  90
   72 17 77        1.0  CLOSED  FLOW-TO  91
   71 17 77        1.0  CLOSED  FLOW-TO  92
   70 17 77        1.0  CLOSED  FLOW-TO  93
   69 17 77        1.0  CLOSED  FLOW-TO  94
   68 17 77        1.0  CLOSED  FLOW-TO  95
   67 17 77        1.0  OPEN    FLOW-TO  96
LAYERXYZ  'U-Shaped Prod'
** perf geometric data: UBA, block entry(x,y,z) block exit(x,y,z), length
   87 17 1   2165.470000  1617.370000  0.000000  2165.470000  1617.370000  80.000000
80.000000
   87 17 2   2165.470000  1617.370000  80.000000  2165.470000  1617.370000  160.000000
80.000000
   87 17 3   2165.470000  1617.370000  160.000000  2165.470000  1617.370000  240.000000
80.000000
   87 17 4   2165.470000  1617.370000  240.000000  2165.470000  1617.370000  320.000000
80.000000
   87 17 5   2165.470000  1617.370000  320.000000  2165.470000  1617.370000  400.000000
80.000000
   87 17 6   2165.470000  1617.370000  400.000000  2165.470000  1617.370000  480.000000
80.000000
   87 17 7   2165.470000  1617.370000  480.000000  2165.470000  1617.370000  560.000000
80.000000
   87 17 8   2165.470000  1617.370000  560.000000  2165.470000  1617.370000  640.000000
80.000000
   87 17 9   2165.470000  1617.370000  640.000000  2165.470000  1617.370000  720.000000
80.000000
   87 17 10  2165.470000  1617.370000  720.000000  2165.470000  1617.370000  800.000000
80.000000
   87 17 11  2165.470000  1617.370000  800.000000  2165.470000  1617.370000  880.000000
80.000000
   87 17 12  2165.470000  1617.370000  880.000000  2165.470000  1617.370000  960.000000
80.000000
   87 17 13  2165.470000  1617.370000  960.000000  2165.470000  1617.370000  1040.000000
80.000000
   87 17 14  2165.470000  1617.370000  1040.000000  2165.470000  1617.370000  1120.000000
80.000000
   87 17 15  2165.470000  1617.370000  1120.000000  2165.470000  1617.370000  1200.000000
80.000000
```

87 17 16 2165.470000 1617.370000 1200.000000 2165.470000 1617.370000 1280.000000 80.000000
87 17 17 2165.470000 1617.370000 1280.000000 2165.470000 1617.370000 1360.000000 80.000000
87 17 18 2165.470000 1617.370000 1360.000000 2165.470000 1617.370000 1440.000000 80.000000
87 17 19 2165.470000 1617.370000 1440.000000 2165.470000 1617.370000 1520.000000 80.000000
87 17 20 2165.470000 1617.370000 1520.000000 2165.470000 1617.370000 1600.000000 80.000000
87 17 21 2165.470000 1617.370000 1600.000000 2165.470000 1617.370000 1680.000000 80.000000
87 17 22 2165.470000 1617.370000 1680.000000 2165.470000 1617.370000 1760.000000 80.000000
87 17 23 2165.470000 1617.370000 1760.000000 2165.470000 1617.370000 1840.000000 80.000000
87 17 24 2165.470000 1617.370000 1840.000000 2165.470000 1617.370000 1920.000000 80.000000
87 17 25 2165.470000 1617.370000 1920.000000 2165.470000 1617.370000 2000.000000 80.000000
87 17 26 2165.470000 1617.370000 2000.000000 2165.470000 1617.370000 2080.000000 80.000000
87 17 27 2165.470000 1617.370000 2080.000000 2165.470000 1617.370000 2160.000000 80.000000
87 17 28 2165.470000 1617.370000 2160.000000 2165.470000 1617.370000 2240.000000 80.000000
87 17 29 2165.470000 1617.370000 2240.000000 2165.470000 1617.370000 2320.000000 80.000000
87 17 30 2165.470000 1617.370000 2320.000000 2165.470000 1617.370000 2400.000000 80.000000
87 17 31 2165.470000 1617.370000 2400.000000 2165.470000 1617.370000 2480.000000 80.000000
87 17 32 2165.470000 1617.370000 2480.000000 2165.470000 1617.370000 2560.000000 80.000000
87 17 33 2165.470000 1617.370000 2560.000000 2165.470000 1617.370000 2640.000000 80.000000
87 17 34 2165.470000 1617.370000 2640.000000 2165.470000 1617.370000 2720.000000 80.000000
87 17 35 2165.470000 1617.370000 2720.000000 2165.470000 1617.370000 2800.000000 80.000000
87 17 36 2165.470000 1617.370000 2800.000000 2165.470000 1617.370000 2880.000000 80.000000
87 17 37 2165.470000 1617.370000 2880.000000 2165.470000 1617.370000 2960.000000 80.000000
87 17 38 2165.470000 1617.370000 2960.000000 2165.470000 1617.370000 3040.000000 80.000000

87 17 39 2165.470000 1617.370000 3040.000000 2165.470000 1617.370000 3120.000000 80.000000
87 17 40 2165.470000 1617.370000 3120.000000 2165.470000 1617.370000 3200.000000 80.000000
87 17 41 2165.470000 1617.370000 3200.000000 2165.470000 1617.370000 3280.000000 80.000000
87 17 42 2165.470000 1617.370000 3280.000000 2165.470000 1617.370000 3360.000000 80.000000
87 17 43 2165.470000 1617.370000 3360.000000 2165.470000 1617.370000 3440.000000 80.000000
87 17 44 2165.470000 1617.370000 3440.000000 2165.470000 1617.370000 3520.000000 80.000000
87 17 45 2165.470000 1617.370000 3520.000000 2165.470000 1617.370000 3600.000000 80.000000
87 17 46 2165.470000 1617.370000 3600.000000 2165.470000 1617.370000 3680.000000 80.000000
87 17 47 2165.470000 1617.370000 3680.000000 2165.470000 1617.370000 3760.000000 80.000000
87 17 48 2165.470000 1617.370000 3760.000000 2165.470000 1617.370000 3840.000000 80.000000
87 17 49 2165.470000 1617.370000 3840.000000 2165.470000 1617.370000 3920.000000 80.000000
87 17 50 2165.470000 1617.370000 3920.000000 2165.470000 1617.370000 4000.000000 80.000000
87 17 51 2165.470000 1617.370000 4000.000000 2165.470000 1617.370000 4080.000000 80.000000
87 17 52 2165.470000 1617.370000 4080.000000 2165.470000 1617.370000 4160.000000 80.000000
87 17 53 2165.470000 1617.370000 4160.000000 2165.470000 1617.370000 4240.000000 80.000000
87 17 54 2165.470000 1617.370000 4240.000000 2165.470000 1617.370000 4320.000000 80.000000
87 17 55 2165.470000 1617.370000 4320.000000 2165.470000 1617.370000 4400.000000 80.000000
87 17 56 2165.470000 1617.370000 4400.000000 2165.470000 1617.370000 4480.000000 80.000000
87 17 57 2165.470000 1617.370000 4480.000000 2165.470000 1617.370000 4560.000000 80.000000
87 17 58 2165.470000 1617.370000 4560.000000 2165.470000 1617.370000 4640.000000 80.000000
87 17 59 2165.470000 1617.370000 4640.000000 2165.470000 1617.370000 4720.000000 80.000000
87 17 60 2165.470000 1617.370000 4720.000000 2165.470000 1617.370000 4800.000000 80.000000
87 17 61 2165.470000 1617.370000 4800.000000 2165.470000 1617.370000 4880.000000 80.000000

87 17 62 2165.470000 1617.370000 4880.000000 2165.470000 1617.370000 4960.000000 80.000000
87 17 63 2165.470000 1617.370000 4960.000000 2165.470000 1617.370000 5040.000000 80.000000
87 17 64 2165.470000 1617.370000 5040.000000 2165.470000 1617.370000 5120.000000 80.000000
87 17 65 2165.470000 1617.370000 5120.000000 2165.470000 1617.370000 5200.000000 80.000000
87 17 66 2165.470000 1617.370000 5200.000000 2165.470000 1617.370000 5280.000000 80.000000
87 17 67 2165.470000 1617.370000 5280.000000 2165.470000 1617.370000 5360.000000 80.000000
87 17 68 2165.470000 1617.370000 5360.000000 2165.470000 1617.370000 5440.000000 80.000000
87 17 69 2165.470000 1617.370000 5440.000000 2165.470000 1617.370000 5520.000000 80.000000
87 17 70 2165.470000 1617.370000 5520.000000 2165.470000 1617.370000 5600.000000 80.000000
87 17 71 2165.470000 1617.370000 5600.000000 2165.470000 1617.370000 5680.000000 80.000000
87 17 72 2165.470000 1617.370000 5680.000000 2165.470000 1617.370000 5760.000000 80.000000
87 17 73 2165.470000 1617.370000 5760.000000 2165.470000 1617.370000 5840.000000 80.000000
87 17 74 2165.470000 1617.370000 5840.000000 2165.444087 1617.370000 5920.837096 80.000018
87 17 75 2165.444087 1617.370000 5920.837096 2165.324618 1617.370000 6000.000000 80.000081
87 17 76 2165.324618 1617.370000 6004.696414 2149.213860 1617.370000 6077.751708 39.366041
86 17 76 2149.213860 1617.370000 6077.751708 2147.236029 1617.370000 6080.671288 1.977831
86 17 77 2147.236029 1617.370000 6080.671288 2124.889835 1617.370000 6103.529854 22.346193
85 17 77 2124.889835 1617.370000 6103.529854 2099.711199 1617.370000 6116.879374 25.178637
84 17 77 2099.711199 1617.370000 6116.879374 2074.947757 1617.370000 6122.157450 24.763441
83 17 77 2074.947757 1617.370000 6122.157450 2049.999998 1617.370000 6123.110000 24.947759
82 17 77 2049.999998 1617.370000 6123.110000 2024.999998 1617.370000 6123.110000 25.000000
81 17 77 2024.999998 1617.370000 6123.110000 1999.999998 1617.370000 6123.110000 25.000000
80 17 77 1999.999998 1617.370000 6123.110000 1974.999998 1617.370000 6123.110000 25.000000

```
   79 17 77  1974.999998  1617.370000  6123.110000  1949.999998  1617.370000  6123.110000
25.000000
   78 17 77  1949.999998  1617.370000  6123.110000  1924.999998  1617.370000  6123.110000
25.000000
   77 17 77  1924.999998  1617.370000  6123.110000  1899.999998  1617.370000  6123.110000
25.000000
   76 17 77  1899.999998  1617.370000  6123.110000  1845.593760  1617.370000  6123.110000
54.406239
   75 17 77  1845.593760  1617.370000  6123.110000  1783.565581  1617.370000  6123.110000
62.028179
   74 17 77  1783.565581  1617.370000  6123.110000  1738.535959  1617.370000  6123.110000
45.029621
   73 17 77  1738.535959  1617.370000  6123.110000  1704.955549  1617.370000  6123.110000
33.580410
   72 17 77  1704.955549  1617.370000  6123.110000  1689.756000  1617.370000  6123.110000
15.199550
   71 17 77  1689.756000  1617.370000  6123.110000  1680.271007  1617.370000  6123.110000
9.484993
   70 17 77  1680.271007  1617.370000  6123.110000  1671.995165  1617.370000  6123.110000
8.275842
   69 17 77  1671.995165  1617.370000  6123.110000  1667.656562  1617.370000  6123.110000
4.338603
   68 17 77  1667.656562  1617.370000  6123.110000  1665.727320  1617.370000  6123.110000
1.929242
   67 17 77  1665.727320  1617.370000  6123.110000  1665.193551  1617.370000  6123.110000
0.533769

FLX_WELLBORE 'FlexWell-ProductionWell' ATTACHTO 'U-Shaped Prod'
SOLID_BLOCK OFF
SEGREGATION ON
ANNULUS ATTACHTO 'U-Shaped Prod'
TUBULARS VARIABLE
**ID        OD        CEMENT OD        DEVICE
  0.14        0.152        0.178
  0.14        0.152        0.178
  0.14        0.152        0.178
  0.14        0.152        0.178
  0.14        0.152        0.178
  0.14        0.152        0.178
  0.14        0.152        0.178
  0.14        0.152        0.178
  0.14        0.152        0.178
  0.14        0.152        0.178
  0.14        0.152        0.178
  0.14        0.152        0.178
  0.14        0.152        0.178
```

0.14	0.152	0.178
0.14	0.152	0.178
0.14	0.152	0.178
0.14	0.152	0.178
0.14	0.152	0.178
0.14	0.152	0.178
0.14	0.152	0.178
0.14	0.152	0.178
0.14	0.152	0.178
0.14	0.152	0.178
0.14	0.152	0.178
0.14	0.152	0.178
0.14	0.152	0.178
0.14	0.152	0.178
0.14	0.152	0.178
0.14	0.152	0.178
0.14	0.152	0.178
0.14	0.152	0.178
0.14	0.152	0.178
0.14	0.152	0.178
0.14	0.152	0.178
0.14	0.152	0.178
0.14	0.152	0.178
0.14	0.152	0.178
0.14	0.152	0.178
0.14	0.152	0.178
0.14	0.152	0.178
0.14	0.152	0.178
0.14	0.152	0.178
0.14	0.152	0.178
0.14	0.152	0.178
0.14	0.152	0.178
0.14	0.152	0.178
0.14	0.152	0.178
0.14	0.152	0.178
0.14	0.152	0.178
0.14	0.152	0.178
0.14	0.152	0.178
0.14	0.152	0.178
0.14	0.152	0.178
0.14	0.152	0.178
0.14	0.152	0.178
0.14	0.152	0.178
0.14	0.152	0.178
0.14	0.152	0.178

```
  0.14        0.152        0.178
  0.14        0.152        0.178
  0.14        0.152        0.178
  0.14        0.152        0.178
  0.14        0.152        0.178
  0.14        0.152        0.178
  0.14        0.152        0.178
  0.14        0.152        0.178
  0.14        0.152        0.178
  0.14        0.152        0.178
  0.14        0.152        0.178
  0.14        0.152        0.178
  0.14        0.152        0.178
  0.14        0.152        0.178
  0.14        0.152        0.178
  0.14        0.152        0.178
  0.14        0.152        0.178
  0.14        0.152        0.178
  0.14        0.152        0.178
  0.14        0.152        0.178
  0.14        0.152        0.178
  0.14        0.152        0.178
  0.14        0.152        0.178
  0.14        0.152        0.178
  0.14        0.152        0.178
  0.14        0.152        0.178
  0.14        0.152        0.178
  0.14        0.152        0.178
  0.14        0.152        0.178
  0.14        0.152        0.178
  0.14        0.152        0.178
  0.14        0.152        0.178
  0.14        0.152        0.178
  0.14        0.152        0.178
  0.14        0.152        0.178
  0.14        0.152        0.178
  0.14        0.152        0.178
  0.14        0.152        0.178
  0.14        0.152        0.178
WALL_CP  3.61288e+06
WALL_HCN 6.48e+06
CEMENT_HEAT_PROP 2e+06 172800
REL_ROUGH 0.0001
MAX_NUSSELT 10000

REPORTING-GROUP 'FlexWell: FlexWell-ProductionWell'
   'U-Shaped Prod'
```

```
   1.0
REPORTING-GROUP 'FlexWell: FlexWell-InjectionWell'
   'U-Shaped Inj'
   1.0
WSRF GRID TNEXT
DATE 2020 2  1.00000
WSRF GRID TNEXT
DATE 2020 3  1.00000
WSRF GRID TNEXT
DATE 2020 4  1.00000
WSRF GRID TNEXT
DATE 2020 5  1.00000
WSRF GRID TNEXT
DATE 2020 6  1.00000
WSRF GRID TNEXT
DATE 2020 7  1.00000
WSRF GRID TNEXT
DATE 2020 8  1.00000
WSRF GRID TNEXT
DATE 2020 9  1.00000
WSRF GRID TNEXT
DATE 2020 10  1.00000
WSRF GRID TNEXT
DATE 2020 11  1.00000
WSRF GRID TNEXT
DATE 2020 12  1.00000
WSRF GRID TNEXT
DATE 2021 1  1.00000
WSRF GRID TNEXT
DATE 2022 1  1.00000
WSRF GRID TNEXT
DATE 2023 1  1.00000
WSRF GRID TNEXT
DATE 2024 1  1.00000
WSRF GRID TNEXT
DATE 2025 1  1.00000
WSRF GRID TNEXT
DATE 2026 1  1.00000
WSRF GRID TNEXT
DATE 2027 1  1.00000
WSRF GRID TNEXT
DATE 2028 1  1.00000
WSRF GRID TNEXT
DATE 2029 1  1.00000
WSRF GRID TNEXT
DATE 2030 1  1.00000
```

```
WSRF GRID TNEXT
DATE 2031 1  1.00000
WSRF GRID TNEXT
DATE 2032 1  1.00000
WSRF GRID TNEXT
DATE 2033 1  1.00000
WSRF GRID TNEXT
DATE 2034 1  1.00000
WSRF GRID TNEXT
DATE 2035 1  1.00000
WSRF GRID TNEXT
DATE 2036 1  1.00000
WSRF GRID TNEXT
DATE 2037 1  1.00000
WSRF GRID TNEXT
DATE 2038 1  1.00000
WSRF GRID TNEXT
DATE 2039 1  1.00000
WSRF GRID TIME
WSRF GRID TIME
WSRF GRID TNEXT
DATE 2040 1  1.00000
WSRF GRID TNEXT
DATE 2041 1  1.00000
WSRF GRID TNEXT
DATE 2042 1  1.00000
WSRF GRID TNEXT
DATE 2043 1  1.00000
WSRF GRID TNEXT
DATE 2044 1  1.00000
WSRF GRID TNEXT
DATE 2045 1  1.00000
WSRF GRID TNEXT
DATE 2046 1  1.00000
WSRF GRID TNEXT
DATE 2047 1  1.00000
WSRF GRID TNEXT
DATE 2048 1  1.00000
WSRF GRID TNEXT
DATE 2049 1  1.00000
WSRF GRID TNEXT
DATE 2050 1  1.00000
WSRF GRID TNEXT
DATE 2051 1  1.00000
WSRF GRID TNEXT
DATE 2052 1  1.00000
```

```
WSRF GRID TNEXT
DATE 2053 1  1.00000
WSRF GRID TNEXT
DATE 2054 1  1.00000
WSRF GRID TNEXT
DATE 2055 1  1.00000
WSRF GRID TNEXT
DATE 2056 1  1.00000
WSRF GRID TNEXT
DATE 2057 1  1.00000
WSRF GRID TNEXT
DATE 2058 1  1.00000
WSRF GRID TNEXT
DATE 2059 1  1.00000
WSRF GRID TNEXT
DATE 2060 1  1.00000
WSRF GRID TNEXT
DATE 2061 1  1.00000
WSRF GRID TNEXT
DATE 2062 1  1.00000
WSRF GRID TNEXT
DATE 2063 1  1.00000
WSRF GRID TNEXT
DATE 2064 1  1.00000
WSRF GRID TNEXT
DATE 2065 1  1.00000
WSRF GRID TNEXT
DATE 2066 1  1.00000
WSRF GRID TNEXT
DATE 2067 1  1.00000
WSRF GRID TNEXT
DATE 2068 1  1.00000
WSRF GRID TNEXT
DATE 2069 1  1.00000
WSRF GRID TNEXT
DATE 2070 1  1.00000
WSRF GRID TNEXT
DATE 2071 1  1.00000
WSRF GRID TNEXT
DATE 2072 1  1.00000
WSRF GRID TNEXT
DATE 2073 1  1.00000
WSRF GRID TNEXT
DATE 2074 1  1.00000
WSRF GRID TNEXT
DATE 2075 1  1.00000
```

```
WSRF GRID TNEXT
DATE 2076 1  1.00000
WSRF GRID TNEXT
DATE 2077 1  1.00000
WSRF GRID TNEXT
DATE 2078 1  1.00000
WSRF GRID TNEXT
DATE 2079 1  1.00000
WSRF GRID TNEXT
DATE 2080 1  1.00000
WSRF GRID TNEXT
DATE 2081 1  1.00000
WSRF GRID TNEXT
DATE 2082 1  1.00000
WSRF GRID TNEXT
DATE 2083 1  1.00000
WSRF GRID TNEXT
DATE 2084 1  1.00000
WSRF GRID TNEXT
DATE 2085 1  1.00000
WSRF GRID TNEXT
DATE 2086 1  1.00000
WSRF GRID TNEXT
DATE 2087 1  1.00000
WSRF GRID TNEXT
DATE 2088 1  1.00000
WSRF GRID TNEXT
DATE 2089 1  1.00000
WSRF GRID TNEXT
DATE 2090 1  1.00000
WSRF GRID TNEXT
DATE 2091 1  1.00000
WSRF GRID TNEXT
DATE 2092 1  1.00000
WSRF GRID TNEXT
DATE 2093 1  1.00000
WSRF GRID TNEXT
DATE 2094 1  1.00000
WSRF GRID TNEXT
DATE 2095 1  1.00000
WSRF GRID TNEXT
DATE 2096 1  1.00000
WSRF GRID TNEXT
DATE 2097 1  1.00000
WSRF GRID TNEXT
DATE 2098 1  1.00000
```

```
WSRF GRID TNEXT
DATE 2099 1  1.00000
WSRF GRID TIME
WSRF GRID TNEXT
DATE 2100 1  1.00000
STOP
```

APPENDIX B

V-SHAPE CASE .DAT CODE

The following is the code used by CMG-STARS to read and run the V-Shaped model evaluated in Chapter 3. The .dat file shown in this appendix is for the V-Shaped configuration:

```
WPRN FLEXWELL GRID 1
INUNIT SI
WSRF WELL 1
WSRF GRID 1
OUTPRN WELL ALL
OUTSRF GRID PRES TEMP
OUTSRF FLEXLAYER ALL
** ***************************************************************************
** Definition of fundamental cartesian grid
** ***************************************************************************
GRID VARI 141 59 86
KDIR DOWN
DI IVAR
 33*25 23.45849 26.54151 9*25 24.49771 25.50229 11*25 65.34148 60.70843
 45.15225 30.72313 15.49412 9.455536 7.353459 4.220635 1.744516 0.5337693
 1.929242 4.338603 8.275842 9.484993 15.19955 33.58041 45.02962 62.02818
 54.40624 65*25
DJ JVAR
 219.6155 184.6332 194.9864 177.731 168.0679 131.1413 198.0924 154.6087
 97.32065 63.84511 83.86141 63.84511 53.83696 45.45232 32.34713 36.437
 32.34713 36.437 39.78325 32.34713 36.437 34.54402 32.63547 37.48895
 21.08753 14.7278 10.8743 0.5456838 14.68839 14.56044 29.28824 40.83618
 34.14172 45.68966 52.04939 57.07023 74.9779 57.99526 64.52908 68.01714
 76.80607 93.124 108.0698 115.7344 111.9021 104.2376 119.5666 119.1834
 96.95626 126.8479 100.7885 111.9021 93.50723 104.2376 93.124 115.0915
 3*80
DK ALL
 715434*80
DTOP
 8319*0
**  0 = null block, 1 = active block
NULL CON          1
*PLNRFRAC_TEMPLATE 'Planar Template'
   *PLNR_REFINE *INTO  7 7 3
   *BWHLEN 1100
   *IDIR
   *INNERWIDTH 0.6096
```

```
   *WF1 0.001
   *K_CENT 50000
   *KH_TYPE LINEAR
   *KH_TIP 50000 50000
   *KV_TYPE LINEAR
   *KV_TIP 50000 50000
   *HEIGHTUP 50
   *HEIGHTDOWN 50
   *POR MATRIX *FZ 0.0016
*END_TEMPLATE
POR CON         0.01
*MOD
  67:67 28:28 77:77   = 0.996
  67:67 28:28 77:77   = 0.75
  67:67 28:28 77:77   = 0.996
PERMI CON        1E-06
*MOD
  67:67 28:28 77:77   = 10000
PERMJ  EQUALSI
PERMK  EQUALSI
**  0 = pinched block, 1 = active block
PINCHOUTARRAY CON            1
*NFZG-ALIGN ON
END-GRID
ROCKTYPE 1
CPOR 4.35e-7
ROCKCP 2667500 0
THCONR 252720
THCONW 53500
** Model and number of components
MODEL 1 1 1 1
COMPNAME 'H2O'
CMM
0
PCRIT
0
TCRIT
0
MASSDEN
1000
AVISC
0.0047352
BVISC
1515.7
ROCKFLUID
RPT 1 WATWET
```

```
**       Sw       krw      krow
SWT

0        0        1
1        1        0
**       Sl       krg      krog
SLT

0        1        0
1        0        1
INITIAL
VERTICAL OFF

INITREGION 1
REFPRES 5820
REFDEPTH 5820
PRES KVAR
 800 1600 2400 3200 4000 4800 5600 6400 7200 8000 8800 9600 10400 11200
 12000 12800 13600 14400 15200 16000 16800 17600 18400 19200 20000
 20800 21600 22400 23200 24000 24800 25600 26400 27200 28000 28800
 29600 30400 31200 32000 32800 33600 34400 35200 36000 36800 37600
 38400 39200 40000 40800 41600 42400 43200 44000 44800 45600 46400
 47200 48000 48800 49600 50400 51200 52000 52800 53600 54400 55200
 56000 56800 57600 58400 59200 60000 60800 61600 62400 63200 64000
 64800 65600 66400 67200 68000 68800
TEMP KVAR
 20 23.68421 27.36842 31.05263 34.73684 38.42105 42.10526 45.78947
 49.47368 53.15789 56.84211 60.52632 64.21053 67.89474 71.57895 75.26316
 78.94736 82.63158 86.31579 90 93.68421 97.36842 101.0526 104.7368
 108.4211 112.1053 115.7895 119.4737 123.1579 126.8421 130.5263 134.2105
 137.8947 141.5789 145.2632 148.9474 152.6316 156.3158 160 163.6842
 167.3684 171.0526 174.7368 178.4211 182.1053 185.7895 189.4737 193.1579
 196.8421 200.5263 204.2105 207.8947 211.5789 215.2632 218.9474 222.6316
 226.3158 230 233.6842 237.3684 241.0526 244.7368 248.4211 252.1053
 255.7895 259.4737 263.1579 266.8421 270.5263 274.2105 277.8947 281.5789
 285.2632 288.9474 292.6316 296.3158 300 303.6842 307.3684 311.0526
 314.7368 318.4211 322.1053 325.7895 329.4737 333.1579
NUMERICAL
AUTOTUNE ON
RUN
DATE 2020 1 1
DTWELL 0.1
**
**
WELL  'Injection Well'
INJECTOR MOBWEIGHT IMPLICIT 'Injection Well'
```

```
INCOMP  WATER  1.0
TINJW  60.0
QUAL  0.0
PINJW  6875.0
OPERATE  MAX  STW  3000.0  CONT
OPERATE  MAX  BHP  1200000.0  CONT
**        rad  geofac  wfrac  skin
GEOMETRY  K  0.0762  0.249  1.0  0.0
    PERF      GEOA  'Injection Well'
   47 11 1         1.0  OPEN    FLOW-FROM  'SURFACE'    'CMGTEMP_000.inc'
LAYERXYZ  'Injection Well'
   47 11 1   1165.470000  1617.370000  0.000000  1165.   'CMGTEMP_001.inc'
SHUTIN 'Injection Well'


**
**
WELL  'Production Well'
PRODUCER 'Production Well'
OPERATE  MAX  STW  3000.0  CONT
**        rad  geofac  wfrac  skin
GEOMETRY  K  0.0762  0.249  1.0  0.0
    PERF      GEOA  'Production Well'
   87 11 1         1.0  OPEN    FLOW-TO  'SURFACE'  R   'CMGTEMP_002.inc'
LAYERXYZ  'Production Well'
   87 11 1   2165.470000  1617.370000  0.000000  2165.   'CMGTEMP_003.inc'
SHUTIN 'Production Well'
**
WELL  'InjectionWell-Inclined'
INJECTOR MOBWEIGHT IMPLICIT 'InjectionWell-Inclined'
INCOMP  WATER  1.0
TINJW  60.0
QUAL  0.0
PINJW  6875.0
OPERATE  MAX  STW  3000.0  CONT
**        rad  geofac  wfrac  skin
GEOMETRY  K  0.0762  0.249  1.0  0.0
    PERF      GEOA  'InjectionWell-Inclined'
   87 11 1         1.0  OPEN    FLOW-FROM  'SURFACE'    'CMGTEMP_004.inc'
LAYERXYZ  'InjectionWell-Inclined'
   87 11 1   2165.470000  1617.370000  0.000000  2165.   'CMGTEMP_005.inc'
SHUTIN 'InjectionWell-Inclined'



**
```

```
WELL  'ProductionWell - Inclined'
PRODUCER 'ProductionWell - Inclined'
OPERATE  MAX  STW  3000.0  CONT
OPERATE  MIN  BHP  5900.0  CONT
**        rad  geofac  wfrac  skin
GEOMETRY  K  0.0762  0.249  1.0  0.0
     PERF      GEOA  'ProductionWell - Inclined'
   47 11 1         1.0  OPEN    FLOW-TO  'SURFACE'  R   'CMGTEMP_006.inc'
LAYERXYZ  'ProductionWell - Inclined'
   47 11 1   1165.470000  1617.370000  0.000000  1165.   'CMGTEMP_007.inc'
SHUTIN 'ProductionWell - Inclined'
**
WELL  'HorizTraj3'
PRODUCER 'HorizTraj3'
OPERATE  MAX  STW  3000.0  CONT
OPERATE  MIN  BHP  5900.0  CONT
**        rad  geofac  wfrac  skin
GEOMETRY  K  0.0762  0.249  1.0  0.0
  PERF_FLX      GEOA  'HorizTraj3'
   87 11 1         1.0  CLOSED  FLOW-TO  'SURFACE'  R   'CMGTEMP_008.inc'
LAYERXYZ  'HorizTraj3'
   87 11 1   2165.470000  1617.370000  0.000000  2165.   'CMGTEMP_009.inc'
FLX_WELLBORE 'FlexWell-ProductionWell' ATTACHTO 'HorizTraj3'
SOLID_BLOCK OFF
SEGREGATION ON
ANNULUS ATTACHTO 'HorizTraj3'
TUBULARS VARIABLE
  0.1397          0.1524          0.1778   'CMGTEMP_010.inc'
WALL_CP  3.63e+06
WALL_HCN 3.888e+06
CEMENT_HEAT_PROP 3283 16800
REL_ROUGH 0.0001
MAX_NUSSELT 10000



**
WELL  'HorizTraj11'
INJECTOR MOBWEIGHT IMPLICIT 'HorizTraj11'
INCOMP  WATER  1.0
TINJW  60.0
QUAL  0.0
PINJW  6875.0
OPERATE  MAX  STW  3000.0  CONT
```

```
**        rad  geofac  wfrac  skin
GEOMETRY  K  0.0762  0.249  1.0  0.0
  PERF_FLX      GEOA  'HorizTraj11'
    47 11 1         1.0  CLOSED  FLOW-FROM  'SURFACE'    'CMGTEMP_011.inc'
LAYERXYZ  'HorizTraj11'
    47 11 1   1165.470000  1617.370000  0.000000  1165.   'CMGTEMP_012.inc'
FLX_WELLBORE 'FlexWell-InjectionWell' ATTACHTO 'HorizTraj11'
SOLID_BLOCK OFF
SEGREGATION ON
ANNULUS ATTACHTO 'HorizTraj11'
TUBULARS VARIABLE
  0.1397          0.1524          0.1778   'CMGTEMP_013.inc'
WALL_CP  3.61288e+06
WALL_HCN 6.48e+06
CEMENT_HEAT_PROP 2e+06 172800
REL_ROUGH 0.0001
MAX_NUSSELT 10000

REPORTING-GROUP 'FlexWell: FlexWell-InjectionWell'
    'HorizTraj11'
    1.0
REPORTING-GROUP 'FlexWell: FlexWell-ProductionWell'
    'HorizTraj3'
    1.0
```

APPENDIX C

EGS CASE .DAT CODE

The following is the code used by CMG-STARS to read and run the EGS model evaluated in Chapter 3. The .dat file shown in this appendix is for the EGS configuration:

```
WPRN FLEXWELL GRID 1
INUNIT SI
WSRF WELL 1
WSRF GRID 1
OUTPRN WELL ALL
OUTSRF GRID PRES TEMP
OUTSRF FLEXLAYER ALL
** ***************************************************************************
** Definition of fundamental cartesian grid
** ***************************************************************************
GRID VARI 59 59 86
KDIR DOWN
DI IVAR
 59*80
DJ JVAR
 59*80
DK ALL
 299366*80
DTOP
 3481*0

**  0 = null block, 1 = active block
NULL CON          1
*PLNRFRAC_TEMPLATE 'Planar Template'
   *PLNR_REFINE *INTO  3 3 1
   *BWHLEN 1100
   *IDIR
   *INNERWIDTH 0.6096
   *WF1 0.001
   *K_CENT 50000
   *KH_TYPE LINEAR
   *KH_TIP 50000 50000
   *KV_TYPE LINEAR
   *KV_TIP 50000 50000
   *HEIGHTUP 50
   *HEIGHTDOWN 50
   *POR MATRIX *FZ 0.0016
```

```
*END_TEMPLATE
RESULTS PLNRSTAGE NAME 'Planar Stage 1'
RESULTS PLNRSTAGE WELL 'Injection'
RESULTS PLNRSTAGE DATE 2020-01-01
RESULTS PLNRSTAGE TRAJECTORY 'Injection'
RESULTS PLNRSTAGE BASENAME 'Injection - Frac'
RESULTS PLNRSTAGE FRACS 'Injection - Frac_1' 'Injection - Frac_2' 'Injection - Frac_3'
RESULTS PLNRSTAGE FRACS 'Injection - Frac_4' 'Injection - Frac_5' 'Injection - Frac_6'
RESULTS PLNRSTAGE FRACS 'Injection - Frac_7' 'Injection - Frac_8' 'Injection - Frac_9'
RESULTS PLNRSTAGE FRACS 'Injection - Frac_10' 'Injection - Frac_11' 'Injection - Frac_12'
RESULTS PLNRSTAGE MINFRACSPACING 0
RESULTS PLNRSTAGE STARTMD 6250
RESULTS PLNRSTAGE ENDMD 7165.58
RESULTS PLNRSTAGE PERFOPTION 1
RESULTS PLNRSTAGE LAYERMIN 1
RESULTS PLNRSTAGE LAYERMAX 78
RESULTS PLNRSTAGE END
*PLNRFRAC 'Planar Template' 21,24,78 *BG_NAME 'Injection - Frac_1'
*PLNRFRAC 'Planar Template' 21,25,78 *BG_NAME 'Injection - Frac_2'
*PLNRFRAC 'Planar Template' 21,26,78 *BG_NAME 'Injection - Frac_3'
*PLNRFRAC 'Planar Template' 21,27,78 *BG_NAME 'Injection - Frac_4'
*PLNRFRAC 'Planar Template' 21,28,78 *BG_NAME 'Injection - Frac_5'
*PLNRFRAC 'Planar Template' 21,29,78 *BG_NAME 'Injection - Frac_6'
*PLNRFRAC 'Planar Template' 21,30,78 *BG_NAME 'Injection - Frac_7'
*PLNRFRAC 'Planar Template' 21,31,78 *BG_NAME 'Injection - Frac_8'
*PLNRFRAC 'Planar Template' 21,32,78 *BG_NAME 'Injection - Frac_9'
*PLNRFRAC 'Planar Template' 21,33,78 *BG_NAME 'Injection - Frac_10'
*PLNRFRAC 'Planar Template' 21,34,78 *BG_NAME 'Injection - Frac_11'
*PLNRFRAC 'Planar Template' 21,35,78 *BG_NAME 'Injection - Frac_12'
*NFZG-ALIGN ON
POR CON        0.01
PERMI CON        1E-06
PERMJ  EQUALSI
PERMK  EQUALSI
**  0 = pinched block, 1 = active block
PINCHOUTARRAY CON           1
END-GRID
ROCKTYPE 1
CPOR 4.35e-7
ROCKCP 2.66e6 0
THCONR 2.59e5
THCONW 53500
** Model and number of components
MODEL 1 1 1 1
COMPNAME 'H2O'
CMM
```

```
0
PCRIT
0
TCRIT
0
MASSDEN
1000
AVISC
0.0047352
BVISC
1515.7
ROCKFLUID
RPT 1 WATWET
**      Sw      krw     krow
SWT

0       0       1
1       1       0
**      Sl      krg     krog
SLT

0       1       0
1       0       1
INITIAL
VERTICAL OFF

INITREGION 1
REFPRES 5820
REFDEPTH 5820
PRES KVAR
 800 1600 2400 3200 4000 4800 5600 6400 7200 8000 8800 9600 10400 11200
 12000 12800 13600 14400 15200 16000 16800 17600 18400 19200 20000
 20800 21600 22400 23200 24000 24800 25600 26400 27200 28000 28800
 29600 30400 31200 32000 32800 33600 34400 35200 36000 36800 37600
 38400 39200 40000 40800 41600 42400 43200 44000 44800 45600 46400
 47200 48000 48800 49600 50400 51200 52000 52800 53600 54400 55200
 56000 56800 57600 58400 59200 60000 60800 61600 62400 63200 64000
 64800 65600 66400 67200 68000 68800
TEMP KVAR
 20 23.68421 27.36842 31.05263 34.73684 38.42105 42.10526 45.78947
 49.47368 53.15789 56.84211 60.52632 64.21053 67.89474 71.57895 75.26316
 78.94736 82.63158 86.31579 90 93.68421 97.36842 101.0526 104.7368
 108.4211 112.1053 115.7895 119.4737 123.1579 126.8421 130.5263 134.2105
 137.8947 141.5789 145.2632 148.9474 152.6316 156.3158 160 163.6842
 167.3684 171.0526 174.7368 178.4211 182.1053 185.7895 189.4737 193.1579
 196.8421 200.5263 204.2105 207.8947 211.5789 215.2632 218.9474 222.6316
```

```
 226.3158 230 233.6842 237.3684 241.0526 244.7368 248.4211 252.1053
 255.7895 259.4737 263.1579 266.8421 270.5263 274.2105 277.8947 281.5789
 285.2632 288.9474 292.6316 296.3158 300 303.6842 307.3684 311.0526
 314.7368 318.4211 322.1053 325.7895 329.4737 333.1579

SW CON          1
SO CON          0
SG CON          0
MFRAC_WAT 'H2O' CON          1
MFRAC_GAS 'H2O' CON          0
NUMERICAL
AUTOTUNE ON
RUN
DATE 2020 1 1
DTWELL 0.1
**
WELL  'Injection'
INJECTOR MOBWEIGHT IMPLICIT 'Injection'
INCOMP  WATER  1.0
TINJW  60.0
QUAL  0.0
PINJW  6894.76
OPERATE  MAX  STW  3000.0  CONT
**        rad  geofac  wfrac  skin
GEOMETRY  K  0.0762  0.249  1.0  0.0
  PERF_FLX     GEOA  'Injection'
   21 21 1              1.0  CLOSED  FLOW-FROM  'S   'CMGTEMP_000.inc'
LAYERXYZ  'Injection'
   21 21 1         1642.970000  1662.560000  0.00000   'CMGTEMP_001.inc'
FLX_WELLBORE 'FlexWell-1' ATTACHTO 'Injection'
SOLID_BLOCK OFF
SEGREGATION ON
ANNULUS ATTACHTO 'Injection'
TUBULARS VARIABLE
  0.14         0.152         0.178   'CMGTEMP_002.inc'
WALL_CP  3.61288e+06
WALL_HCN 6.48e+06
CEMENT_HEAT_PROP 2e+06 172800
REL_ROUGH 0.0001
MAX_NUSSELT 10000

**
WELL  'Production'
PRODUCER 'Production'
OPERATE  MAX  STW  3000.0  CONT
OPERATE  MIN  BHP  5900.0  CONT
```

```
**        rad  geofac  wfrac  skin
GEOMETRY  K  0.0762  0.249  1.0  0.0
  PERF_FLX      GEOA  'Production'
    34 21 1                1.0  CLOSED  FLOW-TO  'SUR   'CMGTEMP_003.inc'
LAYERXYZ  'Production'
    34 21 1          2682.970000  1662.560000  0.00000   'CMGTEMP_004.inc'
FLX_WELLBORE 'FlexWell-2' ATTACHTO 'Production'
SOLID_BLOCK OFF
SEGREGATION ON
ANNULUS ATTACHTO 'Production'
TUBULARS VARIABLE
  0.14          0.152          0.178   'CMGTEMP_005.inc'
WALL_CP  3.61288e+06
WALL_HCN 6.48e+06
CEMENT_HEAT_PROP 2e+06 172800
REL_ROUGH 0.0001
MAX_NUSSELT 10000

REPORTING-GROUP 'FlexWell: FlexWell-1'
    'Injection'
    1.0
REPORTING-GROUP 'FlexWell: FlexWell-2'
    'Production'
    1.0
```

APPENDIX D

LIST OF SUPPLEMENTAL FILES FOR COPYRIGHT PERMISSIONS

1. Reprinted permission of EGS, Inc. team for Figure 1.1.
2. Reprinted permission of Colorado Geological Survey for Figure 1.2.
3. Reprinted permission of U.S. Geological Survey for Figure 1.3.
4. Reprinted permission of Karla Panchuk for Figure 2.1.
5. Reuse permission provided by Elsevier and Copyright Clearance Center for Figure 2.2.
6. Reuse permission provided by Elsevier and Copyright Clearance Center for Figure 2.3.
7. Reuse permission provided by Elsevier and Copyright Clearance Center for Figure 2.4.
8. Reuse permission provided by Elsevier and Copyright Clearance Center for Figure 2.5.
9. Reuse permission provided by Elsevier and Copyright Clearance Center for Figure 2.6.
10. Reuse permission provided by Elsevier and Copyright Clearance Center for Figure 2.7.